Global and specific responses of the histone acetylome to systematic perturbation

Christian Feller§, Ignasi Forné, Axel Imhof and Peter B. Becker*

Adolf-Butenandt-Institute and Center for Integrated Protein Science Munich, Ludwig-Maximilians-University, Munich, Germany

§ Present address: Department of Biology, Institute of Molecular Systems Biology, Eidgenössische Technische Hochschule Zurich (ETH-Z), Zurich 8093, Switzerland

Corresponding author

Peter B. Becker

Email: pbecker@med.uni-muenchen.de

Adolf-Butenandt-Institute

Schillerstrasse 44, 80336 München, Germany

Phone: 089-2180-75-431

Fax: 089-2180-75-425

Running title

A comprehensive inventory of the histone acetylome

SUMMARY

Regulation of histone acetylation is fundamental to the utilisation of eukaryotic genomes in chromatin. Aberrant acetylation contributes to disease and can be clinically combated by inhibiting the responsible enzymes.

Our knowledge of the histone acetylation system is patchy because we so far lacked the methodology to describe acetylation patterns and their genesis by integrated enzyme activities. We devised a generally applicable, mass spectrometry-based strategy to precisely and accurately quantify combinatorial modification motifs. This was applied to generate a comprehensive inventory of acetylation motifs on histones H3 and H4 in *Drosophila* cells.

Systematic depletion of known or suspected acetyltransferases and deacetylases revealed specific alterations of histone acetylation signatures, established enzyme-substrate relationships and unveiled an extensive crosstalk between neighboring modifications. Unexpectedly, overall histone acetylation levels remained remarkably constant upon depletion of individual acetyltransferases. Conceivably, the acetylation level is adjusted to maintain the global charge neutralisation of chromatin and the stability of nuclei.

INTRODUCTION

The problem of packaging and organising complex genomes in the nuclei of cells was elegantly solved by the evolution of chromatin. The wrapping of DNA around octamers of histone proteins to form an ever-repeating succession of nucleosomes is universal among all eukaryotes. The increasing complexity of organisms due to the differentiation of cell types necessitates a structural and functional diversification of chromatin. This is mainly achieved by post-translational, chemical modifications of histones.

Currently, we know of more than 10 different types of chemical modifications (such as methylation, acetylation, phosphorylation) that alter the properties of amino acids in histones. Collectively, these modifications locally define chromatin structure and are fundamental to establishing the gene expression programmes that characterise healthy and diseased cells. The enzymes that reversibly modify histones are increasingly recognised as targets for therapeutic intervention in cancer tissue and neurodegenerative diseases (Dawson and Kouzarides, 2012; Graff and Tsai, 2013).

Acetylations of histones H3 and H4 are frequent and among the best characterised post-translational modifications (Sterner and Berger, 2000; Kouzarides, 2007; Lee and Workman, 2007). The N-terminal domains of these two histones (the amino-terminal ‘tail’ domains) alone bear a dozen lysine residues subject to acetylation. Additional acetylation has also been reported at internal residues (Tan et al., 2011). Histone acetylation patterns in chromatin result from the interplay between an impressive number of dedicated lysine acetyltransferases (KATs) and antagonising deacetylases (KDACs), yet their individual enzyme-substrate relationships is often controversial or not known.

The acetylation of lysine has structural consequences: charge neutralisation weakens DNA-histone and nucleosome-nucleosome interactions and is often correlated to unfolding of nucleosome fibres and gene activation (Kouzarides, 2007). Acetylated lysines may contribute to marking individual histones as they are recognised by bromodomains of effector proteins.

Acetylation of lysines prevents their methylation or ubiquitylation and may therefore have secondary effects.

Different post-translational modifications (PTMs) may reside on the same histone molecule. Many cases have been reported where PTM combinations (PTM motifs) rather than individual marks bear functional meaning (Fischle et al., 2003). Top/middle-down mass spectrometry suggests the existence of over 200 different PTM motifs on histones – many of which involve site-specific acetylation – yet their exact cellular abundance remains elusive (Pesavento et al., 2008; Young et al., 2009; Jung et al., 2013).

Acetylated lysines may be bound by dedicated bromodomains in effector proteins. Although the affinity towards a single acetyl-lysine is low, multiple adjacent acetyl-lysines not only boost the affinity but may also tune the targeting selectivity (Ruthenburg et al., 2007; Filippakopoulos et al., 2012). It is currently not known whether combinatorial acetylation motifs are generated by a single KAT or whether they require the action of multiple enzymes, with the exception of the cytoplasmic di-acetylation of H4 at K5 and 12, which is catalysed by HAT1 (Parthun, 2012).

Moreover, PTMs neighbouring acetylated lysines can strongly alter the affinity of bromodomains – and likewise the enzymatic activity of KATs and KDACs may be modulated by close-by PTMs (Fischle et al., 2003; Filippakopoulos et al., 2012).

Our ability to detect and reliable quantify low abundant histone acetylation, or acetylation as part of a PTM motif, are currently rather limited. Traditionally, histone PTMs are detected with antibodies raised against appropriately modified peptides. However, recent studies alarm that antibodies raised against individually acetylated lysines (e.g. H4.K12ac) primarily recognise multiply-acetylated peptides (e.g. tetra-acetylated H4) and may display substantial off-target reactivity (Fuchs et al., 2011; Rothbart et al., 2012). Moreover, antibody detection systems have a limited linear dynamic range, precluding a quantitative analysis. Finally, most antibodies are unable to differentially display acetylation in combinatorial motifs.

Peptide modifications are commonly detected by mass spectrometry (MS), however, most current MS protocols are hampered by low precision and accuracy to reliably quantify combinatorial histone PTM motifs. We optimised an MS workflow and applied it to generate a quantitative and comprehensive inventory of motifs involving acetylation of histones H3 and H4 in *Drosophila melanogaster* cells and the changes in these motifs in response to ablation of many known or suspected KATs and KDACs. The comprehensiveness of the dataset not only allows us to define class-specific features that are shared among members of enzyme families but also to describe the histone modification system as a highly interconnected, responsive network that compensates for the loss of individual components.

RESULTS

Optimising liquid chromatography mass spectrometry (LC-MS) workflows for accurate and precise quantification of single and combinatorial PTMs

Identifying and quantifying rare, combinatorial modification motifs currently poses a major analytical challenge. We optimised LC-MS workflows for sensitive, precise and accurate quantification of PTM motifs containing lysine acetylation and methylation.

We rapidly isolated histones from cells by acid extraction and chemically acetylated all unmodified and mono-methylated lysines with deuterated acetic anhydride (D3AA method, (Smith et al., 2003)). The deuterated (d3) mass tag adds three Daltons to distinguish endogenous from chemical acetylation. This also ensures that digestion by trypsin only occurs after arginine, yielding peptides of an intermediate size necessary for bottom-up analysis of PTM motifs (Figure 1A). Unlike the more common propionylation (Garcia et al., 2007; Schotta et al., 2008; Zheng et al., 2013), chemical acetylation yields peptides with similar physicochemical properties to those bearing endogenous acetylation. This ensures comparability during the entire LC-MS workflow, including the MS quantification.

We developed a generally applicable targeted MS workflow to reliably quantify PTM motifs that require MS^n measurements (Figures 1A-C, S1-S3, Supplemental Experimental Procedure Note (SEP) 1 and Table S1). Motifs containing methylated lysines in addition to acetylation displayed characteristic shifts in retention time and thus were quantified based on their MS1 peak area (Figures 1A, S1). However, positional isomers carrying one or multiple acetylations are not separated chromatographically using the D3AA method. Their individual intensities can be quantified using signals generated by a high occurrence of targeted MS2 scans (Figures 1A, S2; Table S1). Because four of the di-acetylated histone H4 combinations, including H4.K5acK12ac, cannot be identified and quantified with MS1 and MS2 only, we optimised procedures to quantitatively read out prognostic MS3 ions and thereby measured those isoforms by successive MS1-MS2-MS3 scans (Figures S2A, S2B, SEP 1.2). To our knowledge, this is the first direct MS-based quantification of all six histone H4 di-acetylated isoforms. Validating the LC-MS workflow using synthetic peptides and performing technical and biological whole-workflow replicates demonstrated high precision and accuracy (Figures 1B, C, S2B, Tables S2, S3 and SEP 1).

Correction of LC-MS signal bias

Modifications change the physicochemical properties of peptides, which may influence several steps during the LC-MS workflow and thereby impair accurate quantification (Marx et al., 2013). To assess this phenomenon, we determined the LC-MS response factor by measuring a library of synthetic peptides containing acetylation and methylation motifs to H3 and normalising the proteotypic signals relative to the abundance of the cleaved quantification (Q) tag (Figure 1C, SEP 2). Equimolar solutions of peptides with different methylation signatures displayed very drastic differences in the LC-MS response factor, corroborating a recent study by Garcia and colleagues (Lin et al., 2014). The effect is most dramatic for peptides containing H3.K9me3, whose Q tag normalised LC-MS response factor is 34 times lower than that of the K9me1 peptide. Therefore, the interpretation of the cellular

abundance of K9me3 is underestimated by an order of magnitude if not corrected for LC-MS bias (see below). On the other hand, H3 peptides bearing K9ac or K14ac have almost identical LC-MS response factors, confirming that the D3AA method achieves accurate quantification of acetylation motifs.

In summary, experimentally determined LC-MS response factors allowed introducing a correction factor specific to histone motifs. Table S2 summarises these factors for a selected set of peptides. Our catalogue of correction factors will facilitate the interpretation of published and future PTM datasets for relative and absolute abundances of peptides and their PTMs.

The histone acetylation motifs fall into three abundance classes

We measured the acetylation and methylation levels of all lysines on histone H3 and H4 in *Drosophila melanogaster* KC cells and quantified 45 of over 55 motifs detected (Figure 1D, Table S3, SEP 1.3). This included acetylation of K5, K8, K12 and K16 as well as methylation of K20 on histone H4 and seven acetylation (K9, K14, K18, K23, K27, K36, K37) as well as five methylation sites (K4, K9, K27, K36, K79) on H3. We did not detect acetylation or methylation on the remaining six lysines of histone H4 and four lysines on histone H3. Although other lysine acetylation sites had been reported before (H4.K91ac, H3.K4ac, H3.K56ac, H3.K122ac), their abundance in *Drosophila* cells is likely below our detection limit of approximately 0.003% or 182 histone molecules per cell, at least on average in an asynchronous population (see below and SEP 1.3).

Knowledge of the cellular abundances of histone motifs facilitates the interpretation of chromatin maps and may contribute to developing quantitative models for the function of histone modifications. For example, H3.K9me3 constitutes a hallmark of repressive chromatin that covers significant regions of the fly and mammalian genomes. In support of this widespread notion, we measured K9me3 on 39% of H3 molecules, but only if we

corrected for the differential LC-MS response (without correction: 4.2% H3.K9me3, Table S3).

The abundances among individual acetylation motifs differ by four orders of magnitude (Figure 1D). The abundance distribution of the 29 histone acetylation motifs revealed three classes. H3.K23ac is by far the most abundant acetylation (47% of H3, corresponding to 2.8 million molecules/cell). It is present, on average, on every second nucleosome or even on all nucleosomes if the arrangement was heterotypic. Eleven motifs were of intermediate abundance (1–12% of histones, class median: 3.7%). Most combinatorial acetylation motifs, however, are present on less than 1% of histones (17 motifs, class median: 0.3%). For example, the H4.K5acK8acK16ac motif is present in only about 7600 estimated copies per cell (for reference, a KC cell has about 6000 active gene promoters). It is tempting to speculate that highly abundant histone acetylation motifs contribute to global features of chromatin structure, whereas rare and combinatorial histone acetylation motifs constitute marks for bromodomain-mediated signalling.

The contributions of known or suspected KAT and KDAC enzymes to histone acetylation motifs

The inventory of all histone acetylation motifs serves as a point of entry to study the histone acetylome as a structural and regulatory system that is installed by KATs and KDACs according to cell-specific programmes. The properties of this system depend on the substrate specificity or redundancy of the enzymes. Which KATs and KDACs contribute to a specific histone acetylation motif? What are the global effects on the histone acetylation landscape if a single enzyme is depleted? Addressing these questions we systematically evaluated the contribution of every KAT and KDAC to the inventory.

Drosophila melanogaster is particularly suited for a single gene perturbation strategy, since most KATs, KDACs and KAT/KDAC-associated proteins are well conserved between the fly

and human cells, yet, the fly genome does not contain extensive KAT and KDAC paralogues, which are common for most mammalian genomes.

We created and curated a list of putative acetyltransferases and deacetylases in *D. melanogaster,* including novel candidate genes coding for proteins with acetyltransferase-related domains (Table S5). Of the at least 44 putative lysine acetyltransferases with recognisable KAT domains, we focused on the 23 KATs that are expressed in most cell types and developmental stages and thus are likely to constitute the most relevant determinants of *Drosophila's* histone acetylation system. This list includes (1) the extensively studied 'model' KATs (GCN5/PCAF, CBP/P300, MOF, HAT1, TIP60), (2) less well characterised KATs (KAT6 [MOZ/MORF], HBO1, ELP3, TAF1, ATAC2), (3) a mostly uncharacterised class of GCN5-related KATs (NAT6, NAT9, NAT10), (4) N-terminal acetyltransferases suggested to also acetylate internal lysines (NAA10, NAA20, NAA30, NAA40, NAA50, NAA60), (5) putative acetyltransferases with no recognisable direct homologue in non-*Drosophilid* species (CG5783, CG12560), (6) the acetyltransferase ECO and (7) a bi-functional enzyme containing a O-GlcNAcase - activity and potentially a KAT activity (MGEA5, also known as NCOAT or OGA).

The *D. melanogaster* genome encodes five recognisable zinc-dependent lysine deacetylases of the HDAC class (RPD3/HDAC1, HDAC3, HDAC4, HDAC6, HDAC11) und five NAD-dependent Sirtuins (SIR2/SIRT1, SIRT2, SIRT4, SIRT6, SIRT7). With the exception of HDAC11 and SIRT7, all KDACs are ubiquitously expressed und analysed in our study.

Because the majority of KATs and KDACs are not or only poorly characterised and consequently mutants and antibodies are lacking, we depleted KAT and KDAC proteins by RNA interference (RNAi) in the *Drosophila* model cell line KC (Table S6). RNAi efficiently depletes proteins in *Drosophila* cell lines within 4 – 7 days.

As a proof of concept we initially focused on the acetyltransferase MOF, for which well characterised mutants and antibodies exist. MOF levels were strongly diminished after incubating cells for 4 days with interfering RNAs directed against MOF transcript, and were

undetectable after 5.5 days (Figures S4A, B). At this time H4.K16ac, the known product of MOF activity, was most strongly reduced (Figure S4C). The two different interfering RNAs yielded very similar results (Table S4). Because MOF is considered to be responsible for the majority of H4.K16ac in *Drosophila* and human cells (Smith et al., 2005; Conrad et al., 2012), we were surprised to observe that depletion of MOF in the female KC cell line reduced the amounts of H4.K16ac by only 40%. Apparently, other KATs besides MOF contribute to setting the H4.K16ac mark.

To compare the acute RNAi depletion strategy with constitutive loss of gene function, we analysed the status of H4.K16ac in adult flies mutated for MOF (Gu et al., 1998). Similar to KC cells, mof^2 mutant females retained over 50% of H4.K16ac (Figure S4D). Therefore, RNAi against MOF led to quantitatively similar reduction of H4.K16ac as loss-of-function mutation of the MOF gene. We conclude that RNAi is an appropriate method for our survey of KAT and KDAC activities.

We next ablated each KAT and KDAC in KC cells with two distinct interfering RNAs for 5.5 days and measured the abundance of 22 acetylation, 6 mixed acetylation-methylation and 11 methylation motifs as well as the 5 unmodified peptide backbones. Using RT-qPCR, we determined a mean knockdown efficiency of 80% across the 31 gene knockdowns (Figure S5). Multiple biological replicates increased the confidence to measure even subtle differences and demonstrated a high reproducibility among the RNAi pairs and across replicates (Table S4, SEP 3). We observed no major growth and cell cycle phenotypes upon depleting individual KATs and KDACs (data not shown), in agreement with a previous report (Kondo and Perrimon, 2011). Notable exceptions were cells in which CBP, TAF1 and RPD3 were targeted, which slowed their proliferation after four days of RNAi (data not shown).

The heat map in Figure 2A shows the relative changes of 24 histone acetylation motifs upon depletion of 23 KATs. Most KATs show a clear specificity for certain acetylation motifs, but CBP and NAA10 contribute to many motifs. KAT depletion leads to decreased levels of 104 acetylation motifs, with interesting specific effects. Many relations between KATs and

particular histone motifs would have been missed had a conventional instead of a combinatorial analysis been applied (compare Figure 2B with 2A). Contrary to expectation, acetylation motifs did not only decline but at the same time the abundances of 160 motifs increased. Detailed analysis (see below) reveals that pre-existing acetylation and methylation patterns modulate the substrate selectivity for further modification.

Our analysis reports the response of the system to enzyme depletion, including primary effects reflecting direct enzyme-substrate relationships, and secondary effects for example of compensatory nature. To our knowledge, these 1364 individual enzyme - histone PTM relationships – monitoring the involvement of 23 KATs and 8 KDACs in 39 acetylation and methylation motifs – constitute the most comprehensive functional histone PTM dataset reported so far.

Mining the database for testable hypotheses and characteristics of acetyltransferase classes

An in-depth analysis of the data summarised in Figure 2 allows not only to shed light on controversial enzyme-substrate relationships but also to derive testable hypotheses about pathways that generate complex acetylation motifs. In the Supplemental Experimental Procedure Note 4, this is illustrated with two examples, the cytoplasmic HAT1 and with HBO1, substrates of which are currently debated (SEP 4 and Figures 2, 3A,B).

Mining the data underlying Figure 2 demonstrates that many KATs specifically contribute to low abundant and combinatorial motifs. Most KATs have a narrow yet not absolute substrate specificity, which is modulated by adjacent acetylation (markedly observed for HAT1, HBO1, MOF, ATAC2, NAT10 and MGEA5) and methylation (KAT6, HBO1, NAT10 and others). This hitherto unappreciated level of crosstalk between neighbouring methylation and acetylation sites (see below) suggests that, like bromodomain recognition of histone tails, the interactions of KATs with substrate peptides are sensitive to the context of specific combinatorial motifs.

The realisation that most KATs have restricted substrate selectivity is in stark contrast to the widespread notion that most KATs are rather promiscuous enzymes (Sterner and Berger, 2000; Kouzarides, 2007; Lee and Workman, 2007). This view may have arisen by studies of the model acetyltransferase CBP, which, however, is a clear outlier within the KAT class (Figures 2, 3C, D). Loss of CBP leads to a reduction of many acetylation motifs, including acetylation at K5 and K8 of H4 and K14, K18, K27 and K36 on H3. Furthermore, whereas most KAT depletions reduce only a distinct subset of the motifs containing the putative primary target lysine, CBP RNAi reduces almost all H4 combinations containing acetylated K5 and K8 (Figure 3C). Evidently, CBP is a rather promiscuous KAT, which may explain its robust acetylation activity of many substrates *in vitro* (Sterner and Berger, 2000). Clearly, the enzymatic properties of CBP do not reflect common properties of KATs as a class.

Commonly, several KATs contribute to setting a histone acetylation motif. This fundamental conclusion echoes the combinatorial nature of histone modifications at the level of the enzymes that bring it about. While on average three KATs contribute to setting an acetylation motif, one often finds a dominant KAT with minor contributions by others. For example, CBP depletion leads to a reduction of H4.K5acK8ac by 61% whereas MGEA5 and NAA10 each contribute only 30% and 23%, respectively (Figure 3E). Although HAT1 is the dominant KAT that sets H4.K5acK12ac, NAA10 and NAA60 also contribute substantially. Figure 3F plots the cumulative contributions of all KATs, calculated from the extent of motif reduction upon KAT depletion to all acetylation motifs. Notably, several bars approximate a cumulative depletion of 100% if all KAT RNAi effects are summed up (median = 113%, mean = 129%), suggesting that our systematic KAT depletion approach captures the majority of the cell's acetylation events. Cases were the cumulative contributions stay below 100% may be explained by functional redundancy between enzymes: the effect of an individual knockdown is underestimated because an alternative KAT takes over. For several rare and highly combinatorial motifs the cumulative contributions add up to more than 100%, which points to potential contributions of KDACs to the steady-state levels of acetylation motifs.

The relaxed specificity of deacetylases restricts the levels of rare, combinatorial motifs

The immediate reversibility that endows acetylation marks with regulatory potential requires strong deacetylase activities. Unlike KATs, KDACs are characterised by relaxed substrate specificity. Depletion of any of the eight commonly expressed KDACs increased the levels of many H4 and most H3 acetylation motifs in a similar way (Figure 4). RPD3 is by far the dominant deacetylase in KC cells, and its depletion leads to strong gains of those rare, combinatorial motifs on H4 that bear regulatory potential.

Overall, motifs with multiple acetylation sites increase stronger than individually acetylated motifs. For example, di-acetylated H3.K9acK14ac increases more than 4 fold after ablation of RPD3. At the same time, the levels of the highly abundant H3.K14ac mark were only marginally increased by 20% whereas the ubiquitous H3.K23ac mark was not affected at all. We also did not detect any new acetylation of the lysines of the H3 and H4 tails that were not acetylated in unperturbed KC cells.

The system's response to KAT deprivation effectively maintains global histone acetylation levels

Contrary to wide-held expectations we observed that the levels of many histone motifs *increased* if cells are deprived of histone acetyltransferases (Figure 2A). To explore this phenomenon more systematically, we summed up all gains and losses of the individual H3 and H4 acetylation motifs. To our surprise, we found that cells have balanced or even higher histone acetylation levels when depleted for most individual lysine acetyltransferases (Figures 5A and S6B). Ablation of only three KATs (KAT6, NAA10 and GCN5) lead to the expected significant reduction of global histone H3 and H4 acetylation. For a major group of 17 KATs, among them CBP and HBO1, the depletion did not change the cell's total number of acetylated histone H3 and H4 peptides relative to non-acetylated peptides significantly, despite the fact that the abundance of some 'primary' acetylation motifs (the presumed direct

products of KAT activity) were severely reduced (Figure 5). We arrived at a similar conclusion when we counted the total number of *acetyl groups* instead of the number of *acetylated peptides* (Figure S6B). These losses were accompanied by gains in other, sometimes unrelated motifs, even on the other histone's tail (Figures 2A, 5B).

For a number of enzymes (NAT6, GC5783, NAA40 and TAF1) we do not detect any loss of acetylation upon depletion, but only gains (Figure 2A). These enzymes may not be KATs after all, or may strictly depend on cofactors that are not present in KC cells. Moreover, some KATs may only acetylate non-histone proteins (Sterner and Berger, 2000; Choudhary et al., 2009). Conceivably, the losses and gains in acetylation motifs upon perturbation of KATs reflect the response of a system that strives to compensate structural perturbations. Such system's response may be brought about in different ways, including feedback responses to modulate gene expression or enzyme activity of other KATs and KDACs. For examples of the modulation of KAT expression levels after depletion of key KATs, see Figure S5B and SEP 5.

The methylation response to KAT depletion allows their functional classification

Depletion of most KATs lead to global changes in histone methylation marks. Hierarchical clustering of the methylation responses upon KAT deprivation revealed a clear grouping of KATs (Figure 6A). Many KAT depletions led to a substantial reduction of H3.K36me2/3, a mark associated with transcribed chromatin, as well as to a massive increase in the repressive H3.K27me3 mark, which indicates polycomb repression. This response is well expected for those KATs that are known transcription co-activators (GCN5, CBP, TIP60). The similarity of the response scored upon ablation of MGEA5 suggests that this poorly characterised KAT also functions as a transcription activator. Interestingly, the putative acetyltransferases CG5783 and NAT6 are the only enzymes whose absence is accompanied by a substantial *increase* of K36me2. Similar, loss of NAA40 is accompanied with a severe

reduction of the repressive K9me2 mark. These results suggest that CG5783, NAT6 and NAA40 may confer repressive functions.

Primary and secondary contributions of KATs to mixed acetylation/methylation motifs

For PTM motifs involving both, acetylation and methylation, it is difficult to conclude about the individual contribution of candidate enzymes. Figures 6B and 6C exemplify this challenge for KAT6 and HBO1.

Cells lacking KAT6 have reduced levels of H3.K14ac only in the context of tri-methylated lysine 9. Because H3.K9me3 alone is not reduced under these conditions, it is reasonable to assume that KAT6 directly acetylates K14ac on a tri-methylated K9 substrate. A similar argument can be made to conclude that KAT6 does not acetylate K14 if K9 is acetylated or mono-/di-methylated. The recognition of K14ac by antibodies may be modulated by adjacent methylation. By contrast, cells deprived of HBO1 not only reduce the H3.K9me3K14ac motif, but also the K9me3 mark alone, a secondary effect that may confuse the analysis of HBO1 substrates by other means.

Modulation of substrate specificity by molecular context

Acetyltransferases are commonly found in complexes with associated proteins that may target the enzyme to specific chromosomal loci and fine-tune substrate selectivity. Variation in associated complex subunits may harness a KAT activity for cell-specific and developmental functions. This is well illustrated using the case of MOF, which is found in two distinct multi-protein complexes. In the context of the ubiquitous NSL (MBDR-2) complex MOF regulates housekeeping genes as a classical transcription co-activator (Feller et al., 2012; Lam et al., 2012). In male somatic cells, MOF additionally associates with the so-called male-specific-lethal (MSL) proteins to form the dosage compensation complex (MSL-DCC). The MSL-DCC compensates the X chromosome monosomy by an increased transcription

output, which involves MOF-dependent H4.K16 acetylation of transcribed gene sequences (Prestel et al., 2010a).

In order to determine whether the protein complex environment modulates MOF's substrate selectivity we monitored changes in histone acetylation motifs after depleting male or female cells of MOF or of the diagnostic subunits of the NSL and MSL-DCC complex. RNA interference targeting MOF expression led to a reduction of H4.K16ac by about 40% in female cells or 60% in male cells (Figures 7A, S4D). MOF depletion in KC cells has to be seen against a robust increase of the almost three-fold more abundant H4.K12ac and additional gains in H3K9- and K14-containing acetylation motifs, leading to overall elevated levels of H3 + H4 acetylation. Likewise, H4.K16ac loss in male S2 cells was accompanied by a clear increase in H4.K12ac and H4.K5ac. Ablation of the MSL-DCC subunit MSL1 in male cells essentially mirrored this effect (with less crosstalk to H4.K5ac), indicating that most MOF effects in S2 cells are mediated by the MSL-DCC. By comparison, interference with the NSL complex through ablation of its core subunit NSL1 only modestly affected H4.K16ac levels. Interestingly, we detected a strong decrease of H3.K27ac in both cell types and of H4.K5ac in female cells lacking NSL1, but not MSL1 (Figure 7A, B). These findings illustrate the male-specific acetylation of H4.K16 over and above a lower, more general level. They also suggest that the NSL complex affects histone acetylation independent of MOF.

X chromosome dosage compensation is accompanied by global redistribution of acetylation and methylation marks

Due to the specific dosage compensation mechanism, male *Drosophila* cells contain more H4.K16ac than female cells (Figure 7C, D). In light of the observed global balancing of total acetylation levels (Figure 5) we wondered whether such chromosome-wide regulation had any consequences for the acetylation system as a whole. We, therefore, compared histone acetylation and methylation motifs in male and female cells as well as in male cells lacking MOF. Remarkably, male and female cells showed similar total histone acetylation levels, if all

H3 and H4 acetylation motifs were summed up (Figure 7C). However, the distribution of acetyl groups between motifs in male cells differs dramatically from that of female cells, and the differences are due to MOF (Figures 7C, D, see also Table S3). Male cells displayed twice the amount of H4.K16ac, but reduced levels of several other acetylation motifs including H4.K5ac, H4.K12ac and H3.K14ac as compared to female cells. Conversely, depletion of MOF in male S2 cells reduced H4.K16ac and increased H4.K5ac, H4.K12ac and H3.K14ac to levels found in female cells.

Comparing methylation signatures between male and female flies indicate that dosage compensation correlates with an increased abundance of the repressive K27me3 mark as well as increased H3.K36me2/3 (Figure 7E). Abolishing dosage compensation in S2 cells by ablation of MOF converts the methylation pattern to a one that resembles females. Together, these results indicate that the evolution of dosage compensation not only boosted the levels of H4.K16 acetylation, but also triggered a network of secondary effects that may be interpreted as adaptations of the system to a global change in acetylation state.

The global response of the histone modification system upon MOF depletion is conserved between *Drosophila* and human cells

One of the surprise findings of our study is that a reduction of H4.K16 acetylation, which is thought to be a histone mark with unique structural implications, led to an inevitable increase of acetylation at the neighbouring K12. The robustness of the effect suggests K12ac may structurally compensate for a loss of K16ac. Since H4.K16 acetylation is thought to affect the basic properties of the chromatin fibre, such an effect should be observable in other species as well. To test this prediction we deprived human cells of MOF. In mammalian cells, MOF preferentially associates with subunits of the NSL complex, but its substrate specificity is still under debate (Cai et al., 2010; Chelmicki et al., 2014). The ablation of MOF in HeLa cells not only reduced its supposed primary product, H4.K16ac, but also increased acetylation of the adjacent lysine 12, in striking resemblance to the effect in *Drosophila* (Figures 7F, S4F).

Moreover, similar to female flies, where MOF functions as a global transcriptional co-regulator, human cells lacking MOF showed increased levels of H3.K9me2 and K27me3, while K9me3 and K36me3 are reduced (Figure 7G).

These results suggest that the global response of the system of histone modifications that we observed through our comprehensive, quantitative study of the acetylation motifs after depletion of critical enzymes, is a conserved feature of higher eukaryotic nuclei.

DISCUSSION

Although lysine acetylation was the first chemical modification described for histones already more than 50 years ago, our knowledge of the contributions of acetylation to the complex, combinatorial histone modification system is still superficial. Optimising LC-MS workflows and correcting for its inherent detection bias we generated a comprehensive inventory of all acetylation sites and many combinatorial motifs for histones H3 and H4 in an asynchronous population of *Drosophila* cells. Some highly abundant motifs may contribute to the general structure of chromatin, whereas rare, often combinatorial, motifs may transmit regulatory signals via bromodomain adaptor proteins.

Knowing the abundance of acetylation sites helps designing and interpreting genomic experiments, distinguishing rate-limiting from saturating components in a chromatin pathway and assessing the dynamic turnover of acetylation motifs (Zheng et al., 2013).

Acetyltransferases were the first histone modifying enzymes to be cloned, yet the substrate specificity of some KATs has remained controversial or even not known (Lee and Workman, 2007). Traditionally, identifying KAT substrates involved testing the acetylation status of selected lysines with antibodies, whose specificities have recently been questioned. Further problems arise from relating the apparent KAT substrate specificities determined *in vitro* to their physiological activities, which are commonly modulated by the molecular environment of the multi-subunit complexes they reside in. Remarkably, we found that most KATs display a

narrow, yet not absolute, substrate specificity in cells, which is influenced by adjacent modifications. This contrasts common perceptions of rather promiscuous KAT activities that originate from the prominent characterisation of a few 'model' enzymes with relaxed substrate selectivity, such as CBP, which is a clear outlier of the class of KATs in this respect.

Our catalogue of the quantitative changes in histone acetylation and methylation motifs in response to ablating all known or suspected acetyltransferases and deacetylases allowed to re-evaluate controversial enzyme-substrate relationships and to discover putative primary targets of uncharacterised KATs. This database can be further mined to derive testable hypotheses about the functional crosstalk between histone modifying enzymes and the assignment of KATs and KDACs to cellular pathways and disease states.

Surprisingly, we found that ablation of many KATs not only reduced acetylation of its putative primary target but also led to acetylation gains at secondary sites, such that the global level of histone acetylation in cells were maintained. Our survey of the secondary effects upon KAT depletion serves as point of entry to study the intertwined regulatory network of histone modifications as a *system*.

Related phenomena that suggest 'compensation' of a modification loss by corresponding gains on other proteins have occasionally been observed before. Analysing the phospho-proteome of a collection of yeast kinase and phosphatase mutants, Aebersold and colleagues reported a similar number of gains and losses in phosphorylation sites across all mutants together (Bodenmiller et al., 2010). Voss and colleagues found that reduced levels of H3.K14ac in *hbo1* knockout mice were accompanied by increases in H4.K16ac and to a lesser extent in H4.K5ac and H3.K9ac (Kueh et al., 2011). Ge and co-workers made similar findings for *cbp/p300* double deletion lines, which displayed increased levels of H3.K23ac and H3.K9me1K14ac (Jin et al., 2011). These related findings in several species may point to a fundamental, conserved principle.

Conceivably, the loss of a particular acetylation motif evokes a compensatory acetylation of a different, but functionally redundant motif by another KAT. The reciprocal responses between H4.K12ac and H4.K16ac (HBO1, MOF) and involving H4.K5 and H4.K8 (CBP) support such a view. However, particularly critical alterations in acetylation, such as losses in highly abundant, structural acetylation motifs, or of motifs with very specific functions during organismal development may not be compensated for (Voss and Thomas, 2009).

Considering histone modifying complexes as components of a system that satisfies local functional heterogeneity as well as global structural constraints, sudden perturbation may trigger feedback regulation to attenuate the impact. In this respect, global charge distribution and neutralisation comes to mind. Histone acetylation significantly diminishes the total number of positive charges in chromatin. We speculate that ablating KATs triggers a homeostatic re-adjustment of global charge to maintain the stability of chromatin according to polyelectrolyte theory (Clark and Kimura, 1990).

The fact that lysines can be modified with several mutually exclusive chemical groups constitutes a basic principle of functional crosstalk between diverse modification-based signalling pathways. Further crosstalk is evident at the level of the modification enzymes, which are sensitive to pre-set modifications on histone tails. Monitoring lysine methylation and mixed acetylation-methylation motifs enabled us to identify new candidates, where a pre-set methylation mark may promote (KAT6: H3.K9me3 → K14ac) or inhibit (NAA10: H3.K9me2 --| K14ac) acetylation. Moreover, we observed that ablating individual KATs led to reduction (GCN5: H3.K79me2) or increase (CBP: H3.K27me3) in methylation sites. Reciprocal correlations between the loss of histone lysine methyltransferases and altered histone acetylation have been documented before (Plazas-Mayorca et al., 2010; Sinha et al., 2010). Our study suggests that crosstalk among lysine acetylation and methylation is widespread and must be considered within the system of a comprehensive modification landscape.

The targeting and substrate selectivity of a KAT may be tuned by associated cofactors. Using the example of MOF, which resides in two distinct complexes with non-overlapping function, we show that while the primary targets are similar across cell types and species (with notable quantitative differences), secondary effects are strongly influenced by the associated co-factors. Depletion of the NSL complex, but not the MSL-DCC complex, caused a massive reduction of the enhancer mark H3.K27ac, an interesting coincidence with the recent mapping of the human NSL complex to enhancers (Chelmicki et al., 2014).

Ablation of MOF activity in the context of the dosage compensation complex led to the expected reduction of H4.K16ac, but surprisingly, this was associated with a pronounced increase in the neighbouring H4.K12ac. Since the only known function of H4.K16 acetylation is to hinder the folding of the nucleosome fibre, we conclude that acetylation of lysine 12 can also fulfil this function to some extent. Interestingly, the depletion of the dosage compensation system led to a significant reduction of bulk H3.K36me3, a mark that is placed co-transcriptionally, which may reflect the two-fold reduction of transcription on the X chromosome.

Furthermore, depletion of MOF in male cells triggered a co-depletion of repressive methyl marks, leading us to speculate that repressive chromatin attenuates the powerful activation potential of H4.K16 acetylation to arrive at the balanced levels that characterise dosage compensation (Prestel et al., 2010b). Our results define a point of entry into a quantitative assessment of the epigenetic principles that enable the chromosome-wide transcriptional fine-tuning in vital processes, such as dosage compensation.

KAT and KDAC inhibitors are considered promising therapeutic agents in the combat against complex diseases including cancer and neurodegenerative disorders. Our work shows that depleting single KAT activities leads to complex alterations of the epigenome, of which we monitored the reduction of *bona fide* primary substrates, the global re-distribution of acetyl groups to secondary sites and changes to methylation of histones. Increased knowledge of

the systemic response of the chromatin modification network will be required for a more targeted utilisation of drugs in a clinical setting.

EXPERIMENTAL PROCEDURES

Cell Lines and RNAi

Cultivation of KC and S2 cells and RNAi were carried out essentially as described before (Feller et al., 2012). For detailed information, see Supplemental Experimental Procedures.

LC-MS for histone PTM quantification

Acid extracted, chemically acetylated and trypsinised histone peptides were separated on a HPLC C18 analytical column and electrosprayed into an LTQ-Orbitrap Classic. MS was operated in a targeted mode and data was analysed with Thermo Xcalibur, Excel and R.

Detailed information can be found in the Supplemental Experimental Procedures.

SUPPLEMENTAL INFORMATION

Supplemental Information includes six figures, six tables and Supplemental Experimental Procedures incl. Supplemental Experimental Procedure Notes (SEP).

AUTHOR CONTRIBUTIONS

P.B.B. and C.F. conceived and designed the study. C.F. coordinated the project, performed most of the wet-laboratory experiments and analysed the data. I.F. and C.F. developed the LC-MS workflow. I.F. processed most samples for LC-MS and performed most MS measurements. A.I. supervised LC-MS experiments and contributed important reagents.

P.B.B. supervised the project. P.B.B. and C.F. wrote the manuscript and all authors revised the final version.

ACKNOWLEDGMENTS

We are grateful to the following colleagues: Dirk Schwarzer for providing synthetic peptides, Matthias Prestel and Heike Mitlöhner for help with fly genetics and maintenance, Thomas Blasi, Tobias Straub and Sascha Trostorff for advice on calculations and statistics, Ana Villar-Garea, Carsten Marr, Tobias Straub and Thomas Blasi for critical comments on the manuscript and members of the Becker lab for helpful discussions. This work was supported by the European Research Council under the European Union's Seventh Framework Programme (FP7/2007-2013) / ERC grant agreement n°293948. C.F. is a fellow of the International Max-Planck Research School (IMPRS-LS).

The mass spectrometry proteomics data have been deposited to the ProteomeXchange Consortium (Vizcaino et al., 2014) via the PRIDE partner repository with the dataset identifier PXD001394. We acknowledge the PRIDE team for support of data deposition to the ProteomeXchange Consortium.

The authors declare no competing financial interests.

REFERENCES

Allis, C.D., Berger, S.L., Cote, J., Dent, S., Jenuwien, T., Kouzarides, T., Pillus, L., Reinberg, D., Shi, Y., Shiekhattar, R.*, et al.* (2007). New nomenclature for chromatin-modifying enzymes. Cell *131*, 633-636.

Bodenmiller, B., Wanka, S., Kraft, C., Urban, J., Campbell, D., Pedrioli, P.G., Gerrits, B., Picotti, P., Lam, H., Vitek, O.*, et al.* (2010). Phosphoproteomic analysis reveals interconnected system-wide responses to perturbations of kinases and phosphatases in yeast. Science signaling *3*, rs4.

Cai, Y., Jin, J., Swanson, S.K., Cole, M.D., Choi, S.H., Florens, L., Washburn, M.P., Conaway, J.W., and Conaway, R.C. (2010). Subunit composition and substrate specificity of a MOF-containing histone acetyltransferase distinct from the male-specific lethal (MSL) complex. The Journal of biological chemistry *285*, 4268-4272.

Chelmicki, T., Dundar, F., Turley, M.J., Khanam, T., Aktas, T., Ramirez, F., Gendrel, A.V., Wright, P.R., Videm, P., Backofen, R.*, et al.* (2014). MOF-associated complexes ensure stem cell identity and Xist repression. eLife *3*, e02024.

Choudhary, C., Kumar, C., Gnad, F., Nielsen, M.L., Rehman, M., Walther, T.C., Olsen, J.V., and Mann, M. (2009). Lysine acetylation targets protein complexes and co-regulates major cellular functions. Science *325*, 834-840.

Clark, D.J., and Kimura, T. (1990). Electrostatic mechanism of chromatin folding. Journal of molecular biology *211*, 883-896.

Conrad, T., Cavalli, F.M., Holz, H., Hallacli, E., Kind, J., Ilik, I., Vaquerizas, J.M., Luscombe, N.M., and Akhtar, A. (2012). The MOF chromobarrel domain controls genome-wide H4K16 acetylation and spreading of the MSL complex. Developmental cell *22*, 610-624.

Dawson, M.A., and Kouzarides, T. (2012). Cancer epigenetics: from mechanism to therapy. Cell *150*, 12-27.

Feller, C., Prestel, M., Hartmann, H., Straub, T., Soding, J., and Becker, P.B. (2012). The MOF-containing NSL complex associates globally with housekeeping genes, but activates only a defined subset. Nucleic acids research *40*, 1509-1522.

Filippakopoulos, P., Picaud, S., Mangos, M., Keates, T., Lambert, J.P., Barsyte-Lovejoy, D., Felletar, I., Volkmer, R., Muller, S., Pawson, T.*, et al.* (2012). Histone recognition and large-scale structural analysis of the human bromodomain family. Cell *149*, 214-231.

Fischle, W., Wang, Y., and Allis, C.D. (2003). Histone and chromatin cross-talk. Current opinion in cell biology *15*, 172-183.

Fuchs, S.M., Krajewski, K., Baker, R.W., Miller, V.L., and Strahl, B.D. (2011). Influence of combinatorial histone modifications on antibody and effector protein recognition. Current biology : CB *21*, 53-58.

Garcia, B.A., Mollah, S., Ueberheide, B.M., Busby, S.A., Muratore, T.L., Shabanowitz, J., and Hunt, D.F. (2007). Chemical derivatization of histones for facilitated analysis by mass spectrometry. Nature protocols *2*, 933-938.

Graff, J., and Tsai, L.H. (2013). Histone acetylation: molecular mnemonics on the chromatin. Nature reviews Neuroscience *14*, 97-111.

Gu, W., Szauter, P., and Lucchesi, J.C. (1998). Targeting of MOF, a putative histone acetyl transferase, to the X chromosome of Drosophila melanogaster. Developmental genetics *22*, 56-64.

Jin, Q., Yu, L.R., Wang, L., Zhang, Z., Kasper, L.H., Lee, J.E., Wang, C., Brindle, P.K., Dent, S.Y., and Ge, K. (2011). Distinct roles of GCN5/PCAF-mediated H3K9ac and CBP/p300-mediated H3K18/27ac in nuclear receptor transactivation. The EMBO journal *30*, 249-262.

Jung, H.R., Sidoli, S., Haldbo, S., Sprenger, R.R., Schwammle, V., Pasini, D., Helin, K., and Jensen, O.N. (2013). Precision Mapping of Coexisting Modifications in Histone H3 Tails from Embryonic Stem Cells by ETD-MS/MS. Analytical chemistry *85*, 8232-8239.

Kondo, S., and Perrimon, N. (2011). A genome-wide RNAi screen identifies core components of the G(2)-M DNA damage checkpoint. Science signaling *4*, rs1.

Kouzarides, T. (2007). Chromatin modifications and their function. Cell *128*, 693-705.

Kueh, A.J., Dixon, M.P., Voss, A.K., and Thomas, T. (2011). HBO1 is required for H3K14 acetylation and normal transcriptional activity during embryonic development. Molecular and cellular biology *31*, 845-860.
Lam, K.C., Muhlpfordt, F., Vaquerizas, J.M., Raja, S.J., Holz, H., Luscombe, N.M., Manke, T., and Akhtar, A. (2012). The NSL complex regulates housekeeping genes in Drosophila. PLoS genetics *8*, e1002736.
Lee, K.K., and Workman, J.L. (2007). Histone acetyltransferase complexes: one size doesn't fit all. Nature reviews Molecular cell biology *8*, 284-295.
Lin, S., Wein, S., Gonzales-Cope, M., Otte, G.L., Yuan, Z.F., Afjehi-Sadat, L., Maile, T., Berger, S.L., Rush, J., Lill, J.R.*, et al.* (2014). Stable Isotope labeled histone peptide library for histone post-translational modification and variant quantification by mass spectrometry. Molecular & cellular proteomics : MCP.
Marx, H., Lemeer, S., Schliep, J.E., Matheron, L., Mohammed, S., Cox, J., Mann, M., Heck, A.J., and Kuster, B. (2013). A large synthetic peptide and phosphopeptide reference library for mass spectrometry-based proteomics. Nature biotechnology *31*, 557-564.
Parthun, M.R. (2012). Histone acetyltransferase 1: More than just an enzyme? Biochimica et biophysica acta *1819*, 256-263.
Pesavento, J.J., Bullock, C.R., LeDuc, R.D., Mizzen, C.A., and Kelleher, N.L. (2008). Combinatorial modification of human histone H4 quantitated by two-dimensional liquid chromatography coupled with top down mass spectrometry. The Journal of biological chemistry *283*, 14927-14937.
Plazas-Mayorca, M.D., Bloom, J.S., Zeissler, U., Leroy, G., Young, N.L., DiMaggio, P.A., Krugylak, L., Schneider, R., and Garcia, B.A. (2010). Quantitative proteomics reveals direct and indirect alterations in the histone code following methyltransferase knockdown. Molecular bioSystems *6*, 1719-1729.
Prestel, M., Feller, C., and Becker, P.B. (2010a). Dosage compensation and the global re-balancing of aneuploid genomes. Genome biology *11*, 216.
Prestel, M., Feller, C., Straub, T., Mitlohner, H., and Becker, P.B. (2010b). The activation potential of MOF is constrained for dosage compensation. Molecular cell *38*, 815-826.
Rothbart, S.B., Lin, S., Britton, L.M., Krajewski, K., Keogh, M.C., Garcia, B.A., and Strahl, B.D. (2012). Poly-acetylated chromatin signatures are preferred epitopes for site-specific histone H4 acetyl antibodies. Scientific reports *2*, 489.
Ruthenburg, A.J., Li, H., Patel, D.J., and Allis, C.D. (2007). Multivalent engagement of chromatin modifications by linked binding modules. Nature reviews Molecular cell biology *8*, 983-994.
Schotta, G., Sengupta, R., Kubicek, S., Malin, S., Kauer, M., Callen, E., Celeste, A., Pagani, M., Opravil, S., De La Rosa-Velazquez, I.A.*, et al.* (2008). A chromatin-wide transition to H4K20 monomethylation impairs genome integrity and programmed DNA rearrangements in the mouse. Genes & development *22*, 2048-2061.
Sinha, I., Buchanan, L., Ronnerblad, M., Bonilla, C., Durand-Dubief, M., Shevchenko, A., Grunstein, M., Stewart, A.F., and Ekwall, K. (2010). Genome-wide mapping of histone modifications and mass spectrometry reveal H4 acetylation bias and H3K36 methylation at gene promoters in fission yeast. Epigenomics *2*, 377-393.
Smith, C.M., Gafken, P.R., Zhang, Z., Gottschling, D.E., Smith, J.B., and Smith, D.L. (2003). Mass spectrometric quantification of acetylation at specific lysines within the amino-terminal tail of histone H4. Analytical biochemistry *316*, 23-33.
Smith, E.R., Cayrou, C., Huang, R., Lane, W.S., Cote, J., and Lucchesi, J.C. (2005). A human protein complex homologous to the Drosophila MSL complex is responsible for the majority of histone H4 acetylation at lysine 16. Molecular and cellular biology *25*, 9175-9188.
Sterner, D.E., and Berger, S.L. (2000). Acetylation of histones and transcription-related factors. Microbiology and molecular biology reviews : MMBR *64*, 435-459.
Tan, M., Luo, H., Lee, S., Jin, F., Yang, J.S., Montellier, E., Buchou, T., Cheng, Z., Rousseaux, S., Rajagopal, N.*, et al.* (2011). Identification of 67 histone marks and histone lysine crotonylation as a new type of histone modification. Cell *146*, 1016-1028.
Vizcaino, J.A., Deutsch, E.W., Wang, R., Csordas, A., Reisinger, F., Rios, D., Dianes, J.A., Sun, Z., Farrah, T., Bandeira, N., et al. (2014). ProteomeXchange provides globally

coordinated proteomics data submission and dissemination. Nature biotechnology 32, 223-226.
Voss, A.K., and Thomas, T. (2009). MYST family histone acetyltransferases take center stage in stem cells and development. BioEssays : news and reviews in molecular, cellular and developmental biology *31*, 1050-1061.
Young, N.L., DiMaggio, P.A., Plazas-Mayorca, M.D., Baliban, R.C., Floudas, C.A., and Garcia, B.A. (2009). High throughput characterization of combinatorial histone codes. Molecular & cellular proteomics : MCP *8*, 2266-2284.
Zheng, Y., Thomas, P.M., and Kelleher, N.L. (2013). Measurement of acetylation turnover at distinct lysines in human histones identifies long-lived acetylation sites. Nature communications *4*, 2203.

FIGURE LEGENDS

Figure 1. Optimised liquid chromatography mass spectrometry (LC-MS) workflow for precise and accurate quantification of PTM motifs

(A) Overview of the LC-MS workflow. D3AA method exemplified for H3 PTM isoform with four highly abundant modifications: H3.K9me3K14acK23acK27me2. (1) Chemical acetylation by d6-acetic anhydride transfers a deuterated (d3)-acetyl group to free lysines. (2) The subsequent trypsin digestion yields peptides of intermediate size. (3) Lysine methylation induces characteristic shifts in retention time, which allows quantification only based on MS1 spectra. Shown are ion intensity traces of the parent ions from the H3.K9-R17 peptide. To aid visualisation, intensities among retention time segments are scaled on the intensity of the third segment: Original intensities of the first and second segments are 6.3 and 3.1 fold higher. (4) The positional isomers with permutations of the lysine acetylation sites (H3.K9ac and H3.K14ac) require successive quantification using MS1 (left) and MS2 (right).

(B) High precision quantification for 45 histone motifs in technical and biological replicate experiments. We determined the median coefficient of variations (CV) of 5.2% for three technical whole-workflow replicates using 2 million *Drosophila* KC cells (left), and CVs of 10.4% and 8.9% across five biological replicates for motifs that require successive MS1-MS2 or MS1-MS2-MS3 (centre, n=20) or MS1-only (right, n=25). The 45 histone motifs are shown in (D) and Table S3.

(C) LC-MS response correction factor improves accuracy for motifs containing lysine methylation sites. Synthetic peptides to acetylation and methylation modifications for H3.K9R17 peptide were individually chemically acetylated, trypsinised and measured by LC-MS. To derive the LC-MS response correction factor (right), raw values for the proteotypic peptide (left) were divided by raw values for the quantification tag (grey hexamer, centre) and signals for the H3.K9me1 peptide. Quantified synthetic peptides were obtained from JPT Peptide Technologies GmbH (Berlin). See Table S2 for full dataset.

(D) Abundance for histone PTM motifs after applying LC-MS response correction factor. Low (yellow), intermediate (orange) and high (red) abundance classes of histone acetylation motifs are indicated. Motifs containing no acetyl group are indicated in white. See Table S3 and SEP 1.3 for full dataset and variation estimates.

(E) Same as (D) for motifs where the LC-MS response correction factor had only intermediate confidence.

See Figures S1-S3 and Tables S1-S3.

Figure 2. Global and specific response to comprehensive perturbation of acetyltransferases

(A) Heat map displaying relative changes in abundance of 28 PTMs involving lysine acetylation in response to RNAi depletion of 23 KATs in KC cells. The first eight KATs are sorted according to the systematic listing by (Allis et al., 2007), the subsequent ones according to their sub-classes, including GCN5 related KATs (NATs) and N-terminal acetyltransferases (NAAs). Relative changes are normalised on control RNAi and log2 scaled. Only significant changes are shown ($p < 0.05$, two-sided unpaired t test). Color code of acetylation motifs is as introduced in Figure 1A.

(B) Relative reductions of acetylation at individual lysines upon RNAi as in (A) cumulating all motifs containing the corresponding lysine. This illustrates the best-case outcome of a conventional analysis with hypothetical antibodies recognising individual acetylated lysines with high specificity.

See Figures S5 and S6 and Tables S4-S6.

Figure 3. Most acetyltransferases have a narrow yet not absolute substrate specificity, which is modulated by the context of adjacent modifications

Statistical significance for all data in (A-F) was assessed with two-sided unpaired t test ($p < 0.05$) on log2 (target RNAi/ctr RNAi).

(A) Quantification example of the histone H4 acetylation motifs for HBO1 RNAi. Statistically significant gains (red) and losses (blue) are indicated. Error bars display SEM (n=8).

(B) Scheme visualising the interdependence of combinatorial H4 motifs. HBO1-depleted cells display a highly selective reduction (blue arrows) of two acetylation motifs. Blue arrows point to significantly changed motifs (two-sided unpaired t test, $p < 0.05$).

(C,D) Quantification example and scheme as in (A) and (B), showing that CBP depletion reduces most H4 motifs containing acetylated lysine 5 or 8 (n=7).

(E) Cumulative contributions of KATs, which significantly (two-sided unpaired t test, $p < 0.05$) contribute to H4.K5acK8ac and H4.K5acK12ac.

(F) Cumulative contributions from all KAT depletion experiments reveals functional redundancy and points to the contribution of deacetylases. Cumulative KAT contribution was calculated from the extent of motif reduction upon KAT depletion filtered for statistically significant decreases (two-sided unpaired t test, $p < 0.05$).

Figure 4. KDACs generally show broad substrate specificity, and RPD3 dominates H4 de-acetylation

(A) KDACs display broad substrate specificity. Heat map showing relative changes of acetylation motif abundance in response to KDAC depletions, normalised to control RNAi and log2 scaled. Only significant changes are shown ($p < 0.05$, two-sided unpaired t test on log2 (KDAC/ctr)). Color code of acetylation motifs is as introduced in Figure 1A.

(B) Global increase of histone H3 and H4 acetylation upon depletion of any HDAC and Sirtuin. Relative changes of total H3, H4 and combined H3 and H4 acetylation levels normalised to control RNAi are shown. Significance was assessed on log2 (KDAC/ctr) using two-sided unpaired t test ($p<0.05$). RNAi to RPD3 and HDAC6 cause stronger gains in acetylation on H4 compared to H3. Error bars indicate SEM (for $n>2$) or minimal and maximal value (for $n=2$). See Table S4 for number of replicates ($n = 2 - 6$).

Figure 5. KAT deprivation induces and redistributes acetylation, which balances global histone acetylation levels

(A) KAT depletion may lead to globally reduced (blue), balanced (grey), or increased (red) acetylation levels. Shown is the global histone acetylation score, calculated by summing up all acetylation motifs on H3 and H4, and normalised to control RNAi. Statistically significant changes were assessed using a two-sided unpaired t test ($p<0.05$) on log2 (KAT/ctr). Error bars indicate SEM (for $n>2$) or minimal and maximal value (for $n=2$). See Table S4 for number of replicates ($n = 2 - 5$).

(B) Selective re-distribution of acetyl groups to specific secondary sites. Total loss (blue) and gain (red) of individual histone acetylation motifs are shown for cells deprived of CBP and HBO1. The contributions of the major motif changes of H3 or H4 acetylation are shown (filtered for significant changes, $p< 0.05$, two-sided unpaired t test).

See Figure S6.

Figure 6. Depletion of KATs and KDACs triggers a systemic alteration of the histone methylome

(A) Reorganisation of histone methylation sites after KAT deprivation. Heat map displays relative changes after KAT RNAi normalised to control RNAi. Only significant changes are shown ($p < 0.05$, two-sided unpaired t test.). Dendrograms were generated by unsupervised

hierarchical clustering using the 'ward' algorithm on a Euclidean distance matrix. The H3.K27me2 and H3.K79me1 motifs did not change significantly in any KAT RNAi and therefore were not integrated in the heat map. Color code of methylation motifs is as introduced in Figure 1A.

(B-C) Comparative analysis of acetylation-only, methylation-only and mixed acetylation-methylation motifs facilitates prioritisation of putative KAT targets and identifies acetylation-methylation crosstalk. Significantly reduced (blue) and increased (red) motifs are indicated (two-sided t test, $p < 0.05$). Error bars indicate SEM (n=3 for KAT6, n=4 for HBO1).

Figure 7: X-chromosome dosage dosage compensation is accompanied by global redistribution of acetylation and methylation marks

(A) The MOF-containing MSL-DCC complex dominates the NSL complex for acetylation of H4.K16. Female KC or male S2 cells were depleted of MOF, MSL1 or NSL1, and the relative abundance of the indicated H4 acetylation (red box) was expressed relative to control cells that were treated with interfering RNAs directed against GST and GFP.

(B) Similar type of experiment as in (A), probing the effect of NSL1, MSL1 or MOF depletion on H3.K27ac levels.

(C) Global histone acetylation levels are similar between male S2 and female KC cells, but the distribution of individual sites differs. Cumulative bar plots summing up total levels of individual histone motifs.

(D) Similar experiment as in (A), revealing the re-distribution of acetyl groups upon MOF depletion in S2 cells.

(E) Similar experiment as in (A), revealing the re-distribution of methyl groups upon MOF depletion in S2 cells. Error bars in A, B, D and E indicate SEM (n=3 for NSL1 in S2 and Kc and MOF in S2; n=4 for MOF in Kc (for H3) and n=11 for MOF in Kc (on H4) and minimal/maximal values for MSL1 (n=2).

(F) Similar experiment as in (D), except that MOF was ablated in Hela cells.

(G) Similar experiment as in (E), except that MOF was ablated in Hela cells. Error bars in F and G represent SEM (n=4).

Statistical significance between control – target RNAi and S2 – KC are indicated by asterisks (two-sided t test, $p < 0.05$).

See Figure S4.

Figure 1

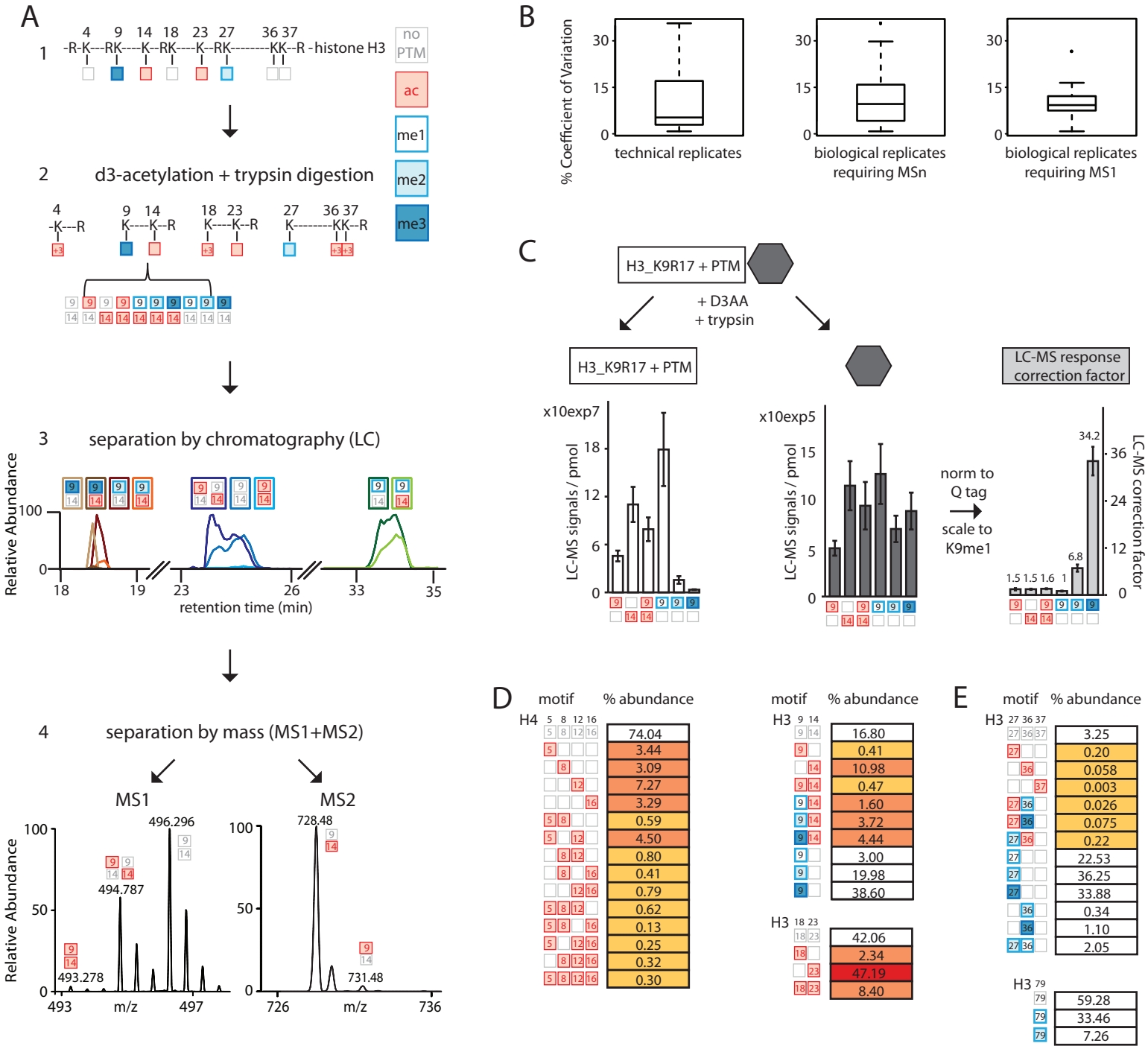

Figure 1

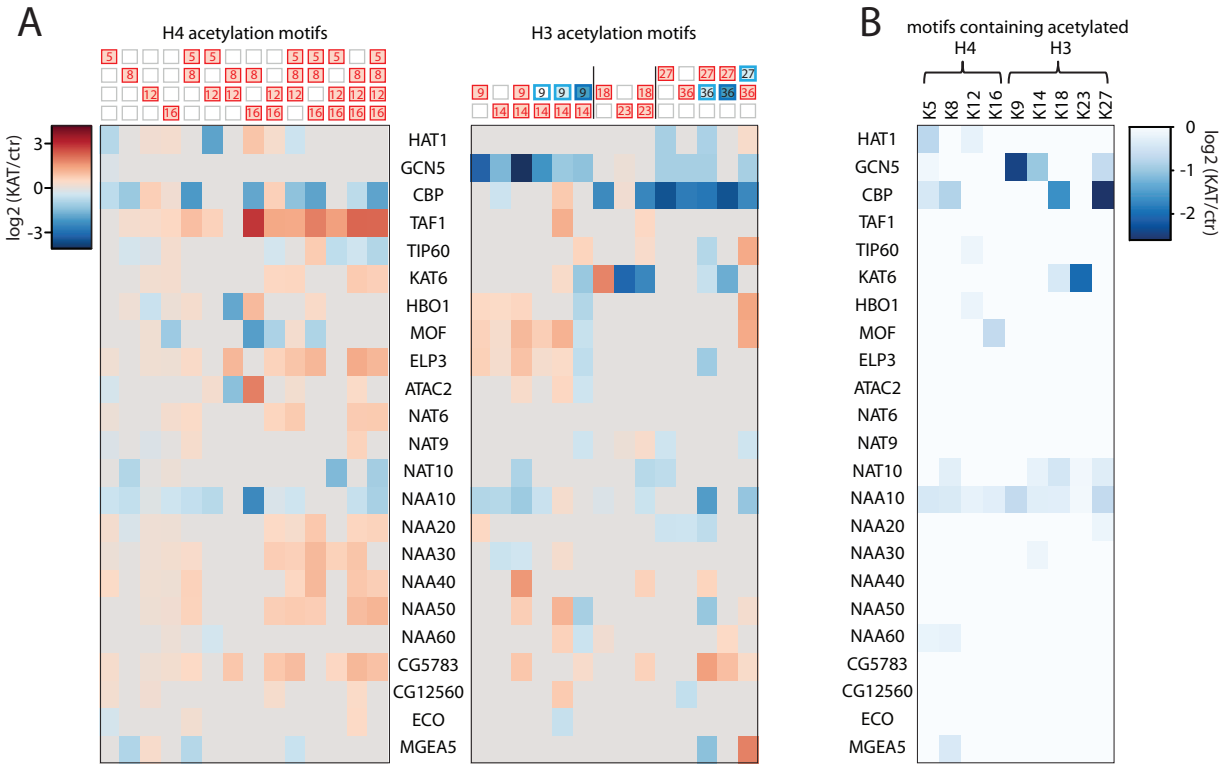
A
H4 acetylation motifs
H3 acetylation motifs
log2 (KAT/ctr)
3
0
-3
HAT1
GCN5
CBP
TAF1
TIP60
KAT6
HBO1
MOF
ELP3
ATAC2
NAT6
NAT9
NAT10
NAA10
NAA20
NAA30
NAA40
NAA50
NAA60
CG5783
CG12560
ECO
MGEA5
B
motifs containing acetylated
H4
H3
K5
K8
K12
K16
K9
K14
K18
K23
K27
0
-1
-2
log2 (KAT/ctr)

Figure 2

Figure 3

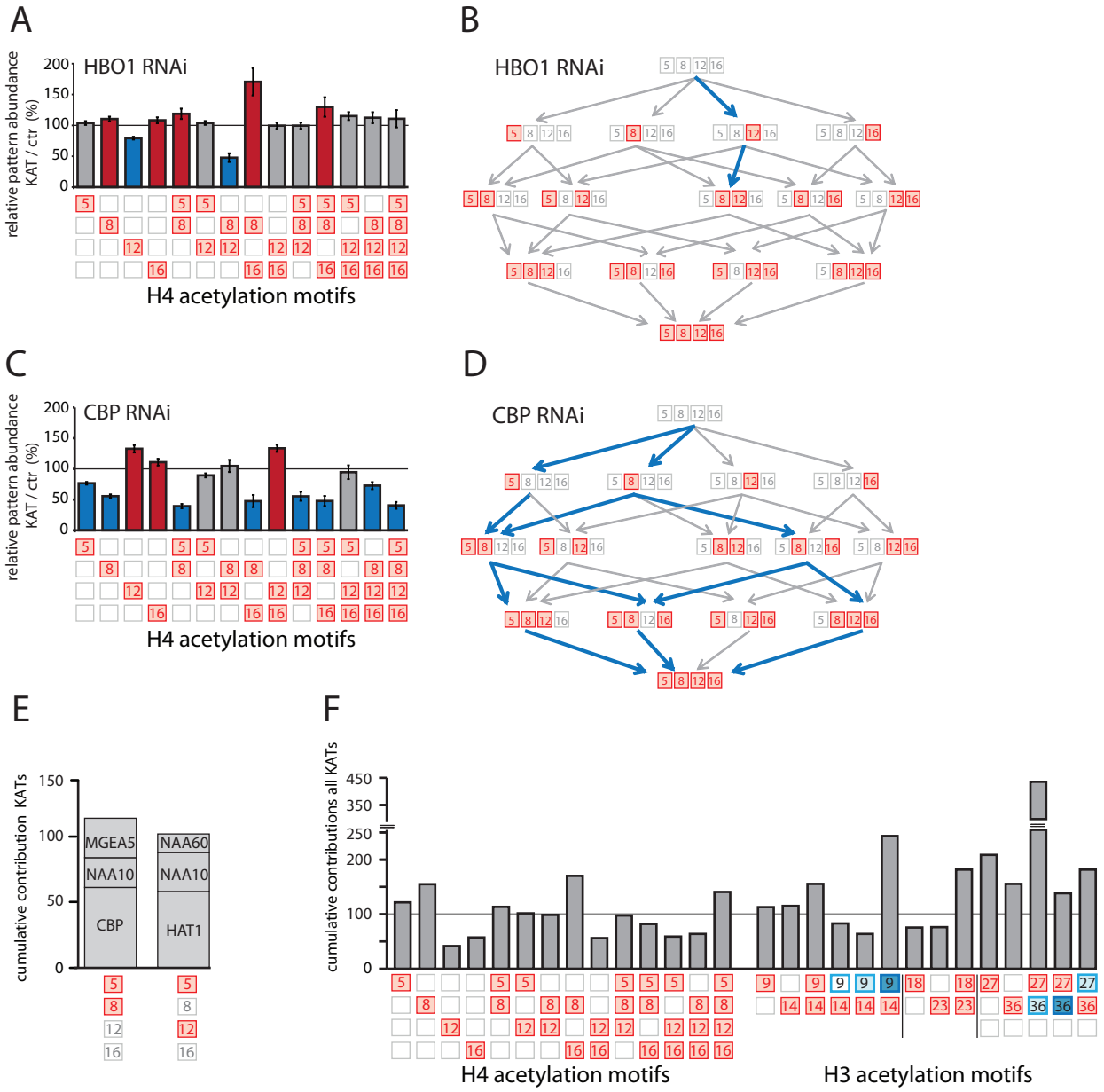

Figure 3

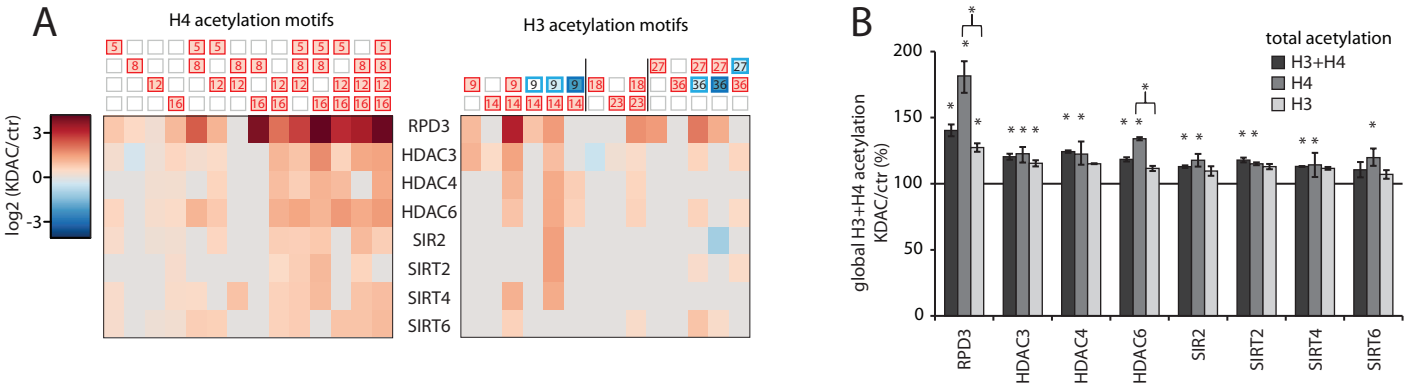
A
H4 acetylation motifs
H3 acetylation motifs
log2 (KDAC/ctr)
3
0
-3
RPD3
HDAC3
HDAC4
HDAC6
SIR2
SIRT2
SIRT4
SIRT6
B
total acetylation
H3+H4
H4
H3
global H3+H4 acetylation
KDAC/ctr (%)
200
150
100
50
0
RPD3
HDAC3
HDAC4
HDAC6
SIR2
SIRT2
SIRT4
SIRT6

Figure 5

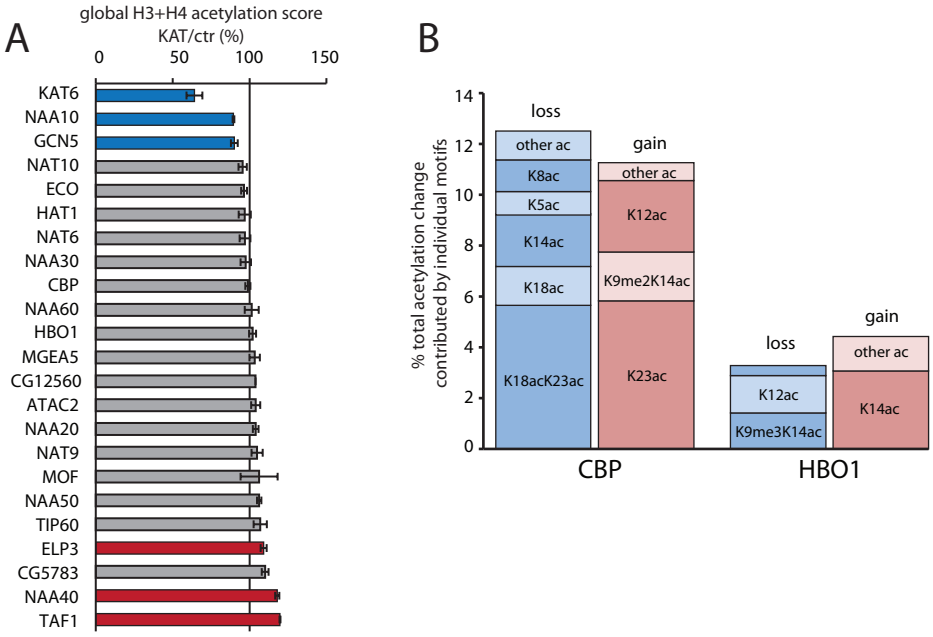

Figure 5

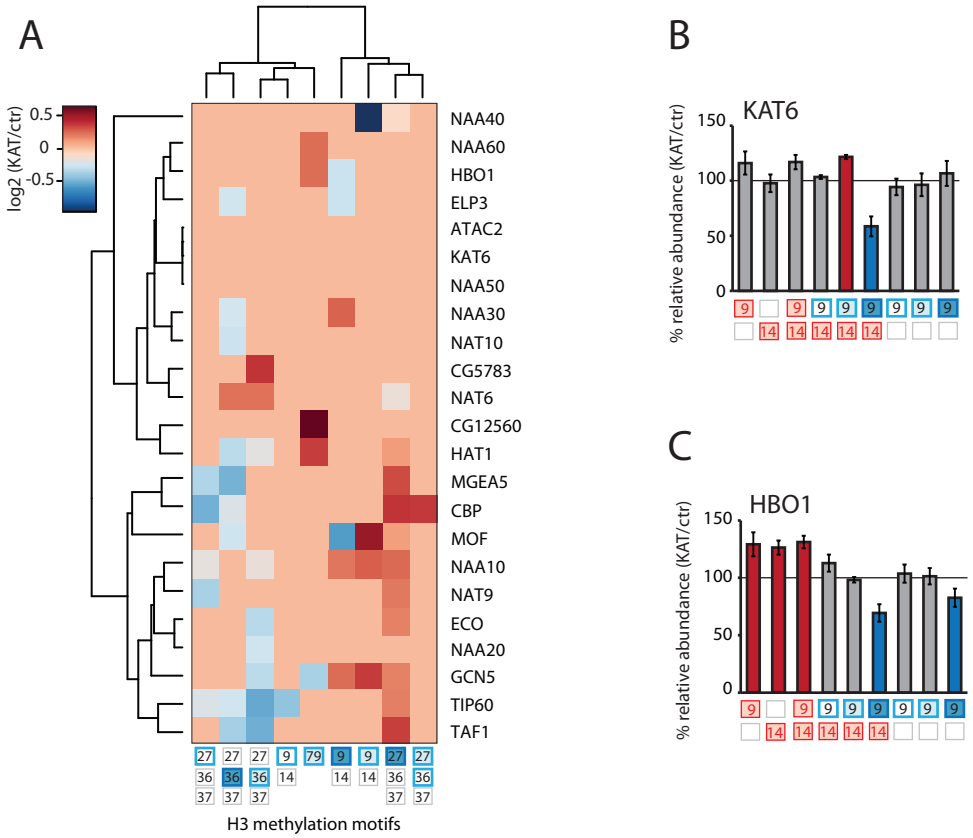
A
log2 (KAT/ctr)
0.5
0
-0.5
NAA40
NAA60
HBO1
ELP3
ATAC2
KAT6
NAA50
NAA30
NAT10
CG5783
NAT6
CG12560
HAT1
MGEA5
CBP
MOF
NAA10
NAT9
ECO
NAA20
GCN5
TIP60
TAF1
H3 methylation motifs
B
KAT6
% relative abundance (KAT/ctr)
150
100
50
0
C
HBO1
% relative abundance (KAT/ctr)
150
100
50
0

Figure 7

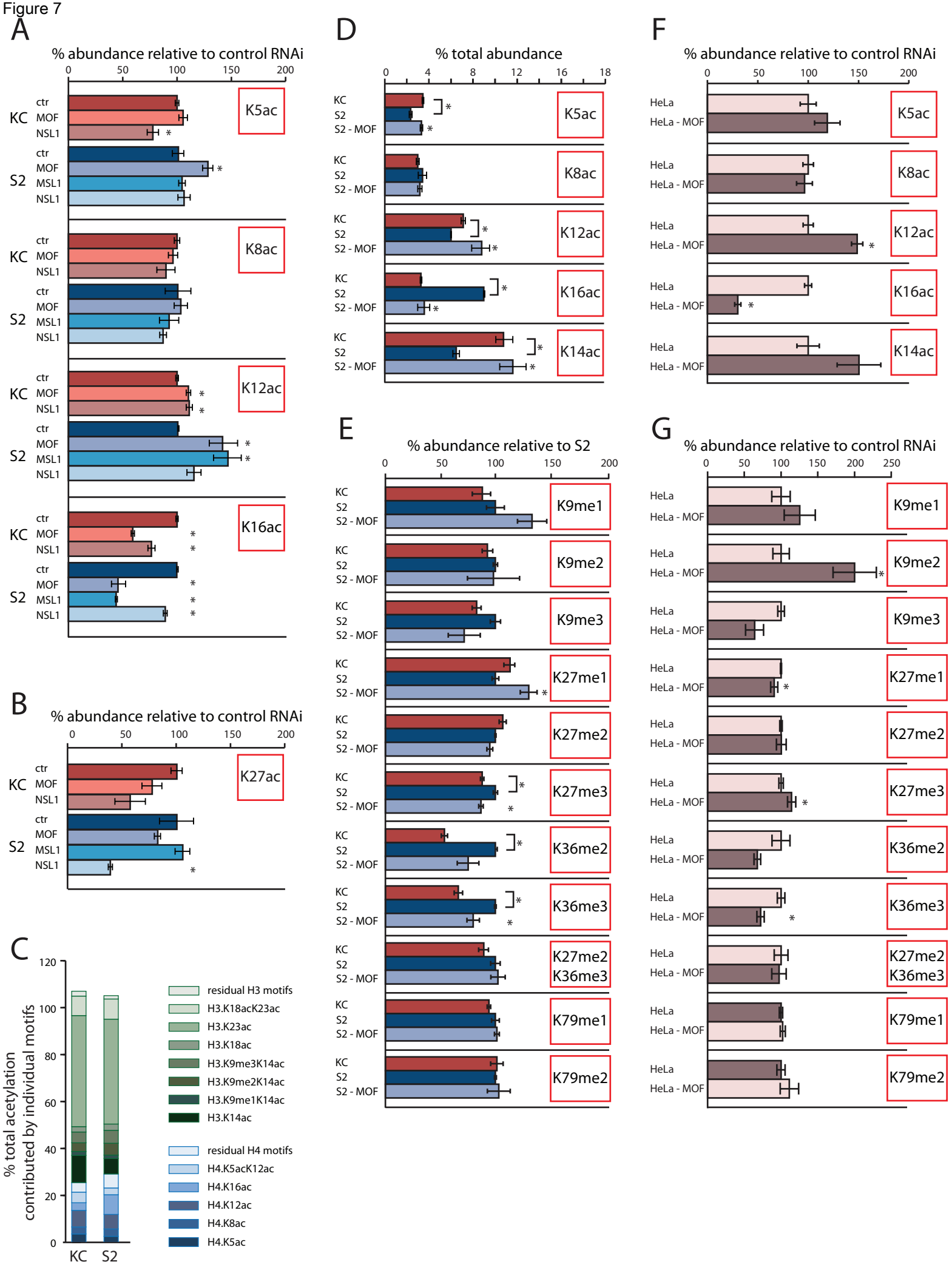

Figure 7

A

Schedule 1: 0 - 24 min

1) MS1. Range 270-505
2) MS2: 495.29 ± 0.8 @35; Range: 250-800

MS quantifier	No. scans
MS1_T3R8_K4me3	3
MS1_T3R8_K4me2	6
MS1_T3R8_noPTM	8
MS1_K9R17_K9me3	14
MS1_K9R17_K9me2	19
MS1_R19L22_K20me2	23
MS1_T3R8_K4me1	24
MS1_K9R17_noPTM	58
MS1_K9R17_1Ac	64
MS1_K9R17_2Ac	65
MS2_K9R17_y7_K14ac	62
MS2_K9R17_y7_K14noAc	57
MS1_R19L22_noPTM	31

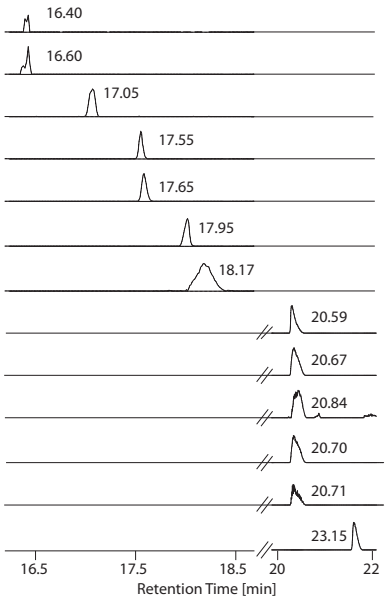

Schedule 2: 24.01 - 33 min

1) MS1. Range 270-550
2) MS2: 495.29 ± 0.8 @35; Range: 250-800
3) MS2: 522.97 ± 0.8 @35 + W. Act. ; Range: 300-800
4) MS2: 522.97 ± 0.8 @35 + W. Act. ; Range: 300-800

MS quantifier	No. scans
MS1_R19L22_K20me1	98

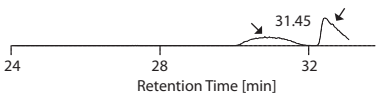

Schedule 3: 33.01- 47 min

1) MS1. Range 440-730
2) MS2: 723.44 ± 1.4 @35 -> MS3: 1215 ± 2 @45 + W.Act.; Range: 700-870
3) MS2: 537.83 ± 0.8 @35, Range: 250-800
4) MS2: 522.97 ± 0.8 @35 + W. Act. ; Range: 300-800
5) MS2: 724.95 ± 0.7 @35; Range: 250-1300
6) MS2: 723.44 ± 0.7 @35; Range: 250-1300
7) MS2: 723.44 ± 1.4 @35 -> MS3: 1215 ± 2 @45 + W.Act.; Range: 700-870
8) MS2: 721.92 ± 0.7 @35 + W.Act.; Range: 250-1300

MS quantifier	No. scans
MS1_K27R40_K27me3	10
MS1_K27R40_K27me2	15
MS1_K18R26_noPTM	13
MS1_K18R26_1Ac	14
MS1_K18R26_2Ac	14
MS2_K18R26_b2_K18ac	15
MS1_K27R40_noPTM	5
MS1_G4R17_noPTM	17
MS1_K27R40_K27me1	8

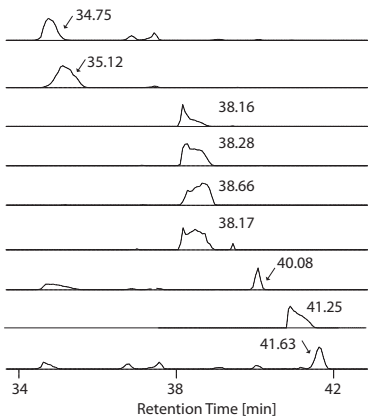

Schedule 4: 47.01- 79 min

1) MS1. Range 440-730

MS quantifier	No. scans
MS1_E73R83_K79me3	18
MS1_E73R83_K79me2	75
MS1_E73R83_noPTM	132
MS1_E73R83_K79me1	99

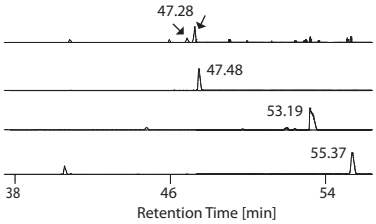

B

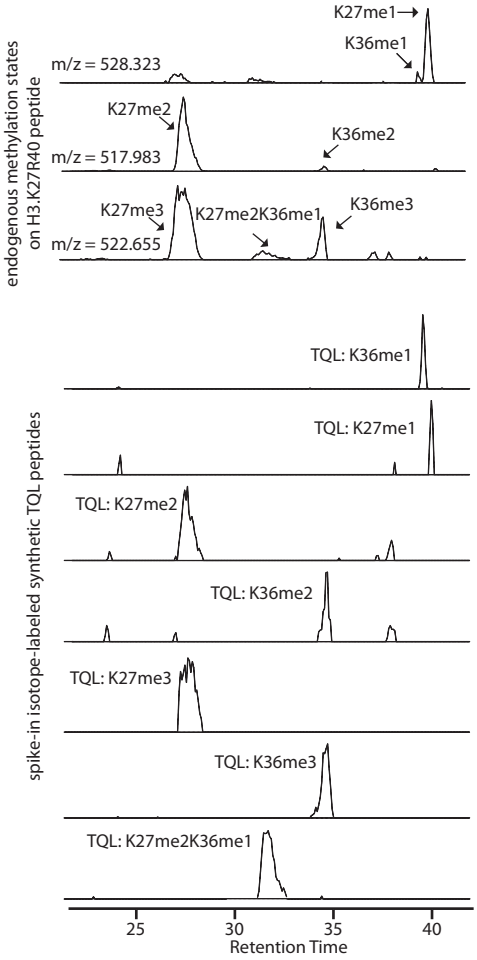

Supplementary Figure 1. Chromatographic separation of histone PTM motifs. Related to Figure 1.

(A) Example of time-scheduled targeted LC-MS experiment. MS recordings were subdivided into four schedules with selected MS1, MS2 and MS3 scan regimes. A selection of MS quantifier and the corresponding number of scans and ion traces are shown. Parameters for each scan schedule is shown above each panel of ion traces. Order within scan cycle, scan range (m/z) and the targeted mass for MS2 and MS3 are indicated. WideBand activation was applied for MS2 of H3.K27R40_1Ac (m/z = 522.97 ± 0.8) and H4.G4R17_3Ac (m/z=721.92 ± 0.7) and MS3 of H4.G4R17_2Ac_y12 (m/z=1215 ± 2). See Table S1 for all MS identifer. (B) Example of chromatographic separation of positional isomers from H3.K27R40 peptide. Three top panels are signals from endogenous histones and bottom seven panels are from experiments with synthetic TQL experiments. Masses corresponding to mono-methylation (m/z= 528.323) belongs to H3.K36me1 and H3.K27me1. Because mono-methylated lysines are still reactive, the resulting d3-proponyl (from endogenous mono-methyl + chemical d3-acetyl) at the N-terminus (H3.K27me1) is more hydrophobic and therefore elutes after H3.K36me1. Masses for di-methylation (m/z= 517.983) correspond to H3.K27me2 and H3.K36me2 and masses for three-methylation (m/z= 522.655) correspond to H3.K27me3, H3.K27me2K36me1 and H3.K36me3. Di-and tri-methylated lysines are not reactive to d6-acetic anhydride, which leaves the methyl-groups.
A more N-terminal methyl group (K27) elutes before a more central methyl group (K36).

Supplementary Figure 1

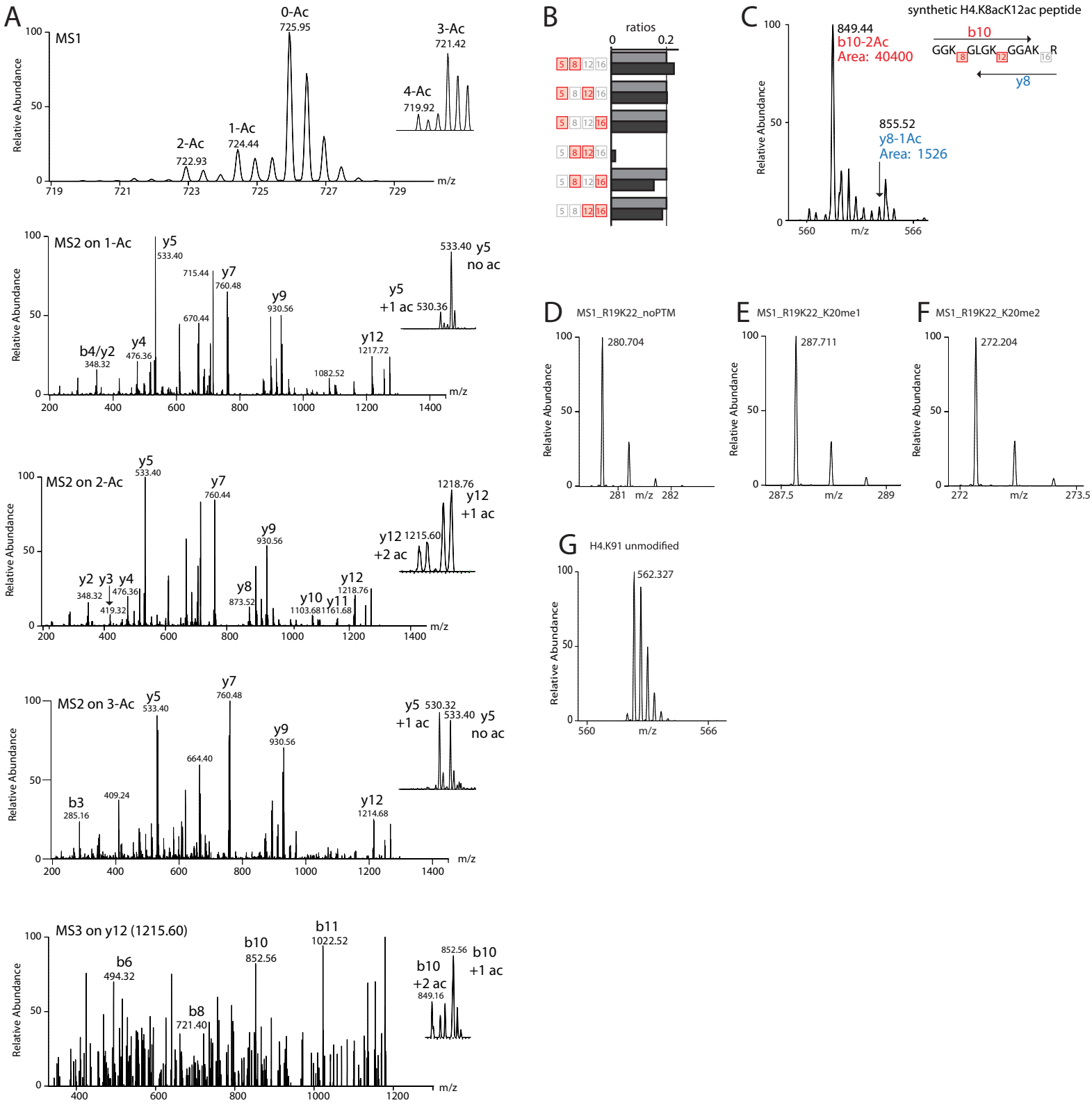

Supplementary Figure 2. MS1-MS2-MS3 analysis for the quantification of isobaric positional isomers to H4.G4-R17. Related to Figure 1.
(A) Spectra for MS1, MS2 and MS3 of the H4.G4-R17 peptide. Note the shift of the MS3 spectrum by -18 caused by the loss of a water molecule. MS3 signals were quantified with b10 fragment ion pairs. Inserts for selected spectra ranges are shown (right). (B) Successive MS1-MS2-MS3 based quantification recovers accurate ratios in experiments with defined concentrations of synthetic peptides. Shown is a representative experiment where five out of six di-acetylated H4 motifs were mixed in equal ratios, processed and quantified via successive MS1-MS2-MS3. Measured ratios (black) are close to expected ratios (grey). (C) The b10 MS3 fragment ions can be used for quantification. The theoretical masses of the b10 MS3 fragment ions (849.52 if di-acetylated and 852.52 if mono-acetylated) are close to the theoretical masses of the y8 ions (852.56 if di-acetylated and 855.56 if mono-acetylated) yet y8 is not observed or only with a minor signals. The MS3 spectrum from an H4.K8acK12ac peptide (gift of D. Schwarzer, Tübingen) generates a dominant b10-2Ac ion at 849.44 (Area: 40400) yet only a minor y8-1Ac signal at 852.52 (Area: 1526), demonstrating that any interference from y8 is minimal, and the b10 ion pair can be used for quantification. (D-F) MS1 spectrum for H4.K20_noPTM (D), H4.K20me1 (E) and H4.K20me2 (F). (G) MS1 spectrum shows triple-charged unmodified H4.K79-R92 peptide, yet no signals for acetylated isoform (theoretical mass of H4.K91ac: 561.220).

Supplementary Figure 2

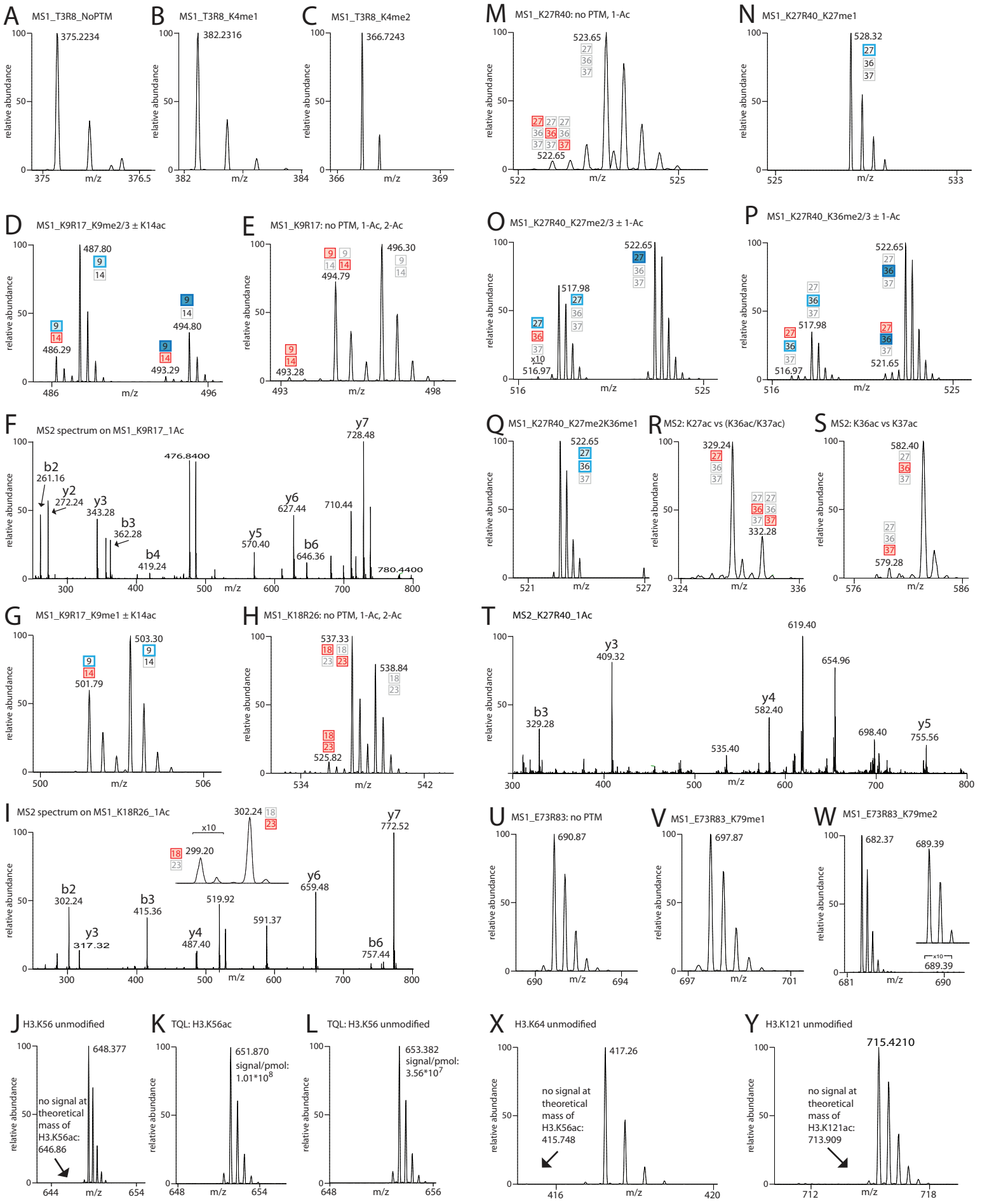

Supplementary Figure 3. MS1 and MS2 spectra for the quantification of H3 motifs. Related to Figure 1.

(A-C) MS1 spectra of H3.T3R-8 peptide, with no modification (A), H3.K4me1 (B) and H3.K4me2 (C). (D, E, G) MS1 spectra of H3.K9-R17 peptide, with H3.K9me2/3 ± K14ac (D), unmodified-, mono- and di-acetylated H3.K9-R17 peptides (E) and H3.K9me1 ± K14ac (G). (F) MS2 on mono-acetylated H3.K9-R17 is required to distinguish H3.K9ac and H3.K14ac. Insert to diagnostic y7 ion pairs is shown in Figure 1A (panel 4). (H) MS1 spectrum of H3.K18-R26 peptide. (I) MS2 on mono-acetylated H3.K18-R26 is required to distinguish H3.K18ac and H3.K23ac. Insert shows diagnostic b2 ion pair. Note that signals around 299.20 were 10x enhanced. (J-L) Spectra for H3.Y54-R63 peptide. Robust identification of unmodified H3.K56 but not acetylated H3.K56ac in histones from KC cells (J), although synthetic TQL peptides to H3.K56ac (K) produce at least similar signals to unmodified H3.K56 TQL peptides (L). (M-Q) MS1 spectra of H3.K27-R40 peptide, with unmodified- and mono-acetylated isoforms of the non-methylated peptide (M), H3.K27me1 (N), H3.K27me2 ± K36ac and H3.K27me3 (O) , H3.K36me2/3 ± K27ac (P), H3.K27me2K36me1 (Q). (R-T) MS2 on mono-acetylated H3.K27-R40 is required to distinguish H3.K27ac, H3.K36ac and H3.K37ac. Full MS2 spectrum (T) and diagnostic b3 (R) and y11 (S) ion pairs are shown. (U-W) MS1 spectra of H3.E73-R83 peptide, with unmodified (U), mono-methylated (V) and di-methylated (W) H3.K79. The insert in W shows minute signals for H3.K79me3 that elutes shortly before H3.K79me2. (Y, X) Robust signals for unmodified H3.K64 and H3.K121, but no signal for acetylated isoforms are detected.

Supplementary Figure 3

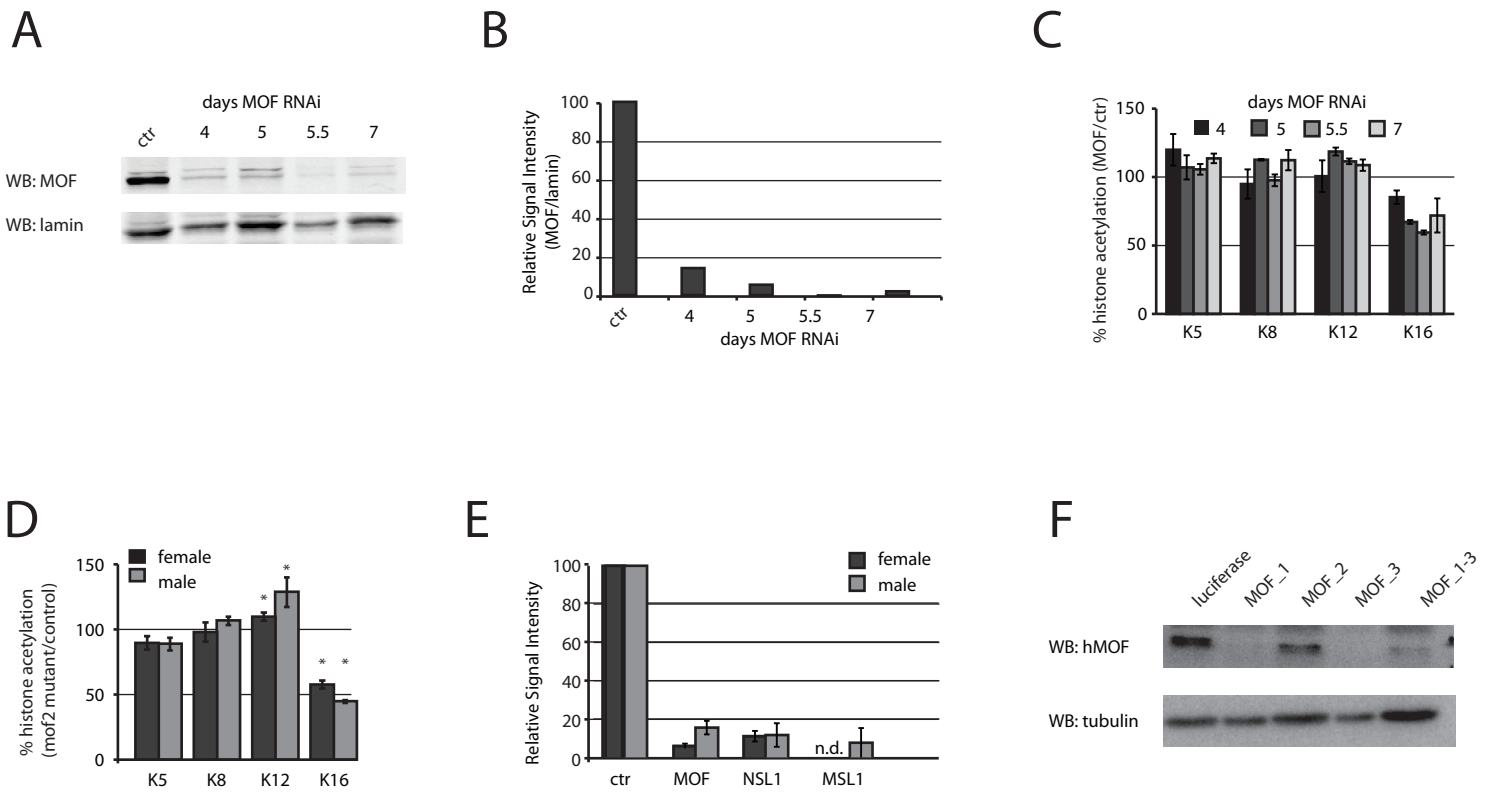

Supplementary Figure 4: Cells lacking MOF still retain substantial levels of H4.K16ac. Related to Figure 7.

(A) Representative example of quantitative immuno blot analysis probing for MOF protein levels during a four to seven days time-course RNAi experiment in female KC cells. Lamin protein levels served as a loading control. (B) Quantification of immuno blot signals from (A) using LI-COR (Biosciences). (C) Quantitative LC-MS analysis of mono-acetylated H4 motifs during a time-course RNAi experiment using two independent MOF RNAi constructs. Values were normalised to control RNAi. Error bars show maximum and minimum from two different RNAi constructs targeting MOF. (D) Quantitative LC-MS analysis of mono-acetylated H4 motifs in adult female (black) and 3rd instar larvae male (grey) mof2 mutants. Error bars represent SEM from 8 (female) and 3 (male) independent biological replicates. The increase of H4.K12ac and the decrease of H4.K16ac is statistically significant ($p < 0.05$ using unpaired two-sided t test). (E) Quantification of immuno blot analysis targeting MOF, NSL1 (NSL complex) and MSL1 (MSL-DCC complex) in KC and S2 cells after 5.5 days of RNAi using LI-COR (Biosciences). Error bars represent SEM of at least three biological replicates. (F) ECL-based immuno blot analysis of RNAi experiment to target hMOF in HeLa cells for 2.5 days using three different siRNA constructs (lanes 2-4), a pool of 3 MOF siRNA constructs (lane 5) and a luciferase sequence as control.

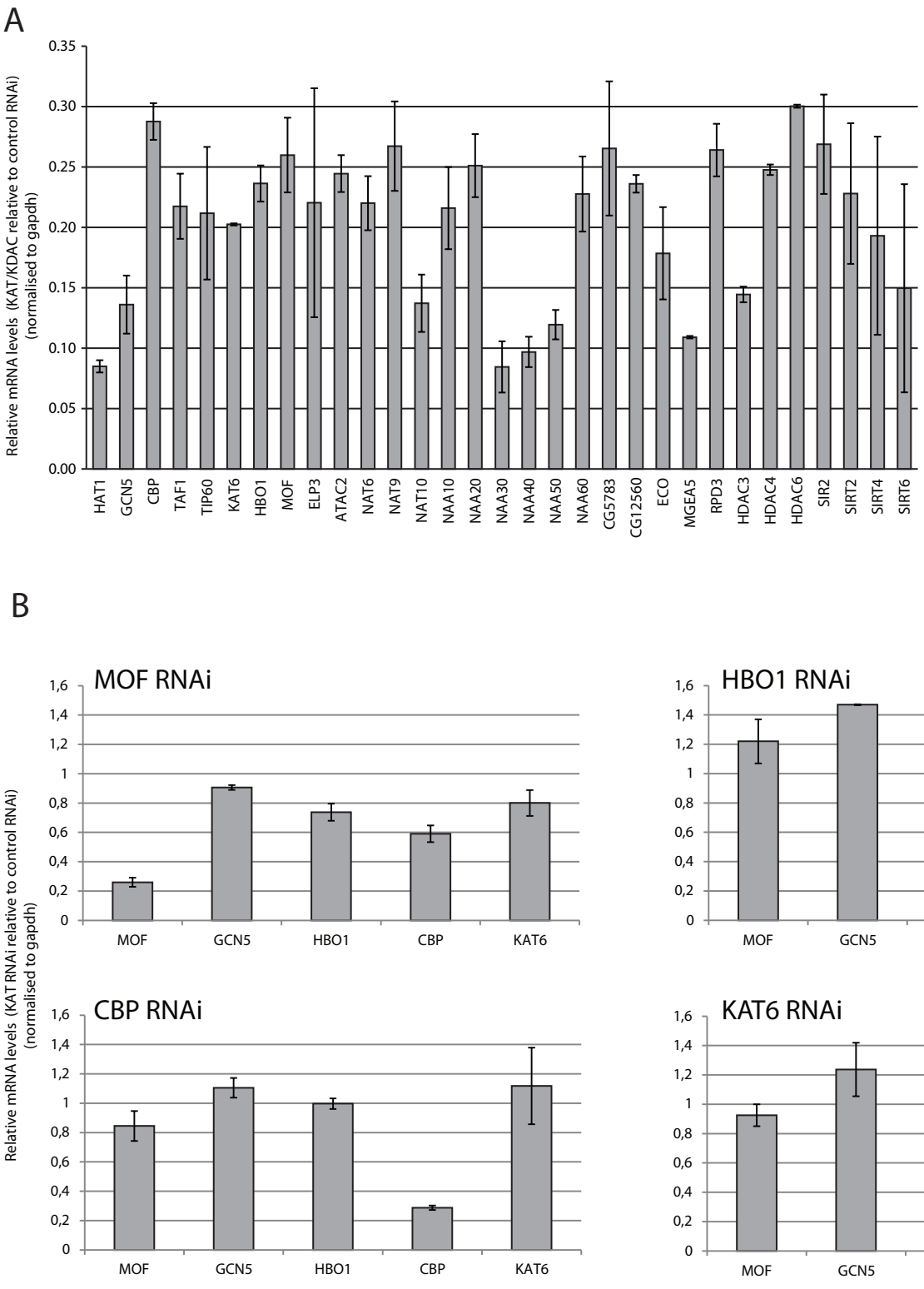

Supplementary Figure 5: Quantification of mRNA levels after KAT and KDAC RNAi. Related to Figure 2.

(A) Bar plot shows results of RT-qPCR measurements after RNAi of indicated KATs and KDACs, normalised to control RNAi and gapdh.

(B) Bar plots show results of RT-qPCR experiments after RNAi of MOF, HBO1, CBP and KAT6 and testing transcripts of MOF, GCN5, HBO1, CBP and KAT6 (normalised to control RNAi and gapdh). See Suppl. Note 5 for discussion.

for (A+B)) Error bars show minimal/maximal value from two different dsRNA RNAi constructs targeting the same KAT/KDAC gene (see Table S7 for RNAi and RT-PCR primers). In cases where only a single dsRNA RNAi construct was used, the replicate experiment was performed on another day.

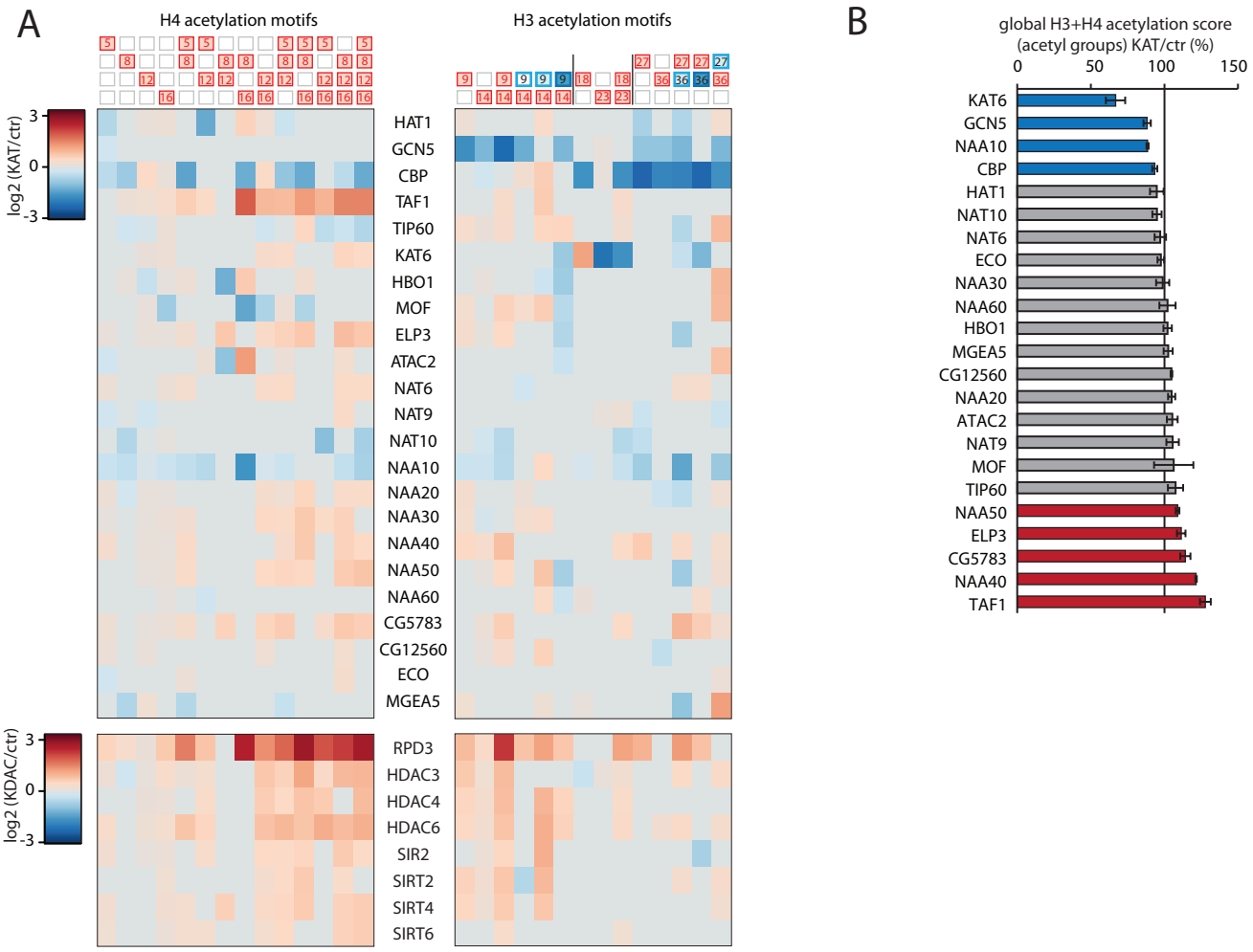

Supplementary Figure 6: Most relative changes of acetylation motifs in response to KAT and KDAC ablation are not affected when correcting for the LC-MS bias. Related to Figure 2.

(A) Heat map displaying relative changes in abundance of 28 histone acetylation motifs in response to KAT and KDAC ablation without appling the LC-MS response correction factor. Only significant changes are shown ($p < 0.05$, two-sided unpaired t test on log2 ratios).

(B) Global acetylation score calculated by counting acetyl groups instead of acetylation motifs. Here, the abundances of motifs with two acetyl-groups are multiplied by two, motifs with three acetyl-groups are multiplied by three etc.

Legends to Supplementary Tables

Table S1: List MS quantifier. Related to Figure 1.
Table S1 provides information on the MS identifier (theoretical m/z, charge state, sequence, retention time and XIC range).

Column Headers
- MS identifier: name of the MS identifier, containing MS scan type (MS1, MS2 or MS3); target peptide (first and last amino acid); PTM type and position (e.g. MS1_K9R17_K9me1: MS1 is sufficient to determine mono-methylation on lysine 9) and for MS2/MS3: y/b fragment ion assignment and m/z (e.g. MS2_K9R17_y7_K14ac_728: MS2 on K9R17 peptide that reports on y7 fragment ion (which has m/z of 728) is necessary to determine acetylation on lysine 14)
- theoretical m/z: theoretical mono-isotopic mass /charge
- charge state: charge state of MS identifier
- sequence: target peptide sequence
- retention time [min]: typical retention time in minutes
- XIC range [min/max]: mass/charge range used for chromatographic peak integration (minimal and maximal value). Note that for individual MS quantifier, the XIC range was adjusted to avoid integration of interfering peaks (e.g. MS1_K27R40_noPTM/1Ac: interfering peak at m/z = 523.79 at similar retention time)

Abbreviations
Kac (lysine acetylation), Kme1/2/3 (lysine mono/di/tri-methylation), noPTM: peptide without PTM, hence all lysines are chemically (d3)-acetylated

Table S2: LC-MS response correction factor. Related to Figure 1.
Table S2 provides the LC-MS response correction factor that has been applied to correct for the LC-MS bias.

Table S3: Histone PTM inventory for KC and S2 cells. Related to Figure 1.
Table S3 details the abundances of histone PTM motifs in KC and S2 cells and the technical and biological coefficients of variations (CV).

Notes:
- % CV for technical replicates (column 9) was derived from three whole-workflow replicates using approximate two million KC cells
- % CV for biological replicates (column 10) was derived from five biological replicates (using 'C' batch control RNAi dataset)
- KC dataset: average of six biological 'replicate batches' (batch A-E and technical whole-workflow replicate);
- S2 dataset: average of three biological replicates.
- For estimation of cellular copy number: see Supplemental Experimental Procedure Note (SEP) 1.3.

Table S4: Histone PTM inventory after KAT and KDAC RNAi in KC. Related to Figure 2.
Table S4 details the abundances of histone PTMs in response to KAT and KDAC RNAi. The table provides the integrated raw values, the relative abundances and the relative changes (target RNAi/control RNAi) to each individual LC-MS experiment as well as the summary statistics (means, p values derived from two-sided unpaired t test and FDR adjusted p values using the Benjamini and Hochberg method). The full legend is provided within the excel spreadsheet.

Table S5: List of *Drosophila melanogaster* KATs and KDACs. Related to Figure 2.
Table S5 lists the *Drosophila melanogaster* KATs and KDACs. Column 1 indicates the name used in this study. Column 2 indicates names according to new nomenclature to histone lysine acetyltransferases according to (Allis et al. 2007). Note that the name KAT14 was introduced after the publication of (Allis et al. 2007) by (Suganuma et al. 2008). Column 3 lists synonyms.

Table S6: List of primers used in this study. Related to Figure 2.
Table S6 lists the primer names and sequences used for RNAi and RT-qPCR.

SUPPLEMENTAL EXPERIMENTAL PROCEDURE

For a detailed discussion on the LC-MS workflow and follow-up discussion of the data, its generation and potential usage, please see the 'supplemental experimental procedure notes (SEP)' below the 'supplemental experimental procedures'.

Inventory for KATs and KDACs in *Drosophila melanogaster*

A list of putative KATs and KDACs was generated using public databases (FlyBase, ENSEMBL, HIstome (Histone Info Database – ACTREC), HomoloGene), primary research articles, reviews and cross-homology search using BLAST. Gene expression data was obtained from FlyBase (FlyAtlas, modENCODE tissue expression data, modENCODE temporal expression data, modENCODE cell line expression data).

Fly stocks, crosses and handling

Flies were raised on standard cornmeal/yeast medium at 18°C - 22°C. OregonR yw flies were used and considered wildtype. The *mof2* allele is described in (Gu et al., 1998) and the MOF(+) rescue transgene is published in (Prestel et al., 2010). Because we did not observe phenotypic effects for female *mof2/mof2* mutants under our culturing conditions, we maintained them as stable stocks and used directly 20 - 50 females either 1 day or 2 - 4 days old for histone PTM analysis. Hemizygous male *mof2* mutants are lethal at the larval stages, as described earlier (Gu et al., 1998), and therefore cannot be analysed at the adult stages of development. MOF(+)/CyO-GFP flies were generated and those males were crossed to homozygous female virgins *mof2/mof2;* +/+ to obtain *mof2*/y; +/CyO-GFP hemizygous male mutants. GFP fluorescence was used to sort male third-instar larval *mof2* mutants.

Cell line cultivation and RNA interference (RNAi)

Cultivation of KC and S2 cells and RNAi were carried out essentially as described before (Feller et al., 2012). Briefly, cells were grown in T75 or T175 flasks, washed in PBS and 1.5 million cells were transferred to each well of a 6-well plate. Cells were treated with 10 µg dsRNA for 60 min in 1 ml serum-free medium. After addition of 2 ml serum-containing medium (10% FCS), cells were incubated for 5.5 days before harvest. Primer sequences used for RNAi are described in Table S7. We used S2 cells of the 'L2-4' subtype, which were obtained from Dr. Patrick Heun (MPI Freiburg, Germany).

Human HeLa Kyoto cells were grown in DMEM medium containing 10% FCS and 1% penicillin/streptomycin at 37°C and 5% CO_2. Cells were transfected with siRNAs using oligofectamine (Invitrogen) according to the manufacturer's instructions. Growth medium was exchanged every day and cells were harvested for histone PTM analysis after 2.5 days. Primer sequences used for RNAi are described in Table S7 and have been published in (Taipale et al., 2005) and (Smith et al., 2005).

RT-qPCR experiments

Total RNA was prepared from KC cells using Trizol followed by the RNeasy Mini Kit (Qiagen) according to the manufacturer's protocol. 600 ng of total RNA was reverse transcribed using random primers and the SuperScript III kit (Life Technologies). Real-time PCR was

performed with a Roche 480 light cycler using the second derivative method for quantification. Primer sequences are described in Supplementary Table S7.

Immuno blotting

Quantification of immunoblots was performed using the LI-COR system (Biosciences). The lamin antibody was obtained from Harald Saumweber (Berlin) and the MOF antibody was described before (Prestel et al., 2010)

Extraction of histones from *Drosophila* tissue and cell lines and peptide processing

Third-instar male larvae were extensively washed in PBS, collected in microcentrifuge tubes, flash frozen in liquid nitrogen and stored at -80°C. Adult female flies were processed in the same manner but the washing step was omitted. Frozen tissue was homogenised in A1 buffer (15 mM HEPES pH 7.6, 60 mM KCl, 15 mM NaCl, 4 mM $MgCl_2$, 0.5% Triton, 0.5 mM DTT, protease inhibitor (Roche)), centrifuged and the pellet was resuspended in 0.2 M sulphuric acid. Acid extraction and all downstream steps were essentially done as with tissue culture cells, as follows.

KC and S2 cells were harvested and collected by centrifugation, washed once with PBS and pellets were flash frozen in liquid nitrogen and stored at -80°C. Frozen cell pellets were suspended in 0.2 M sulphuric acid and histones and other acid-soluble proteins were extracted overnight and precipitated with 26% TCA (trichloroacetic acid). After two to five washes with cold acetone, the histone pellet was resuspended in SDS-PAGE loading buffer. If necessary, pH was adjusted with 1 µl of 1 M Tris pH 8.0. Histones were separated by SDS-PAGE on 15% polyacrylamide gels, stained with Colloidal Blue Staining Kit (Invitrogen) and bands corresponding to histones H3 and H4 were excised from the gels. Recombinant histones were run as a size marker.

Gel pieces containing histones were washed twice with water, twice with 100 mM ammonium bicarbonate (ambic) and incubated in 50 mM ambic/50% acetonitrile for 3 times 10 min while shaking at 37°C for destaining. Gel pieces were successively dehydrated by incubating once with 100 mM ambic, once with 20 mM ambic and 3 times with acetonitrile. Histones were chemically acetylated with d6-deuterated acetic anhydride (99% D, Sigma) for 45 min at 37°C (pH was monitored to be pH 7-8). After acetylation, histones were washed 4 times with 100 mM ambic and thrice with acetonitrile followed by overnight trypsin (Promega) digestion at 37°C. Tryptic peptides were extracted twice with 70% acetonitrile/0.25% TFA and twice with acetonitrile, vacuum concentrated and resuspended in 0.1% TFA. Histone peptides were desalted using C18-StageTips (Rappsilber et al., 2003), eluted in 80% acetonitrile/0.25% TFA, vacuum concentrated, reconstituted in 0.1% TFA and stored at 4°C (short) or -20°C (long).

Processing of TQL spiketides and calculation of LC-MS response correction factor (LCF)

Purified, isotopically labelled and quantified SpikeTides TQL were purchased from JPT Peptide Technologies GmbH (Berlin). 1 nmol of peptides was resuspended in 80% 100 mM ambic, 18% acetonitrile and 2% DMSO, followed by two rounds of 1 min vortexing, 3 min sonication and 15 min shaking at 25°C. Chemical acetylation and trypsinisation was carried

out as described above. Each TQL proteotypic peptide was measured in replicates in different concentrations (1, 5 and 15 pmol) using the same LC parameters but acquiring MS1 scans only.

The LC-MS response correction factor (LCF) was calculated by dividing the raw MS signals for the proteotypic peptide per pmol by the raw MS signals for the Q tag which was followed by scaling to the motif that has the highest signal among all motifs for a given peptide. We experienced technical problems for individual motifs from the H3.K27-R40 and H3.E73-R83 synthetic peptides and therefore can only report LCFs with moderate confidence for those motifs.

LC-MS workflow and peak integration

Tryptic peptides were injected in two different HPLC systems from Dionex depending on the batch: Samples from replicate batch 'A' were separated on an Ultimate and replicate batches 'B' to 'E' were separated on an Ultimate 3000 RSLCnano. Peptides were separated with a gradient from 5-60% acetonitrile in 0.1% formic acid over 40 min at 300 nl/min on a C18 analytical column (75 µm i.d. ×15 cm, packed in-house with Reprosil Pur C18 AQ 2.4 µm; Doctor Maisch). The effluent from the HPLC was directly electrosprayed into an LTQ-Orbitrap Classic mass spectrometer (Thermo Fisher Scientific). MS was operated in a targeted setup (see Suppl. Note 1). Typical MS conditions were spray voltage, 1.5 kV; no sheath and auxiliary gas flow; heated capillary temperature, 200°C; MS1 resolution of 7500 (at 400 m/z); normalised collision-induced dissociation energy 35% (MS2) and 45% (MS3); activation q = 0.25; and activation time = 30 ms.

LC-MS data was quantified using the Xcalibur software package (Thermo Fisher Scientific, version 2.2) based on the area of the peak from the extracted ion chromatogram. A processing method was built using the Xcalibur Processing Setup including the mass-to-charge range and the expected retention time (see Table S1). Further parameters were: peak detection: Genesis; trace: mass range; smoothing points: 3, S/N threshold: 0.5. The identities of the MS quantifiers were verified by MS2 spectra of the natural occurring forms and their corresponding synthetic peptides (JPT Berlin). All chromatograms were manually verified in Quan Browser and re-integrated where necessary. Typically, this involves baseline adjustment and adjustments to integrate the identical retention time across the d0/d3 pair (i. e. endogenous vs. chemical acetylation). Peak integration was optimised to yield the maximal co-eluting chromatogram of the d3/d0 pair. The spectra from suspicious chromatograms (e.g. if peaks with similar m/z were eluting close-by) were manually inspected, and, if necessary, m/z integration range was adjusted (if possible) or MS quantifier were excluded (see Suppl. Note 3).

Data analysis and statistical analysis

After peak integration, the data was exported into an Excel spread sheet and data summarisation and statistical analysis was performed in Excel and R. The relative abundance was calculated according to the formulas provided in Table S2. Each sample was normalised to control RNAi samples within the same biological replicate batch (for details and justification: see Suppl. Note 3) and ratios were log2 scaled. We applied a two-sided unpaired t test over the log2 ratios of relative changes from all target RNAi samples (e.g. HAT1) for a specific motif (e.g. H4.K5acK12ac) relative to all control RNAi samples within the

same replicate batch. Because we considered the purpose of this study in the discovery of changed histone motif abundances upon KAT and KDAC RNAi and we expected only moderate differences, we did not apply a conservative filter by adjusting the p--values by their FDRs. Nevertheless, for convenience of the individual reader, Table S5 provides all MS raw signals, relative and total abundance values to all RNAi samples as well as summarised tables, which report on the mean changes of every KAT/KDAC RNAi (unfiltered) and raw and adjusted p values (two-sided unpaired t test, p values were adjusted per KAT/KDAC RNAi across all motifs according to Benjamini and Hochberg; p-value adjustment was performed in R). This table might be used to discover a potential change of a histone motif upon an individual KAT knockdown and to evaluate its significance considering the number of replicates and technical and biological variation.

Calculations to derive motif abundance from MS quantifier.

Motifs at histone H4

$$\text{H4.G4R17\_noPTM} = \frac{\text{MS1\_G4R17\_noPTM}}{sum(\text{MS1\_G4R17\_noPTM}, \text{MS1\_G4R17\_1Ac}, \text{MS1\_G4R17\_2Ac} \text{MS1\_G4R17\_3Ac} \text{MS1\_G4R17\_4Ac})}$$

$$\text{H4.K5ac} = \frac{\text{MS1\_G4R17\_1Ac}}{sum(\text{MS1\_G4R17\_noPTM}, \text{MS1\_G4R17\_1Ac}, \text{MS1\_G4R17\_2Ac} \text{MS1\_G4R17\_3Ac} \text{MS1\_G4R17\_4Ac})} * \left(1 - \frac{\text{MS2\_G4R17\_1Ac\_y12\_K16K12K8.1Ac\_1217}}{sum(\text{MS2\_G4R17\_1Ac\_y12\_K16K12K8.1Ac\_1217}, \text{MS2\_G4R17\_1Ac\_y12\_K16K12K8.0Ac\_1220})}\right)$$

$$\text{H4.K8ac} = \frac{\text{MS1\_G4R17\_1Ac}}{sum(\text{MS1\_G4R17\_noPTM}, \text{MS1\_G4R17\_1Ac}, \text{MS1\_G4R17\_2Ac} \text{MS1\_G4R17\_3Ac} \text{MS1\_G4R17\_4Ac})} *$$

$$\left(\frac{\text{MS2\_G4R17\_1Ac\_y12\_K16K12K8.1Ac\_1217}}{sum(\text{MS2\_G4R17\_1Ac\_y12\_K16K12K8.1Ac\_1217}, \text{MS2\_G4R17\_1Ac\_y12\_K16K12K8.0Ac\_1220})} - \frac{\text{MS2\_G4R17\_1Ac\_y7\_K16K12.1Ac\_760}}{sum(\text{MS2\_G4R17\_1Ac\_y7\_K16K12.1Ac\_760}, \text{MS2\_G4R17\_1Ac\_y7\_K16K12.0Ac\_763})}\right)$$

$$\text{H4.K12ac} = \frac{\text{MS1\_G4R17\_1Ac}}{sum(\text{MS1\_G4R17\_noPTM}, \text{MS1\_G4R17\_1Ac}, \text{MS1\_G4R17\_2Ac} \text{MS1\_G4R17\_3Ac} \text{MS1\_G4R17\_4Ac})} *$$

$$\left(\frac{\text{MS2\_G4R17\_1Ac\_y7\_K16K12.1Ac\_760}}{sum(\text{MS2\_G4R17\_1Ac\_y7\_K16K12.1Ac\_760}, \text{MS2\_G4R17\_1Ac\_y7\_K16K12.0Ac\_763})} - \frac{\text{MS2\_G4R17\_1Ac\_y5\_K16ac\_530}}{sum(\text{MS2\_G4R17\_1Ac\_y5\_K16ac\_530}, \text{MS2\_G4R17\_1Ac\_y5\_K16NoAc\_533})}\right)$$

$$\text{H4.K16ac} = \frac{\text{MS1\_G4R17\_1Ac}}{sum(\text{MS1\_G4R17\_noPTM}, \text{MS1\_G4R17\_1Ac}, \text{MS1\_G4R17\_2Ac} \text{MS1\_G4R17\_3Ac} \text{MS1\_G4R17\_4Ac})} * \frac{\text{MS2\_G4R17\_1Ac\_y5\_K16ac\_530}}{sum(\text{MS2\_G4R17\_1Ac\_y5\_K16ac\_530}, \text{MS2\_G4R17\_1Ac\_y5\_K16NoAc\_533})}$$

$$\text{H4.K5acK8ac} = \frac{\text{MS1\_G4R17\_2Ac}}{sum(\text{MS1\_G4R17\_noPTM}, \text{MS1\_G4R17\_1Ac}, \text{MS1\_G4R17\_2Ac} \text{MS1\_G4R17\_3Ac} \text{MS1\_G4R17\_4Ac})} * \frac{\text{MS2\_G4R17\_2Ac\_y7\_K16K12.0Ac\_763}}{sum(\text{MS2\_G4R17\_2Ac\_y7\_K16K12.0Ac\_763}, \text{MS2\_G4R17\_2Ac\_y7\_K16K12.1Ac\_760}, \text{MS2\_G4R17\_2Ac\_y7\_K16K12.2Ac\_757})}$$

$$\text{H4.K5acK12ac} = \frac{\text{MS1}_{\text{-G4R17-2Ac}}}{sum(\text{MS1}_{\text{-G4R17-noPTM}}, \text{MS1}_{\text{-G4R17-1Ac}}, \text{MS1}_{\text{-G4R17-2Ac}} \text{MS1}_{\text{-G4R17-3Ac}} \text{MS1}_{\text{-G4R17-4Ac}})} *$$

$$((1 - \frac{\text{MS3}_{\text{-G6R17-2Ac-b10-1Ac-867}}}{sum(\text{MS3}_{\text{-G6R17-2Ac-b10-1Ac-867}}, \text{MS3}_{\text{-G6R17-2Ac-b10-0Ac-870}})} * \frac{\text{MS2}_{\text{-G4R17-2Ac-y12-K16K12K8.2Ac-1214}}}{sum(\text{MS2}_{\text{-G4R17-2Ac-y12-K16K12K8.2Ac-1214}}, \text{MS2}_{\text{-G4R17-2Ac-y12-K16K12K8.1Ac-1217}})} -$$

$$\frac{\text{MS2}_{\text{-G4R17-2Ac-y5-K16ac-530}}}{sum(\text{MS2}_{\text{-G4R17-2Ac-y5-K16ac-530}}, \text{MS2}_{\text{-G4R17-2Ac-y5-K16NoAc-533}})} - \frac{\text{MS2}_{\text{-G4R17-2Ac-y7-K16K12.0Ac-763}}}{sum(\text{MS2}_{\text{-G4R17-2Ac-y7-K16K12.0Ac-763}}, \text{MS2}_{\text{-G4R17-2Ac-y7-K16K12.1Ac-760}}, \text{MS2}_{\text{-G4R17-2Ac-y7-K16K12.2Ac-757}})})$$

$$\text{H4.K5acK16ac} = \frac{\text{MS1}_{\text{-G4R17-2Ac}}}{sum(\text{MS1}_{\text{-G4R17-noPTM}}, \text{MS1}_{\text{-G4R17-1Ac}}, \text{MS1}_{\text{-G4R17-2Ac}} \text{MS1}_{\text{-G4R17-3Ac}} \text{MS1}_{\text{-G4R17-4Ac}})} *((\frac{\text{MS2}_{\text{-G4R17-2Ac-y12-K16K12K8.2Ac-1214}}}{sum(\text{MS2}_{\text{-G4R17-2Ac-y12-K16K12K8.2Ac-1214}}, \text{MS2}_{\text{-G4R17-2Ac-y12-K16K12K8.1Ac-1217}})} *$$

$$(\frac{\text{MS3}_{\text{-G6R17-2Ac-b10-1Ac-867}}}{sum(\text{MS3}_{\text{-G6R17-2Ac-b10-1Ac-867}}, \text{MS3}_{\text{-G6R17-2Ac-b10-0Ac-870}})} -1) + \frac{\text{MS2}_{\text{-G4R17-2Ac-y5-K16ac-530}}}{sum(\text{MS2}_{\text{-G4R17-2Ac-y5-K16ac-530}}, \text{MS2}_{\text{-G4R17-2Ac-y5-K16NoAc-533}})}))$$

$$\text{H4.K8acK12ac} = \frac{\text{MS1}_{\text{-G4R17-2Ac}}}{sum(\text{MS1}_{\text{-G4R17-noPTM}}, \text{MS1}_{\text{-G4R17-1Ac}}, \text{MS1}_{\text{-G4R17-2Ac}} \text{MS1}_{\text{-G4R17-3Ac}} \text{MS1}_{\text{-G4R17-4Ac}})} *$$

$$\frac{\text{MS3}_{\text{-G6R17-2Ac-b10-1Ac-867}}}{sum(\text{MS3}_{\text{-G6R17-2Ac-b10-1Ac-867}}, \text{MS3}_{\text{-G6R17-2Ac-b10-0Ac-870}})} * \frac{\text{MS2}_{\text{-G4R17-2Ac-y12-K16K12K8.2Ac-1214}}}{sum(\text{MS2}_{\text{-G4R17-2Ac-y12-K16K12K8.2Ac-1214}}, \text{MS2}_{\text{-G4R17-2Ac-y12-K16K12K8.1Ac-1217}})}$$

$$\text{H4.K8acK16ac} = \frac{\text{MS1}_{\text{-G4R17-2Ac}}}{sum(\text{MS1}_{\text{-G4R17-noPTM}}, \text{MS1}_{\text{-G4R17-1Ac}}, \text{MS1}_{\text{-G4R17-2Ac}} \text{MS1}_{\text{-G4R17-3Ac}} \text{MS1}_{\text{-G4R17-4Ac}})} * ((\frac{\text{MS2}_{\text{-G4R17-2Ac-y12-K16K12K8.2Ac-1214}}}{sum(\text{MS2}_{\text{-G4R17-2Ac-y12-K16K12K8.2Ac-1214}}, \text{MS2}_{\text{-G4R17-2Ac-y12-K16K12K8.1Ac-1217}})} *$$

$$(1 - -\frac{\text{MS3}_{\text{-G6R17-2Ac-b10-1Ac-867}}}{sum(\text{MS3}_{\text{-G6R17-2Ac-b10-1Ac-867}}, \text{MS3}_{\text{-G6R17-2Ac-b10-0Ac-870}})} - \frac{\text{MS2}_{\text{-G4R17-2Ac-y7-K16K12.2Ac-757}}}{sum(\text{MS2}_{\text{-G4R17-2Ac-y7-K16K12.0Ac-763}}, \text{MS2}_{\text{-G4R17-2Ac-y7-K16K12.1Ac-760}}, \text{MS2}_{\text{-G4R17-2Ac-y7-K16K12.2Ac-757}})}))$$

$$\text{H4.K12acK16ac} = \frac{\text{MS1}_{\text{-G4R17-2Ac}}}{sum(\text{MS1}_{\text{-G4R17-noPTM}}, \text{MS1}_{\text{-G4R17-1Ac}}, \text{MS1}_{\text{-G4R17-2Ac}} \text{MS1}_{\text{-G4R17-3Ac}} \text{MS1}_{\text{-G4R17-4Ac}})} *$$

$$\frac{\text{MS2}_{\text{-G4R17-2Ac-y7-K16K12.2Ac-757}}}{sum(\text{MS2}_{\text{-G4R17-2Ac-y7-K16K12.0Ac-763}}, \text{MS2}_{\text{-G4R17-2Ac-y7-K16K12.1Ac-760}}, \text{MS2}_{\text{-G4R17-2Ac-y7-K16K12.2Ac-757}})}$$

$$\text{H4.K5acK8acK12ac} = \frac{\text{MS1}_{\text{G4R17}_{\text{3Ac}}}}{sum(\text{MS1}_{\text{G4R17}_{\text{noPTM}}}, \text{MS1}_{\text{G4R17}_{\text{1Ac}}}, \text{MS1}_{\text{G4R17}_{\text{2Ac}}} \text{MS1}_{\text{G4R17}_{\text{3Ac}}} \text{MS1}_{\text{G4R17}_{\text{4Ac}}})} * \left(1 - \frac{\text{MS2}_{\text{G4R17}_{\text{3Ac}_{\text{y5\_K16ac\_530}}}}}{sum(\text{MS2}_{\text{G4R17}_{\text{3Ac}_{\text{y5\_K16ac\_530}}}}, \text{MS2}_{\text{G4R17}_{\text{3Ac}_{\text{y5\_K16NoAc\_533}}}})}\right)$$

$$\text{H4.K5acK8acK16ac} = \frac{\text{MS1}_{\text{G4R17}_{\text{3Ac}}}}{sum(\text{MS1}_{\text{G4R17}_{\text{noPTM}}}, \text{MS1}_{\text{G4R17}_{\text{1Ac}}}, \text{MS1}_{\text{G4R17}_{\text{2Ac}}} \text{MS1}_{\text{G4R17}_{\text{3Ac}}} \text{MS1}_{\text{G4R17}_{\text{4Ac}}})} *$$

$$\left(\frac{\text{MS2}_{\text{G4R17}_{\text{3Ac}_{\text{y5\_K16ac\_530}}}}}{sum(\text{MS2}_{\text{G4R17}_{\text{3Ac}_{\text{y5\_K16ac\_530}}}}, \text{MS2}_{\text{G4R17}_{\text{3Ac}_{\text{y5\_K16NoAc\_533}}}})} - \frac{\text{MS2}_{\text{G4R17}_{\text{3Ac}_{\text{y7\_K16K12.2Ac\_757}}}}}{sum(\text{MS2}_{\text{G4R17}_{\text{3Ac}_{\text{y7\_K16K12.1Ac\_757}}}}, \text{MS2}_{\text{G4R17}_{\text{3Ac}_{\text{y7\_K16K12.2Ac\_760}}}})}\right)$$

$$\text{H4.K5acK12acK16ac} = \frac{\text{MS1}_{\text{G4R17}_{\text{3Ac}}}}{sum(\text{MS1}_{\text{G4R17}_{\text{noPTM}}}, \text{MS1}_{\text{G4R17}_{\text{1Ac}}}, \text{MS1}_{\text{G4R17}_{\text{2Ac}}} \text{MS1}_{\text{G4R17}_{\text{3Ac}}} \text{MS1}_{\text{G4R17}_{\text{4Ac}}})} *$$

$$\left(\frac{\text{MS2}_{\text{G4R17}_{\text{3Ac}_{\text{y7\_K16K12.2Ac\_757}}}}}{sum(\text{MS2}_{\text{G4R17}_{\text{3Ac}_{\text{y7\_K16K12.1Ac\_757}}}}, \text{MS2}_{\text{G4R17}_{\text{3Ac}_{\text{y7\_K16K12.2Ac\_760}}}})} - \frac{\text{MS2}_{\text{G4R17}_{\text{3Ac}_{\text{y12\_K16K12K8.3Ac\_1211}}}}}{sum(\text{MS2}_{\text{G4R17}_{\text{3Ac}_{\text{y12\_K16K12K8.3Ac\_1211}}}}, \text{MS2}_{\text{G4R17}_{\text{3Ac}_{\text{y12\_K16K12K8.2Ac\_1214}}}})}\right)$$

$$\text{H4.K8acK12acK16ac} = \frac{\text{MS1}_{\text{G4R17}_{\text{3Ac}}}}{sum(\text{MS1}_{\text{G4R17}_{\text{noPTM}}}, \text{MS1}_{\text{G4R17}_{\text{1Ac}}}, \text{MS1}_{\text{G4R17}_{\text{2Ac}}} \text{MS1}_{\text{G4R17}_{\text{3Ac}}} \text{MS1}_{\text{G4R17}_{\text{4Ac}}})} * \frac{\text{MS2}_{\text{G4R17}_{\text{3Ac}_{\text{y12\_K16K12K8.3Ac\_1211}}}}}{sum(\text{MS2}_{\text{G4R17}_{\text{3Ac}_{\text{y12\_K16K12K8.3Ac\_1211}}}}, \text{MS2}_{\text{G4R17}_{\text{3Ac}_{\text{y12\_K16K12K8.2Ac\_1214}}}})}$$

$$\text{H4.K5acK8acK12acK16ac} = \frac{\text{MS1}_{\text{G4R17}_{\text{4Ac}}}}{sum(\text{MS1}_{\text{G4R17}_{\text{noPTM}}}, \text{MS1}_{\text{G4R17}_{\text{1Ac}}}, \text{MS1}_{\text{G4R17}_{\text{2Ac}}} \text{MS1}_{\text{G4R17}_{\text{3Ac}}} \text{MS1}_{\text{G4R17}_{\text{4Ac}}})}$$

Motifs at histone H3

H3.K9R17_noPTM =

$$\frac{MS1_{\_K9R17\_noPTM}}{sum(MS1_{\_K9R17\_noPTM}, MS1_{\_K9R17\_1Ac}, MS1_{\_K9R17\_2Ac}, MS1_{\_K9R17\_K9me3K14noAc}, MS1_{\_K9R17\_K9me3K14ac}, MS1_{\_K9R17\_K9me2K14noAc}, MS1_{\_K9R17\_K9me2K14ac}, MS1_{\_K9R17\_K9me1K14noAc}, MS1_{\_K9R17\_K9me1K14ac},}$$

H3.K9ac =

$$\frac{MS1_{\_K9R17\_1Ac}}{sum(MS1_{\_K9R17\_noPTM}, MS1_{\_K9R17\_1Ac}, MS1_{\_K9R17\_2Ac}, MS1_{\_K9R17\_K9me3K14noAc}, MS1_{\_K9R17\_K9me3K14ac}, MS1_{\_K9R17\_K9me2K14noAc}, MS1_{\_K9R17\_K9me2K14ac}, MS1_{\_K9R17\_K9me1K14noAc}, MS1_{\_K9R17\_K9me1K14ac},}$$

$$* \quad \frac{MS1_{K9R17_{y7\_K14noAc\_731}}}{sum(MS1_{K9R17_{y7\_K14noAc\_731}}, MS1_{K9R17_{y7\_K14ac\_728}})}$$

H3.K14ac =

$$\frac{MS1_{\_K9R17\_1Ac}}{sum(MS1_{\_K9R17\_noPTM}, MS1_{\_K9R17\_1Ac}, MS1_{\_K9R17\_2Ac}, MS1_{\_K9R17\_K9me3K14noAc}, MS1_{\_K9R17\_K9me3K14ac}, MS1_{\_K9R17\_K9me2K14noAc}, MS1_{\_K9R17\_K9me2K14ac}, MS1_{\_K9R17\_K9me1K14noAc}, MS1_{\_K9R17\_K9me1K14ac},}$$

$$* \quad \frac{MS1_{K9R17_{y7\_K14ac\_728}}}{sum(MS1_{K9R17_{y7\_K14noAc\_731}}, MS1_{K9R17_{y7\_K14ac\_728}})}$$

H3.K9me1K14ac =

$$\frac{MS1_{\_K9R17\_K9me1K14ac}}{sum(MS1_{\_K9R17\_noPTM}, MS1_{\_K9R17\_1Ac}, MS1_{\_K9R17\_2Ac}, MS1_{\_K9R17\_K9me3K14noAc}, MS1_{\_K9R17\_K9me3K14ac}, MS1_{\_K9R17\_K9me2K14noAc}, MS1_{\_K9R17\_K9me2K14ac}, MS1_{\_K9R17\_K9me1K14noAc}, MS1_{\_K9R17\_K9me1K14ac},}$$

H3.K9me2K14ac =

$$\frac{MS1_{\_K9R17\_K9me2K14ac}}{sum(MS1_{\_K9R17\_noPTM}, MS1_{\_K9R17\_1Ac}, MS1_{\_K9R17\_2Ac}, MS1_{\_K9R17\_K9me3K14noAc}, MS1_{\_K9R17\_K9me3K14ac}, MS1_{\_K9R17\_K9me2K14noAc}, MS1_{\_K9R17\_K9me2K14ac}, MS1_{\_K9R17\_K9me1K14noAc}, MS1_{\_K9R17\_K9me1K14ac},}$$

H3.K9me3K14ac =

$$\frac{MS1_{\_K9R17\_K9me3K14ac}}{sum(MS1_{\_K9R17\_noPTM}, MS1_{\_K9R17\_1Ac}, MS1_{\_K9R17\_2Ac}, MS1_{\_K9R17\_K9me3K14noAc}, MS1_{\_K9R17\_K9me3K14ac}, MS1_{\_K9R17\_K9me2K14noAc}, MS1_{\_K9R17\_K9me2K14ac}, MS1_{\_K9R17\_K9me1K14noAc}, MS1_{\_K9R17\_K9me1K14ac},}$$

$$\text{H3.K9me1} = \frac{\text{MS1\_K9R17\_K9me1K14NoAc}}{sum(\text{MS1\_K9R17\_noPTM},\text{MS1\_K9R17\_1Ac},\text{MS1\_K9R17\_2Ac},\text{MS1\_K9R17\_K9me3K14noAc},\text{MS1\_K9R17\_K9me3K14ac},\text{MS1\_K9R17\_K9me2K14noAc},\text{MS1\_K9R17\_K9me2K14ac},\text{MS1\_K9R17\_K9me1K14noAc},\text{MS1\_K9R17\_K9me1K14ac},}$$

$$\text{H3.K9me2} = \frac{\text{MS1\_K9R17\_K9me2K14NoAc}}{sum(\text{MS1\_K9R17\_noPTM},\text{MS1\_K9R17\_1Ac},\text{MS1\_K9R17\_2Ac},\text{MS1\_K9R17\_K9me3K14noAc},\text{MS1\_K9R17\_K9me3K14ac},\text{MS1\_K9R17\_K9me2K14noAc},\text{MS1\_K9R17\_K9me2K14ac},\text{MS1\_K9R17\_K9me1K14noAc},\text{MS1\_K9R17\_K9me1K14ac},}$$

$$\text{H3.K9me3} = \frac{\text{MS1\_K9R17\_K9me3K14NoAc}}{sum(\text{MS1\_K9R17\_noPTM},\text{MS1\_K9R17\_1Ac},\text{MS1\_K9R17\_2Ac},\text{MS1\_K9R17\_K9me3K14noAc},\text{MS1\_K9R17\_K9me3K14ac},\text{MS1\_K9R17\_K9me2K14noAc},\text{MS1\_K9R17\_K9me2K14ac},\text{MS1\_K9R17\_K9me1K14noAc},\text{MS1\_K9R17\_K9me1K14ac},}$$

$$\text{H3.K18R26\_noPTM} = \frac{\text{MS1\_K18R26\_noPTM}}{sum(\text{MS1\_K18R26\_noPTM},\text{MS1\_K18R26\_1Ac},\text{MS1\_K18R26\_2Ac}}$$

$$\text{H3.K18ac} = \frac{\text{MS1\_K18R26\_noPTM}}{sum(\text{MS1\_K18R26\_noPTM},\text{MS1\_K18R26\_1Ac},\text{MS1\_K18R26\_2Ac}} * \frac{\text{MS1\_K18R26\_b2\_K18ac\_299}}{sum(\text{MS1\_K18R26\_b2\_K18ac\_299},\text{MS1\_K18R26\_b2\_K18NoAc\_302})}$$

$$\text{H3.K23ac} = \frac{\text{MS1\_K18R26\_noPTM}}{sum(\text{MS1\_K18R26\_noPTM},\text{MS1\_K18R26\_1Ac},\text{MS1\_K18R26\_2Ac}} * \frac{\text{MS1\_K18R26\_b2\_K18NoAc\_302}}{sum(\text{MS1\_K18R26\_b2\_K18ac\_299},\text{MS1\_K18R26\_b2\_K18NoAc\_302})}$$

$$\text{H3.K18acK23ac} = \frac{\text{MS1\_K18R26\_2Ac}}{sum(\text{MS1\_K18R26\_noPTM},\text{MS1\_K18R26\_1Ac},\text{MS1\_K18R26\_2Ac}}$$

$$\text{H3.K27R40\_noPTM} = \frac{\text{MS1\_K27R40\_noPTM}}{sum(\text{MS1\_K27R40\_noPTM},\text{MS1\_K27R40\_1Ac},\text{MS1\_K27R40\_K27me1},\text{MS1\_K27R40\_K27me2},\text{MS1\_K27R40\_K27me3},\text{MS1\_K27R40\_K36me2},\text{MS1\_K27R40\_K36me3}\,\text{MS1\_K27R40\_K27me2K36me1}}$$

$$\text{MS1\_K27R40\_K27me2K36ac},\text{MS1\_K27R40\_K36me2K27ac},\text{MS1\_K27R40\_K36me3K27ac})$$

$$\text{H3.K27ac} = \frac{\text{MS1\_K27R40\_1Ac}}{sum(\text{MS1\_K27R40\_noPTM},\text{MS1\_K27R40\_1Ac},\text{MS1\_K27R40\_K27me1},\text{MS1\_K27R40\_K27me2},\text{MS1\_K27R40\_K27me3},\text{MS1\_K27R40\_K36me2},\text{MS1\_K27R40\_K36me3}\,\text{MS1\_K27R40\_K27me2K36me1}}$$

$$\frac{}{\text{MS1\_K27R40\_K27me2K36ac},\text{MS1\_K27R40\_K36me2K27ac},\text{MS1\_K27R40\_K36me3K27ac})} *$$

$$(1 - \text{average}((\frac{\text{MS1\_K27R40\_y5\_K27noAc\_752}}{\text{MS1\_K27R40\_y5\_K27noAc\_752},\text{MS1\_K27R40\_y5\_K27ac\_755})}),(\frac{\text{MS1\_K27R40\_b3\_K27noAc\_332}}{\text{MS1\_K27R40\_b3\_K27noAc\_332},\text{MS1\_K27R40\_b3\_K27ac\_329})}))$$

$$\text{H3.K36ac} = \frac{\text{MS1\_K27R40\_1Ac}}{sum(\text{MS1\_K27R40\_noPTM},\text{MS1\_K27R40\_1Ac},\text{MS1\_K27R40\_K27me1},\text{MS1\_K27R40\_K27me2},\text{MS1\_K27R40\_K27me3},\text{MS1\_K27R40\_K36me2},\text{MS1\_K27R40\_K36me3}\,\text{MS1\_K27R40\_K27me2K36me1}}$$

$$\frac{}{\text{MS1\_K27R40\_K27me2K36ac},\text{MS1\_K27R40\_K36me2K27ac},\text{MS1\_K27R40\_K36me3K27ac})} *$$

$$\text{average}((\frac{\text{MS1\_K27R40\_y5\_K27noAc\_752}}{\text{MS1\_K27R40\_y5\_K27noAc\_752},\text{MS1\_K27R40\_y5\_K27ac\_755})}),(\frac{\text{MS1\_K27R40\_b3\_K27noAc\_332}}{\text{MS1\_K27R40\_b3\_K27noAc\_332},\text{MS1\_K27R40\_b3\_K27ac\_329})}))$$

$$* (\frac{\text{MS1\_K27R40\_y4\_K36ac\_582}}{\text{MS1\_K27R40\_y4\_K36ac\_579},\text{MS1\_K27R40\_y4\_K36NoAc\_582})})$$

$$\text{H3.K37ac} = \frac{\text{MS1\_K27R40\_1Ac}}{sum(\text{MS1\_K27R40\_noPTM},\text{MS1\_K27R40\_1Ac},\text{MS1\_K27R40\_K27me1},\text{MS1\_K27R40\_K27me2},\text{MS1\_K27R40\_K27me3},\text{MS1\_K27R40\_K36me2},\text{MS1\_K27R40\_K36me3}\,\text{MS1\_K27R40\_K27me2K36me1}}$$

$$\frac{}{\text{MS1\_K27R40\_K27me2K36ac},\text{MS1\_K27R40\_K36me2K27ac},\text{MS1\_K27R40\_K36me3K27ac})} *$$

$$\text{average}((\frac{\text{MS1\_K27R40\_y5\_K27noAc\_752}}{\text{MS1\_K27R40\_y5\_K27noAc\_752},\text{MS1\_K27R40\_y5\_K27ac\_755})}),(\frac{\text{MS1\_K27R40\_b3\_K27noAc\_332}}{\text{MS1\_K27R40\_b3\_K27noAc\_332},\text{MS1\_K27R40\_b3\_K27ac\_329})}))$$

$$* (1 - \frac{\text{MS1\_K27R40\_y4\_K36ac\_582}}{\text{MS1\_K27R40\_y4\_K36ac\_579},\text{MS1\_K27R40\_y4\_K36NoAc\_582})})$$

$$\text{H3.K27R40\_K27me1} = \frac{\text{MS1\_K27R40\_K27me1}}{sum(\text{MS1\_K27R40\_noPTM},\text{MS1\_K27R40\_1Ac},\text{MS1\_K27R40\_K27me1},\text{MS1\_K27R40\_K27me2},\text{MS1\_K27R40\_K27me3},\text{MS1\_K27R40\_K36me2},\text{MS1\_K27R40\_K36me3}\,\text{MS1\_K27R40\_K27me2K36me1}}$$

$$\frac{}{\text{MS1\_K27R40\_K27me2K36ac},\text{MS1\_K27R40\_K36me2K27ac},\text{MS1\_K27R40\_K36me3K27ac})}$$

$$\text{H3.K27R40\_K27me2} = \frac{\text{MS1\_K27R40\_K27me2}}{sum(\text{MS1\_K27R40\_noPTM},\text{MS1\_K27R40\_1Ac},\text{MS1\_K27R40\_K27me1},\text{MS1\_K27R40\_K27me2},\text{MS1\_K27R40\_K27me3},\text{MS1\_K27R40\_K36me2},\text{MS1\_K27R40\_K36me3}\,\text{MS1\_K27R40\_K27me2K36me1}}$$

$$\frac{}{\text{MS1\_K27R40\_K27me2K36ac},\text{MS1\_K27R40\_K36me2K27ac},\text{MS1\_K27R40\_K36me3K27ac})}$$

$$\text{H3.K27R40\_K27me3} = \frac{\text{MS1\_K27R40\_K27me3}}{sum(\text{MS1\_K27R40\_noPTM},\text{MS1\_K27R40\_1Ac},\text{MS1\_K27R40\_K27me1},\text{MS1\_K27R40\_K27me2},\text{MS1\_K27R40\_K27me3},\text{MS1\_K27R40\_K36me2},\text{MS1\_K27R40\_K36me3}\,\text{MS1\_K27R40\_K27me2K36me1}}$$

$$\frac{}{\text{MS1\_K27R40\_K27me2K36ac},\text{MS1\_K27R40\_K36me2K27ac},\text{MS1\_K27R40\_K36me3K27ac})}$$

$$\text{H3.K27R40\_K36me2} = \frac{\text{MS1\_K27R40\_K36me2}}{sum(\text{MS1\_K27R40\_noPTM},\text{MS1\_K27R40\_1Ac},\text{MS1\_K27R40\_K27me1},\text{MS1\_K27R40\_K27me2},\text{MS1\_K27R40\_K27me3},\text{MS1\_K27R40\_K36me2},\text{MS1\_K27R40\_K36me3}\,\text{MS1\_K27R40\_K27me2K36me1}}$$

$$\frac{}{\text{MS1\_K27R40\_K27me2K36ac},\text{MS1\_K27R40\_K36me2K27ac},\text{MS1\_K27R40\_K36me3K27ac})}$$

$$\text{H3.K27R40\_K36me3} = \frac{\text{MS1\_K27R40\_K36me3}}{sum(\text{MS1\_K27R40\_noPTM},\text{MS1\_K27R40\_1Ac},\text{MS1\_K27R40\_K27me1},\text{MS1\_K27R40\_K27me2},\text{MS1\_K27R40\_K27me3},\text{MS1\_K27R40\_K36me2},\text{MS1\_K27R40\_K36me3}\,\text{MS1\_K27R40\_K27me2K36me1}}$$

$$\frac{}{\text{MS1\_K27R40\_K27me2K36ac},\text{MS1\_K27R40\_K36me2K27ac},\text{MS1\_K27R40\_K36me3K27ac})}$$

$$\text{H3.K27R40\_K27me2K36me1} = \frac{\text{MS1\_K27R40\_K27me2K36me1}}{sum(\text{MS1\_K27R40\_noPTM},\text{MS1\_K27R40\_1Ac},\text{MS1\_K27R40\_K27me1},\text{MS1\_K27R40\_K27me2},\text{MS1\_K27R40\_K27me3},\text{MS1\_K27R40\_K36me2},\text{MS1\_K27R40\_K36me3}\,\text{MS1\_K27R40\_K27me2K36me1}}$$

$$\frac{}{\text{MS1\_K27R40\_K27me2K36ac},\text{MS1\_K27R40\_K36me2K27ac},\text{MS1\_K27R40\_K36me3K27ac})}$$

H3.K27R40_K27me2K36ac =

$$\frac{\mathrm{MS1}_{\_\mathrm{K27R40}\_\mathrm{K27me2K36ac}}}{sum(\mathrm{MS1}_{\_\mathrm{K27R40}\_\mathrm{noPTM}},\mathrm{MS1}_{\_\mathrm{K27R40}\_\mathrm{1Ac}},\mathrm{MS1}_{\_\mathrm{K27R40}\_\mathrm{K27me1}},\mathrm{MS1}_{\_\mathrm{K27R40}\_\mathrm{K27me2}},\mathrm{MS1}_{\_\mathrm{K27R40}\_\mathrm{K27me3}},\mathrm{MS1}_{\_\mathrm{K27R40}\_\mathrm{K36me2}},\mathrm{MS1}_{\_\mathrm{K27R40}\_\mathrm{K36me3}}\mathrm{MS1}_{\_\mathrm{K27R40}\_\mathrm{K27me2K36me1}}}$$

$$\overline{\mathrm{MS1}_{\_\mathrm{K27R40}\_\mathrm{K27me2K36ac}},\mathrm{MS1}_{\_\mathrm{K27R40}\_\mathrm{K36me2K27ac}},\mathrm{MS1}_{\_\mathrm{K27R40}\_\mathrm{K36me3K27ac}})}$$

H3.K27R40_K36me2K27ac =

$$\frac{\mathrm{MS1}_{\_\mathrm{K27R40}\_\mathrm{K36me2K27ac}}}{sum(\mathrm{MS1}_{\_\mathrm{K27R40}\_\mathrm{noPTM}},\mathrm{MS1}_{\_\mathrm{K27R40}\_\mathrm{1Ac}},\mathrm{MS1}_{\_\mathrm{K27R40}\_\mathrm{K27me1}},\mathrm{MS1}_{\_\mathrm{K27R40}\_\mathrm{K27me2}},\mathrm{MS1}_{\_\mathrm{K27R40}\_\mathrm{K27me3}},\mathrm{MS1}_{\_\mathrm{K27R40}\_\mathrm{K36me2}},\mathrm{MS1}_{\_\mathrm{K27R40}\_\mathrm{K36me3}}\mathrm{MS1}_{\_\mathrm{K27R40}\_\mathrm{K27me2K36me1}}}$$

$$\overline{\mathrm{MS1}_{\_\mathrm{K27R40}\_\mathrm{K27me2K36ac}},\mathrm{MS1}_{\_\mathrm{K27R40}\_\mathrm{K36me2K27ac}},\mathrm{MS1}_{\_\mathrm{K27R40}\_\mathrm{K36me3K27ac}})}$$

H3.K27R40_K36me3K27ac =

$$\frac{\mathrm{MS1}_{\_\mathrm{K27R40}\_\mathrm{K36me3K27ac}}}{sum(\mathrm{MS1}_{\_\mathrm{K27R40}\_\mathrm{noPTM}},\mathrm{MS1}_{\_\mathrm{K27R40}\_\mathrm{1Ac}},\mathrm{MS1}_{\_\mathrm{K27R40}\_\mathrm{K27me1}},\mathrm{MS1}_{\_\mathrm{K27R40}\_\mathrm{K27me2}},\mathrm{MS1}_{\_\mathrm{K27R40}\_\mathrm{K27me3}},\mathrm{MS1}_{\_\mathrm{K27R40}\_\mathrm{K36me2}},\mathrm{MS1}_{\_\mathrm{K27R40}\_\mathrm{K36me3}}\mathrm{MS1}_{\_\mathrm{K27R40}\_\mathrm{K27me2K36me1}}}$$

$$\overline{\mathrm{MS1}_{\_\mathrm{K27R40}\_\mathrm{K27me2K36ac}},\mathrm{MS1}_{\_\mathrm{K27R40}\_\mathrm{K36me2K27ac}},\mathrm{MS1}_{\_\mathrm{K27R40}\_\mathrm{K36me3K27ac}})}$$

H3.E73R83_noPTM = $\frac{\mathrm{MS1}_{\_\mathrm{E73R83}\_\mathrm{noPTM}}}{sum(\mathrm{MS1}_{\_\mathrm{E73R83}\_\mathrm{noPTM}},\mathrm{MS1}_{\_\mathrm{E73R83}\_\mathrm{K79me1}},\mathrm{MS1}_{\_\mathrm{E73R83}\_\mathrm{K79me2}}}$

H3.E73R83.K79me1 = $\frac{\mathrm{MS1}_{\_\mathrm{E73R83}\_\mathrm{K79me1}}}{sum(\mathrm{MS1}_{\_\mathrm{E73R83}\_\mathrm{noPTM}},\mathrm{MS1}_{\_\mathrm{E73R83}\_\mathrm{K79me1}},\mathrm{MS1}_{\_\mathrm{E73R83}\_\mathrm{K79me2}}}$

H3.E73R83.K79me2 = $\frac{\mathrm{MS1}_{\_\mathrm{E73R83}\_\mathrm{K79me2}}}{sum(\mathrm{MS1}_{\_\mathrm{E73R83}\_\mathrm{noPTM}},\mathrm{MS1}_{\_\mathrm{E73R83}\_\mathrm{K79me1}},\mathrm{MS1}_{\_\mathrm{E73R83}\_\mathrm{K79me2}}}$

Equation system to derive formulas for di-acetylated H4 motifs

Target variables (acetylation motifs)

H4.K5acK8ac = x1 (directly MS1+MS2)
H4.K5acK12ac = x2 (MS1+MS2+MS3)
H4.K5acK16ac = x3 (MS1+MS2+MS3)
H4.K8acK12ac = x4 (MS1+MS2+MS3)
H4.K8acK16ac = x5 (MS1+MS2+MS3)
H4.K12acK16ac = x6 (directly MS1+MS2)

Relating MS quantifier to target variables (equation system)

b = MS2_G4R17_2Ac_y5_K16.1Ac_530 / (MS2_G4R17_2Ac_y5_K16.1Ac_530 + MS2_G4R17_2Ac_y5_K16.0Ac_533)
= (x3+x5+x6)/(x1+x2+x3+x4+x5+x6)

c = MS2_G4R17_2Ac_y12_K16K12K8.2Ac_1214 / (MS2_G4R17_2Ac_y12_K16K12K8.2Ac_1214 + MS2_G4R17_2Ac_y12_K16K12K8.1Ac_1217)
= (x4+x5+x6)/(x1+x2+x3+x4+x5+x6)

e = MS2_G4R17_2Ac_y7_K16K12.0Ac_763 / (MS2_G4R17_2Ac_y7_K16K12.0Ac_763 + MS2_G4R17_2Ac_y7_K16K12.1Ac_760 + MS2_G4R17_2Ac_y7_K16K12.2Ac_757)
= (x1)/(x1+x2+x3+x4+x5+x6)

f = MS2_G4R17_2Ac_y7_K16K12.2Ac_757 / (MS2_G4R17_2Ac_y7_K16K12.0Ac_763 + MS2_G4R17_2Ac_y7_K16K12.1Ac_760 + MS2_G4R17_2Ac_y7_K16K12.2Ac_757)
= (x6)/(x1+x2+x3+x4+x5+x6)

i = MS3_G6R17_2Ac_b10_2Ac_867 / (MS3_G6R17_2Ac_b10_2Ac_870 + MS3_G6R17_2Ac_b10_2Ac_867)
= x4 / (x4+x5+x6)

o = x1+x2+x3+x4+x5+x6 = 1

Solution of equation system

x1 = e
x2 = 1 – ic – b – e
x3 = c(i – 1) + b
x4 = ic
x5 = c(1 – i) – f
x6 = f

SUPPLEMENTAL EXPERIMENTAL PROCEDURE NOTES (SEPs)

SEP 1: LC-MS workflow

1.1 Improved sensitivity, precision and accuracy to quantify positional isomers containing lysine acetylation

We streamlined the histone extraction protocol to enable rapid processing of many samples (see Supplemental Experimental Procedures). The low requirement of starting material (typically 2 - 5 x 10^6 KC cells) allowed a cost-effective RNAi strategy and histone preparation without chromatographic enrichment. The direct extraction of histones from cells, rather than from nuclei or chromatin reduced preparation time and did not require usage of deacetylase inhibitors. Commonly used deacetylase inhibitors such as sodium butyrate alter the native histone acetylation pattern by inhibiting different deacetylases of the HDAC class with different efficiencies (Thorne et al., 1990; Fraga et al., 2005; Karmodiya et al., 2012). Our procedure aims at minimising the risk of altering the native histone acetylation pattern during sample preparation.

Histones were chemically acetylated using d6-deuterated acetic anhydride rather than propionylated to harmonise the physiochemical properties between the endogenously acetylated and non-acetylated lysines. This ensures similar properties during the LC-MS workflow, including comparable interactions during pre-LC (similar hydrophobicity, tube interactions etc.), LC (positional isomers co-elute and hence are electrosprayed at the same acetonitrile concentration) and MS (similar 'matrix effects' during ionization, fragmentation, MS acquisition), which results in improved accuracy among positional isomers. For example, using equimolar solutions of positional isomers from di-acetylated H4.G4-R17 peptides resulted in very similar ratios (Figure S2B). Furthermore, positional isomers for H3 peptides differing only in their site of acetylation display very similar LC-MS response correction factors (Table S2).

We developed a targeted MS protocol on a standard hybrid linear ion trap Orbitrap instrument (LTQ Orbitrap Classic) but the MS strategy can be implemented on different mass spectrometers capable of MS3 fragmentation. The general rationale is to iteratively acquire full or targeted survey scans (MS1) combined with targeted MS2 or MS3 spectra during the entire peptide elution or scheduled for pre-defined retention time windows (see Figure S1A for an example of scheduled RT windows). The scheduled spectra were recorded using a reduced window (e.g. MS1 acquisition window from 270 to 505 during the first retention time schedule) and less MS2/MS3 were scheduled. This improved the quantification of the MS identifier eluting within narrow LC peaks (e.g. H3.K9me2/3) through achieving a higher number of scans. We noted, however, that a few MS identifiers showed considerable shifts in their retention time within consecutive LC runs (in particular the non-methylated H3.K9R17 identifier with more than 5 minutes shift). Note that most of the data presented in the current study was therefore acquired without retention-time scheduling. In contrast to previously developed targeted MS strategies (Schmidt et al., 2008; Gallien et al., 2012a; Gallien et al., 2012b; Peterson et al., 2012; Jaffe et al., 2013; Tang et al., 2014) our emphasis was on the high-precision quantification of combinatorial PTM motifs. To increase the MS duty cycle, MS1 scans were recorded within the Orbitrap at low resolution (7500 at 400 m/z) after accumulating 100,000 ions over a maximum time of 500 ms. To increase the precision and sensitivity for MS2 and MS3, enhanced zoom scans were acquired within the ion trap targeting the first, second and third isotope, setting a target value to 50,000 and

accumulating for a maximal time of 100 ms. WideBand activation was performed to improve fragmentation for MS2 of the H3.K27R40_1Ac (m/z = 522.97 ± 0.8) and H4.G4R17_3Ac (m/z = 721.92 ± 0.7) identifier and for MS3 of the H4.G4R17_2Ac_y12 (m/z = 1215 ± 2) identifier. The targeted strategy enhanced the precision, reduced the interference and yielded a high density of scans.

Motifs containing methylated lysines in addition to acetylation displayed characteristic shifts in retention time (Figures 1A, S1). A systematic analysis of positional isomers (peptides with identical mass but PTMs at different positions) revealed some rules. A di- or tri-methyl group close to the N-terminus of a peptide results in a lower hydrophobicity and thus earlier retention time as compared to when the methylation is in the middle. For example, an H3 peptide containing tri-methylated lysine 27 (K27me3) elutes a few minutes before the same peptide bearing K36me3 (Figure S1B). Furthermore, tri-methylated peptides elute shortly before di-methylated ones, followed by unmethylated and, lastly, mono-methylated forms. This was true for all histone peptides analysed and allows a precise quantification of peptides carrying methylation-only or mixed acetylation-methylation motifs (with a single acetylation site) solely based on their MS1 values (Figures 1A, S1).

To validate and benchmark the LC-MS workflow, we used synthetic peptides carrying different acetylation motifs at different ratios (Figure S2B, Table S2), which demonstrated a very high accuracy. To assess the level of precision, we performed three whole-workflow replicates starting with 2 million KC cells each. The quantification of 45 histone motifs resulted in a median coefficient of variation (CV) of 5.2% (Figure 1B, Table S3). Next, we measured the level of variation for five independent biological replicates involving control RNAi treatments of between 2 and 8 million cells. Through optimising MS2 and MS3 recordings, the CVs for motifs that require successive MS^n measurements were similar (median CV of 10.4) to those for motifs requiring MS1 only (median CV of 8.9). However, the CVs of the individual histone PTMs varied between 0.8% and 35.7% (Figure 1B, Table S3). Similar results were obtained using 75,000 to 300,000 mammalian cells (data not shown). The differences in CV for histone PTMs reflect their *in vivo* abundances, which differ in several orders of magnitude (Figures 1D, E) and the technical imprecision specific to any MS identifier (Table S3). For example, quantitation of the highly abundant H3.K27me2 motif requires only MS1-based quantification with highly precise MS1 quantifier (CV = 5.3%), whereas the low-abundant H4.K8acK12ac motif requires integration from MS1, MS2 and MS3 peak areas (CV = 35.7%). Overall, our current LC-MS workflow is able to analyse low amounts of sample and the sensitivity, precision and accuracy are improved over state-of-art workflows for quantifying histone PTM motifs.

1.2 Successive MS1-MS2-MS3 to quantify combinatorial motifs of the di-acetylated histone H4 positional isomers

The abundance of peptides with two out of four acetylations cannot be resolved with MS1 and MS2 analysis alone, because the set of linear equations for these motifs cannot be mathematically solved (as noted before by Phanstiel et al. 2008, and see formulas and equation system in Supplemental Experimental Procedures). One possible solution is to separate these positional isomers by chromatography (Young et al., 2009). Potential drawbacks of this strategy include sample-to-sample variation in chromatographic separation of the positional isomers, uneven matrix and acetonitrile effects due to different retention times and high operating skills required for elaborated chromatography systems.

We developed an easy to implement strategy involving iterative loops of targeted MS1-MS2-MS3 scans. The information from the re-fragmented (MS3) ions is necessary to solve the equation system and derive the abundances of H4.K5acK12ac, H4.K8acK12ac, H4.K8acK16ac and H4.K5acK16ac (see formulas and equation system in Supplemental Experimental Procedures). To increase the dynamic range of MS3 acquisition, we performed enhanced zoom scans in the ion trap, targeting an increased window centred on the second isotope of the di-acetylated MS2 fragment ions – but excluding the mono-acetylated precursor ions – and applying WideBand activation to increase the efficiency of fragmentation. Note that the second isotope of the MS2 y12 ion that is subjected to MS3 (theoretical mass: 1215.7096) is often at least as strong as the first isotope (see Figure S1A second panel zoom in). Although a number of MS3 fragment ions could potentially be analysed, we focused on the b10 ion pairs because this gave most reproducible results. The b10 ions with two acetyl groups represent H4.K8acK12ac (theoretical m/z = 867.469) and b10 ions with a single acetyl-group represents H4.K8acK16ac and H4.K12acK16ac (theoretical m/z = 870.492). Note that fragmentation of the water loss ion through WideBand activation shifted the observed spectra by -18 Dalton (see Figures S2A, S2C). Supplemental Experimental Procedures details the formulas that are used to calculate the motif abundances for the di-acetylated isoforms.

Theoretically, the b10 MS3 fragment ion with two acetyl groups (theoretical m/z = 870.492) may interfere with the y8 MS3 fragment ion harbouring a single acetyl group (theoretical m/z = 870.516). To test for this, we recorded MS3 scans for a synthetic peptide (H4.K8acK12ac) for which we only expect signals for the b10 MS3 fragment ion with two acetyl groups (expected m/z at 849) and the y8 MS3 fragment with a single acetyl group (expected m/z at 855). The MS3 signal intensities for the b10 ion are dominant over the y8 ion (40400 vs 1526, b10/y8 > 0.96), demonstrating the usability of the b10 ion for quantification. Alternatively, one may use the b8 MS3 classifier pair (theoretical m/z at 739.41 and 742.43) yet we observed less accurate results using synthetic peptides and overall less signal and more varying results with most biological samples.

To test for accuracy, we performed sets of experiments where we mixed synthetic peptides containing di-acetylated H4 motifs in different ratios and measured their abundances via LC-MS. The representative experiment in Figure S3B shows that the measured ratios are close to the expected ones, verifying the MS3-based assay and demonstrating high accuracy.

In summary, we introduce an easy to implement and robust LC-MS workflow which resolves the abundance of PTMs within complex positional isomers. The assay is general applicable and might be useful to pinpoint acetylation sites within clusters of any protein.

1.3 Detection and quantification of H3 and H4 histone acetylation motifs

Histones are basic proteins with clusters of lysines close to the N-terminal ‘tail’ domains. The goal of this study was to monitor the acetylation status of any lysine on the canonical histones H3 and H4 with a particular focus to probe for potential combinatorial motifs. Because we chemically acetylated lysines which are not acetylated in the cell, peptides from endogenously acetylated and non-acetylated lysines co-elute during chromatography. This procedure not only has the advantage of increasing the precision (see above), but also to increase the confidence in the identification of low abundant acetylation sites. Although the MS signals of low abundant acetylation sites often display more imprecise masses than high-signal MS identifiers, precise co-elution (or slight shift towards later retention times) is a good

indication for the existence of an acetylation site (see below for examples including H3.K27me2K36ac, H3.K36me2/3K27ac) whereas the absence of co-elution is a strong indication for the absence of an acetylation site (see H4.K20ac and H3.K56ac below). A slight shift towards later retention times for endogenously acetylated histones compared to chemically d3-acetylated histones is caused by the slightly decreased interaction of the deuterated (d3) moieties with the C18 column (Goodlett et al., 2001).

We robustly detected MS1 masses corresponding to the mono-, di-, tri- and tetra-acetylated isoforms of the H4.G4-R17 peptide from KC cell histone preparations (Figure S2A). MS2 and MS3 peptide sequencing of histones from KC cells enabled the identification and quantification of all positional isomers on this peptide with one exception (H4.K5acK16ac). Although we detected synthetic peptides to H4.K5acK16ac and accurately determined their abundance in mixtures of synthetic di-acetylated H4.G4-R17 peptides (Figure S2B), the low abundance of this motif together with the more complicated formula to derive this motif (see Supplemental Experimental Procedures) did not allow its reliable quantification in KC cell samples. We therefore do not display the abundance values for this motif. Moreover, to keep the other di-acetylated H4.G4-R17 motifs independent of H4.K5acK16ac, we did not artificially correct for omitting H4.K5acK16ac. Therefore, if we sum up the abundances of all fifteen quantified H4.G4-R17 motifs, we only approximate but do not exactly arrive at 1.

Although we detect all histone H4 peptides in their unmodified form, we did not identify any acetylation to lysines K31, K44, K59, K77, K79 and K91 (Figure S2). Acetylation at H4.K20ac has been detected in plants (Zhang et al., 2007) and recently also in human cancer cells (Zheng et al., 2013; Tang et al., 2014). In contrast, we fail to detect H4.K20ac in *Drosophila* cells. Of note, in a few histone preparations from adult flies we detected a MS1 mass at m/z = 279.1940 which is very close to the theoretical mass of H4.K20ac (m/z = 279.1927). Its very low signal intensity did not allow MS2 analysis. Importantly, because the peaks that may indicate H4.K20ac did not co-elute with (or elute slightly after) the peaks of the unmodified H4.K20-R23 peptide, we conclude that we are currently unable to detect H4.K20ac in *Drosophila* cells.

Similar to H4.K20ac, we also did not detect acetylated H4.K91. H4.K91ac has been found in yeast and mammalian cells and is associated with histone maturation in the cytoplasm (Ye et al., 2005; Yang et al., 2011). Figure S2G shows the existence of a high-signal triple charged MS1 spectrum for the unmodified H4.K79R92 peptide, yet we do not detect any signal for the acetylated isoform at a similar retention time.

Consecutive MS1-MS2 analysis on histone H3 peptides identified acetylation to lysines 9, 14, 18, 23, 27, 36 and 37 in the combinations detailed in Table S3. Figure S3 documents the MS1 and MS2 spectra. Co-elution of H3.K27me2K36ac, H3.K36me2K27ac and H3.K36me3K27ac with the unmodified isoforms H3.K27me2, H3.K36me2 and H3.K36me3 provides high confidence in the identification of these motifs. The b3 and y11 fragment ion pairs derived from targeting the mono-acetylated H3.K27-R40 peptide revealed that while most acetylation is, as expected, on lysine 27 (0.20% of all H3 motifs corresponding to estimated 12000 molecules/cell), there was also detectable acetylation on lysine 36 (0.058% of H3 motifs or estimated 3500 molecules/cell; for calculations: see below). Moreover, we detected minute amounts of acetylation on lysine 37 (0.003% of H3 motifs or estimated 182 molecules/cell, Figure S3R-T). Although the signals of the MS2_K27R40_y4_K36ac_579 identifier reporting on H3.K37ac is above background, the current number of replicates within the RNAi dataset did not allow its high-confidence quantification. We therefore display only 28 out of 29 acetylation motifs for the KAT and KDAC RNAi datasets. Using the motif

abundance of H3.K37ac, we estimate that our lowest detection limit is at around 0.003% or estimated 182 molecules per cell for those motifs that require consecutive MS1 and MS2 analysis. Motifs that require solely MS1 analysis likely have lower detection limits (including H4.K20ac, H3.K56ac).

We did not detect the long hydrophobic peptide H3.F84-R116 and thus cannot interrogate acetylation to lysine H3.K115. Furthermore, although we robustly detected all other unmodified H3 peptides, we did not detect acetylation to lysines K4, K56, K64, K79 and K122 (Figure S3).

Acetylation of H3.K56 is high in yeast cells and very low in mammalian cells (see (Drogaris et al., 2012) and references therein). Using antibodies to detect H3.K56ac, Tyler and colleagues reported that deprivation of SIR2 in *Drosophila* S2 cells increased the levels of H3.K56ac (Das et al., 2009). We did not detect H3.K56ac in KC cells treated with control RNAi or RNAi targeting SIR2 (Figure S3J). We also did not detect this modification in S2 cells. Measuring synthetic peptides of unmodified and acetylated K56 yielded strong signals for both isoforms, arguing that our LC-MS approach is capable to detect acetylated K56ac if present on synthetic peptides (Figures S3K, L).

Acetylation of H3.K64 and H3.K122 was recently observed in mammalian cells (Tropberger et al., 2013; Di Cerbo et al., 2014), but similar to H3.K56ac, we detected the unmodified but not acetylated isoforms in histones from KC cells (Figure S3X, Y).

We detected methylation at lysine 20 of H4 and lysines K4, K9, K27, K36 and K79 of H3 (Table S3 and Figure S2, S3). Although occasionally we observed a mass corresponding to a mono-methylated H3.K9-R17 peptide, which elutes 3 minutes after H3.K9me1 and thus might be H3.K14me1, MS2 analysis did not confirm the identity of H3.K14me1. The same applies to MS1 masses, which may indicate mono-methylation at the H3.K18-R26 peptide. MS2 analysis targeting this parent ion did not yield any fragment ion that would indicate the presence of the mono-methylated H3.K18-R26 peptide.

Apart from the methyllysine-containing motifs detailed in Figure 1D, E and Table S3, we also detected low levels of H3.K36me1, H3.K27me1K36me1 and minute amounts of H3.K79me3. Under our conditions, H3.K36me1 elutes very close to the positional isomer of the more dominant H3.K27me1 (Figure S1B) and in some samples H3.K36me1 (m/z = 528.3226) elutes close to acetylated K27ac from the histone variant H3.3, which lead to an interference with its second isotope at m/z = 528.3157. We therefore currently cannot reliably report H3.K36me1 throughout all KAT and KDAC RNAi samples. We also excluded H3.K27me1K36me1 for a high-confidence comparative analysis, because its measured abundance varied substantially even throughout control RNAi samples. Similar to other di- and tri-methyl pairs, H3.K79me3 elutes shortly before H3.K79me2 (Figure S1A, lowest panel in schedule 4). Because of its very low signal intensity and the observed variability across control RNAi samples, we excluded H3.K79me3 for a high-confidence quantitative analysis. We estimated the abundance of H3.K79me3 in KC cells to be below 0.2% (Figure S3W), supporting that, similar to human DOT1L but unlike to yeast Dot1, *D. melanogaster* DOT1 almost exclusively generates H3.K79me1/2.

In this study, we do not report on the methylation states of H4.K20 and H3.K4. Although we robustly identified the more hydrophobic un-methylated und mono-methylated states to each of these peptides (Figures S2D-F, S3A, B), H3.K4me2 showed much lower signal intensities and the me3 states of each peptide are only occasionally detected. Reliable quantification of these small hydrophilic peptides would require additional or alternative peptide purification

strategies. To not compromise quantification of the other 45 histone PTM motifs, we excluded the analysis of the H3.T3-R8 and H4.K20-R23 peptides.

Calculation of motif abundance and estimation of cellular copy number

To calculate the relative abundance of a histone motif, its specific peak intensity (area under curve of each MS chromatogram) was divided by the sum of all peak intensities of motifs that contribute to a peptide (See Supplemental Experimental Procedures for formulas). For example, the relative abundance of H3.K14ac was calculated by multiplying the fraction of MS2 identifiers that distinguish H3.K14ac from H3.K9ac (MS2_K9R17_y7_K14ac_728 / (MS2_K9R17_y7_K14ac_728 + MS2_K9R17_y7_K14noAc_731)) with the fraction of the non-methylated but mono-acetylated MS1 signals relative to all MS1 signals for the H3.K9-R17 peptide (H3.K9-R17_1Ac / (H3.K9-R17_noPTM + H3.K9-R17_1Ac + H3.K9-R17_2Ac + H3.K9-R17_K9me1/2/3 ± K14ac)). Of note, any other modification that occurs on this motif but was not quantified in this study will cause an overestimation of the abundances for the quantified motifs. This includes, for instances, the phosphorylation sites at H3.S10 and H3.T11 – which would require alternative purification strategies – as well as PTMs that have not yet been identified.

We attempted to determine the exact cell copy number of all histone molecules and specific histone acetylation and methylation motifs by spiking-in highly purified, precisely quantitated synthetic peptides (TQL-spiketide, JPT Berlin) into known quantities of KC cells. However, as described below, we observed already strong variations in the abundance of the Q tag dissociated by trypsin digestion from different proteotypic peptides, which complicates its faithful accurate quantitative interpretation. Moreover, we observed strong variations of the LC-MS response throughout replicate experiments with cells and spike-in TQL-peptide mixes. Lastly, we observed ion suppression effects when we titrated the number of cells against the concentration of TQL synthetic peptides, or *vice versa*.

Because of the technical problems described above, we estimated the number of histone motifs per cell assuming i) a D. *melanogaster* genome size of 196 mega base pairs (Mb) for females and 170 Mb for males (http://flybase.org/reports/FBsp00000001.html) ii) an average nucleosome repeat length of 197 base pairs (Becker and Wu, 1992), iii) a minimal pool of free histones while most histones are organised as nucleosomes (Loyola et al., 2006) and iv) equal number of cells in G1 (n=2) and G2 (n=4) phase. Accordingly, multiplying the relative abundances measured in this study with 5 969 543 and 5 177 664 million histone molecules of a diploid female or male cell, respectively, the estimated abundance for the rare H3.K37ac motif is around 182 molecules per female cell whereas the high abundant H3.K23ac motif is present on approximately 2.8 million histone molecules.

SEP 2: Introducing an LC-MS response factor to increase the accuracy of histone PTM quantification

Post-translational modifications can have a substantial impact on several steps of the LC-MS workflow – including column interactions during liquid chromatography and ionisation and fragmentation within the mass spectrometer – and can therefore severely bias accurate quantitation between different PTMs signatures of the same peptide (Schotta et al., 2008; Farley and Link, 2009; Marx et al., 2013). For the current study, we needed to know accurate

relative abundances to reliable interpret the abundance levels in the light of their roles as high abundant structural motifs or rare motifs with signalling character.

As expected, the D3AA method applied in this study reduced the inherent bias in MS signals for motifs that contain a single or multiple acetylations as the only PTM. Measuring defined amounts of different synthetic di-acetylated H4.G4-R17 peptides recovered the expected ratios (see above and Figures S2B, C). Furthermore, we observed very similar LC-MS response factors among positional isomers of H3 peptides that contain lysine acetylation as the only PTM (Table S2).

In contrast, we observed dramatically different MS signals when we measured the same amount of peptides that differed in their methylation status. A similar observation has been made before by Jenuwein and colleagues who observed up to 5 fold differences when comparing the raw MS signals among synthetic peptides to H4.K20me1/2/3 and the unmodified H4.K20-R23 peptide (Schotta et al., 2008). We measured synthetic peptides to methylation motifs that contain methylated K9, K27, K36 and K79. The most dramatic effect was measured between the different methylation states of lysine 9, where the raw MS signals of the H3.K9me3 peptide was 50-fold less than the raw MS signals for the H3.K9me1 motif (Table S2).

Some of the differences might be due to different *initial* peptide concentrations, which may vary in a peptide-specific manner due to peptide processing workflows between the quantitation of peptides (at JPT, Berlin) and their digestion with trypsin (in our laboratory). For example, the exact quantitation of the TQL-synthetic peptide by fluorescence might be influenced by the physicochemical properties of the peptide sequence including their modification pattern. Furthermore, peptides with different physicochemical properties, such as the ones with different methylation states, might be differentially affected by peptide loss during the early pre-LC workflows, including insufficient resuspension and different interactions with the tube walls.

To test for this ‘pre-LC error’, we measured the MS signals of the Q tag, which is cleaved off the proteotypic peptide by trypsin digestion. Indeed, we observed substantial differences in the Q tag signals between experiments with different TQL-synthetic peptides (Figure 1C, middle panel). Normalising the MS signals of the proteotypic peptides by the MS signals of the Q tag not only reduced the variation between replicate measurements by two-fold (compare the SEM between columns 4 and 6 in Table S2) but also yielded more similar LC-MS response correction factors among motifs that differ only in their site of acetylation. For example, while the LC-MS response correction factors without applying the Q tag normalisation differed markedly between H3.K9ac (3.92), H3.K14ac (1.62) and H3.K9acK14ac (2.26), applying the normalisation with the Q tag signals converged the LC-MS response correction factors (H3.K9ac: 1.46, H3.K14ac: 1.46 and H3.K9acK14ac: 1.58). In addition, the Q tag normalisation also reduced the overall differences between the highest and lowest LC-MS response correction factor (e.g. H3.K9me3 before Q tag normalisation: 50.49, after Q tag normalisation: 34.17).

Theoretically, the accuracy of the LC-MS response factors for motifs that elute during different retention times can be increased by measuring them in the background of the endogenous histone sample. However, because we observed a dose-dependent interference between the synthetic spike-in peptides with their co-eluting endogenous counterpart, we did not proceed with this strategy, which is also the reason why we refrained from using the spike-in peptides for absolute quantitation.

Application of the LC-MS response correction factor had a significant impact on estimating the cellular copy number of histone acetylation and methylation motifs (Table S3). For example, without applying the LC-MS response correction factor, we estimated that H3.K27ac is found on 0.7% of H3 molecules (estimated 41,000 molecules/cell). This number is unexpectedly high, considering that this dynamic mark is preferentially detected at active enhancers (> 10,000) (Kharchenko et al., 2011; Yanez-Cuna et al., 2014). If we correct for the LC-MS bias, we arrive at a 3.5 times lower number for H3.K27ac (0.2% or estimated 12,000 molecules/cell). By contrast, we underestimated the abundance of the repressive H3.K9me3 mark by almost ten-fold (4.2% vs. 39%). Combining the numbers for the cellular abundance, genome-wide occupancy and half-live allows deriving testable quantitative models on genome organisation and function.

Application of the LC-MS response correction factor did not change the conclusions of most KAT and KDAC RNAi experiments, with a few notable exceptions (Figure S6 and Table S4). While H3.K14ac appeared to be elevated in many KAT depletion experiments without applying the LC-MS correction factor, this trend was weaker when correcting for the LC-MS bias. Another example is the depletion of HBO1, that appeared to cause a moderate reduction of H3.K9me2K14ac (85% of control), which was not observable anymore after applying the correction factor (98% of control).

SEP 3: Experimental design and statistical analysis

During the course of this study, we continuously developed the LC-MS protocol while expanding the scope of KAT and KDACs and histone motifs to be analysed. Therefore, the current manuscript summarises datasets that were generated using different LC-MS workflows and different KC cell batches grown and processed during different months and years (time span from 2012 to 2014). As a consequence, we observed technical and biological variations, which we addressed by normalising KAT/KDAC RNAi samples within each ‘batch’ to their corresponding control RNAi samples (Tables S3, S4 and see below).

We aimed to ablate each KAT and KDAC with two distinct non-overlapping RNAi constructs (Table S6) in at least two independent biological experiments for each RNAi construct. For most RNAi experiments, we used two dsRNA sequences from the *Drosophila* RNAi Screening Center (DSRC, Harvard). Most of those constructs have an average size of 500 base pairs and are widely used in genome-wide RNAi screens. For some genes, we designed new RNAi constructs using the NEXT-RNAi platform (www.nextrnai.org) because there was only a single RNAi construct at DSRC (e.g. MGEA5) or we expected an insufficient knockdown or elevated off-target reactivity when using short DSRC constructs (e.g. NAA10 < 250 bp). Because of their short mRNA size or unfavourable sequence composition, we could only target NAT9, NAA40, CG12560 and SIRT6 with a single dsRNA construct.

For most RNAi experiments, we observed an overall high similarity of the responses that are caused by different dsRNA constructs targeting the same KAT or KDAC gene (Table S4). However, this was not the case for each one dsRNA-CBP and dsRNA-TIP60 construct, which were therefore not incorporated in the analysis (see note in Table S4).

While many KAT RNAi samples where acquired during three different ‘replicate batch groups’ (see Table S4), some KAT RNAi samples were acquired in fewer batches (e.g. MGEA5: 3 biological replicates in the ‘C’ batch; NAT10: 2 biological replicates each in the ‘B’ and ‘C’ batch). In some cases, we conducted several independent RNAi experiments with the same batch of cells yet on different days or weeks. For example, we conducted two

independent RNAi experiments each with the single NAA40_1 RNAi construct during times of the 'A' batch (NAA40_1_1_A and NAA40_1_2_A) and the 'B' batch (NAA40_1_1_B and NAA40_1_2_B).

Normalisation to control RNAi samples within each batch was necessary because, while most histone motifs did not show major differences in their abundance across the different batches, some motifs showed considerable variation. For example, while the abundance of H4.K5ac was similar across the batches 'A' to 'E' (3.38%, 3.42%, 3.75%, 3.15% and 3.38%), the abundance values scattered stronger for H4.K12ac (6.95%, 8.20%, 7.66%, 5.98% and 8.03%). Because our interest was primarily in the relative change of a motif comparing a KAT/KDAC RNAi with its control (GST RNAi, GFP RNAi, EGFP RNAi or mock), this normalisation step reduced biological variation across *paired* groups of KAT/KDAC and control RNAi (= samples between 'batches') and thereby increased statistical power to detect minor differences. Although we note that some motif abundances systematically varied more than others, we currently suspect not only technological reasons (such as noise within LC-MS signals due to different quantitation requirements, see formulas in Supplemental Experimental Procedures) but also biological explanations, such as the time we kept cells in culture or environmental conditions. For example, we observed varying levels of H4.K12ac and H3.K18acK23ac in cells, which were either kept for very short or extended periods of time in culture (preliminary observation, samples not used during this study). Similarly, we suspect altered serum conditions to be responsible for some batch-to-batch variations.

We excluded MS values for histone motifs that we either did not measure in a particular sample or in case the MS values were not reliable. For example, we did not measure histone H3 motifs of samples within batch 'A'. Common sources for non-reliable MS values were low MS signals due to technical shortcomings at the LC or MS, interference with other ions (sometimes caused by problems with the LC gradient) or ion suppression effects. In case we identified a problem with a single MS identifier (e.g. the early eluting MS1_K9R17_K9me3 identifier, which reports on the H3.K9me3 motif), we excluded all motifs of this peptide (H3.K9-R17), even if individual motifs, which elute at later retention times, appeared fine (H3.K9me1 and acetylated K9 and K14). However, in many cases, other peptides were not affected (e.g. H3.R18-K26) and thus remained in the analysis. In these special cases where we could not reliably quantify peptides, we did not calculate summarised values (e.g. global acetylation score).

SEP 4: Mining the database to derive testable hypotheses and to shed light into controversial enzyme-substrate relationships

HAT1 is the well-known cytoplasmic HAT that renders histone H4 competent for nucleosome assembly by acetylation at lysines 5 and 12. Up to now, current methodology did not allow measuring the di-acetylated motif *per se* (see SEP 1.2). Our analysis shows that the main effect of HAT1 knockdown is a reduction of the H4.K5acK12ac mark (Figure 2A). Interestingly, it also reveals a reduction of K5ac, but not of K12ac. Together with *in vitro* data on recombinant HAT1 that demonstrates efficient acetylation of unmodified and pre-acetylated templates on either positions 5 or 8 yet not on other sites or combinatorial motifs (K12ac, K5acK12ac, K8acK16ac; Makowski et al. 2001), this leads us to hypothesise that HAT1 first acetylates H4 at K5, releases a fraction of H4.K5ac to the cellular histone pool and di-acetylates another fraction to produce H4.K5acK12ac. Notably, we detect a minor decrease of the tri-acetylated H4.K5acK8acK12ac upon HAT1 depletion, which suggests that HAT1 further acetylates K8 on a small fraction of its di-acetylated product. This is in line with

previous reports indicating that cytosolic H4 bound to chaperones is not only acetylated at lysines 5 and 12, but that a minor acetylation of K8 can be detected as well (Verreault et al., 1996).

The physiological substrates of HBO1 are controversially discussed. Whereas some groups report HBO1 as the major H4 acetyltransferase with specificity for K5, K8 and K12, others found that inactivation of the *hbo1* gene in mice did not cause a decline of H4 acetylation, yet led to dramatic loss of H3.K14ac (Miotto and Struhl, 2010; Kueh et al., 2011; Lalonde et al., 2013). Indeed, HBO1 ablation in *Drosophila* affects H4.K12ac levels only very modestly, if the values of all motifs including this mark are combined (as if one used an antibody that does not differentiate H4.K12ac-containing motifs) (Figure 2B). However, monitoring individual motifs reveals that HBO1-lacking cells show a moderate reduction of mono-acetylated H4.K12, but a severe loss of the di-acetylated H4.K8acK12ac motif (Figures 2A, 3A, 3B). One of the possible scenarios to explain this finding is that HBO1 initially acetylates H4.K12 and then further acetylates K8 on a fraction of its first acetylation product.

SEP 5: Homeostatic control of acetylation levels upon deprivation of KATs

To determine whether deprivation of KATs reduces the global acetylation levels of histones, we calculated a 'global H3 + H4 acetylation score' and compared it between cells lacking a specific KAT and cells treated with control RNAi constructs (Figure 5A and Table S4, column 59). The 'global H3 + H4 acetylation score' is calculated by summing up all fractional acetylation events observed on the four histone peptides that are subject to acetylation (H4.G4-R17, H3.K9-R17, H3.K18-R26 and H3.K27-R40). For example, depletion of CBP in the CBP_2_3_C experiment (targeting CBP with the CBP_2 RNAi construct, using the third biological replicate experiment in the batch 'C') displayed a relative 'global H3 + H4 acetylation score' of 96% (Table S4, row 74, column 59). In other words, the cumulative acetylation on the four acetylated peptides (H4.G4-R17, H3.K9-R17, H3.K18-R26 and H3.K27-R40) was reduced by only 4% relative to control RNAi. This value is derived by dividing the 'global H3 + H4 acetylation score' for CBP_2_3_C of 100.57 (see row 74, column 117) by the mean of the 'global H3 + H4 acetylation score' for the control RNAi samples from the 'C' batch, which has a value of 105.02 (Table S4, row 266, column 117). The 'global H3+H4 acetylation score' (column 117) is the sum of the 'global acetylation score for H4' (column 115) and the 'global acetylation score for H3' (column 116). The 'global acetylation score for H4' represents the fraction of histone H4 peptides that is acetylated, which is 27.14% for the CBP_2_3_C sample. The 'global acetylation score for H3' is the sum of all fractional acetylation events on the three acetylated H3 peptides (19.78% for H3.K9-R17, 53.59% for H3.K18-R26, and 0.06% for H3.K27-R40, total of 73.43%).

To calculate the % total acetylation change that is contributed by individual motifs (Figure 5B), we scaled the relative change of each KAT RNAi/ctr RNAi experiment (filtered for significant losses, using unpaired two-sided t test on log2 ratios) to the relative abundance of each motif in KC cells. This was done to circumvent the batch effects between different 'replicate batch groups' (see SEP 3).

The system's response that causes increases of acetylation upon ablation of individual acetyltransferases may be brought about in different ways, e.g. by modulating the expression or activities of other acetyltransferases or deacetylases. To address cross-regulation on the transcriptional level in an exemplary manner, we choose to monitor the mRNA levels of selected KATs (MOF, HBO1, CBP, KAT6 and GCN5) because many of their acetylation

motifs were increased in other KAT knockdown experiments (Figures 2, S5B). For example, one may expect increased levels of HBO1 and GCN5 after MOF RNAi, because H4.K12ac (HBO1) and K9ac/K14ac-containing motifs (GCN5) were increased under these conditions. We found, on the contrary, almost unchanged levels of GCN5 and only very moderately reduced HBO1 mRNA. Similar to the example of MOF RNAi, we found all kinds of mostly very moderate effects for HBO1, KAT6 and CBP RNAi, some of which in line and some contrary to expectations (Figure S5B).

SUPPLEMENTAL REFERENCES

Allis, C.D., Berger, S.L., Cote, J., Dent, S., Jenuwien, T., Kouzarides, T., Pillus, L., Reinberg, D., Shi, Y., Shiekhattar, R.*, et al.* (2007). New nomenclature for chromatin-modifying enzymes. Cell *131*, 633-636.

Becker, P.B., and Wu, C. (1992). Cell-free system for assembly of transcriptionally repressed chromatin from Drosophila embryos. Molecular and cellular biology *12*, 2241-2249.

Das, C., Lucia, M.S., Hansen, K.C., and Tyler, J.K. (2009). CBP/p300-mediated acetylation of histone H3 on lysine 56. Nature *459*, 113-117.

Di Cerbo, V., Mohn, F., Ryan, D.P., Montellier, E., Kacem, S., Tropberger, P., Kallis, E., Holzner, M., Hoerner, L., Feldmann, A.*, et al.* (2014). Acetylation of histone H3 at lysine 64 regulates nucleosome dynamics and facilitates transcription. eLife *3*, e01632.

Drogaris, P., Villeneuve, V., Pomies, C., Lee, E.H., Bourdeau, V., Bonneil, E., Ferbeyre, G., Verreault, A., and Thibault, P. (2012). Histone deacetylase inhibitors globally enhance h3/h4 tail acetylation without affecting h3 lysine 56 acetylation. Scientific reports *2*, 220.

Farley, A.R., and Link, A.J. (2009). Identification and quantification of protein posttranslational modifications. Methods in enzymology *463*, 725-763.

Feller, C., Prestel, M., Hartmann, H., Straub, T., Soding, J., and Becker, P.B. (2012). The MOF-containing NSL complex associates globally with housekeeping genes, but activates only a defined subset. Nucleic acids research *40*, 1509-1522.

Fraga, M.F., Ballestar, E., Villar-Garea, A., Boix-Chornet, M., Espada, J., Schotta, G., Bonaldi, T., Haydon, C., Ropero, S., Petrie, K.*, et al.* (2005). Loss of acetylation at Lys16 and trimethylation at Lys20 of histone H4 is a common hallmark of human cancer. Nature genetics *37*, 391-400.

Gallien, S., Duriez, E., Crone, C., Kellmann, M., Moehring, T., and Domon, B. (2012a). Targeted proteomic quantification on quadrupole-orbitrap mass spectrometer. Molecular & cellular proteomics : MCP *11*, 1709-1723.

Gallien, S., Peterman, S., Kiyonami, R., Souady, J., Duriez, E., Schoen, A., and Domon, B. (2012b). Highly multiplexed targeted proteomics using precise control of peptide retention time. Proteomics *12*, 1122-1133.

Goodlett, D.R., Keller, A., Watts, J.D., Newitt, R., Yi, E.C., Purvine, S., Eng, J.K., von Haller, P., Aebersold, R., and Kolker, E. (2001). Differential stable isotope labeling of peptides for quantitation and de novo sequence derivation. Rapid communications in mass spectrometry : RCM *15*, 1214-1221.

Gu, W., Szauter, P., and Lucchesi, J.C. (1998). Targeting of MOF, a putative histone acetyl transferase, to the X chromosome of Drosophila melanogaster. Developmental genetics *22*, 56-64.

Jaffe, J.D., Wang, Y., Chan, H.M., Zhang, J., Huether, R., Kryukov, G.V., Bhang, H.E., Taylor, J.E., Hu, M., Englund, N.P.*, et al.* (2013). Global chromatin profiling reveals NSD2 mutations in pediatric acute lymphoblastic leukemia. Nature genetics *45*, 1386-1391.

Karmodiya, K., Krebs, A.R., Oulad-Abdelghani, M., Kimura, H., and Tora, L. (2012). H3K9 and H3K14 acetylation co-occur at many gene regulatory elements, while H3K14ac marks a subset of inactive inducible promoters in mouse embryonic stem cells. BMC genomics *13*, 424.

Kharchenko, P.V., Alekseyenko, A.A., Schwartz, Y.B., Minoda, A., Riddle, N.C., Ernst, J., Sabo, P.J., Larschan, E., Gorchakov, A.A., Gu, T.*, et al.* (2011). Comprehensive analysis of the chromatin landscape in Drosophila melanogaster. Nature *471*, 480-485.

Kueh, A.J., Dixon, M.P., Voss, A.K., and Thomas, T. (2011). HBO1 is required for H3K14 acetylation and normal transcriptional activity during embryonic development. Molecular and cellular biology *31*, 845-860.
Lalonde, M.E., Avvakumov, N., Glass, K.C., Joncas, F.H., Saksouk, N., Holliday, M., Paquet, E., Yan, K., Tong, Q., Klein, B.J.*, et al.* (2013). Exchange of associated factors directs a switch in HBO1 acetyltransferase histone tail specificity. Genes & development *27*, 2009-2024.
Loyola, A., Bonaldi, T., Roche, D., Imhof, A., and Almouzni, G. (2006). PTMs on H3 variants before chromatin assembly potentiate their final epigenetic state. Molecular cell *24*, 309-316.
Marx, H., Lemeer, S., Schliep, J.E., Matheron, L., Mohammed, S., Cox, J., Mann, M., Heck, A.J., and Kuster, B. (2013). A large synthetic peptide and phosphopeptide reference library for mass spectrometry-based proteomics. Nature biotechnology *31*, 557-564.
Makowski, A.M., Dutnall, R.N., and Annunziato, A.T. (2001). Effects of acetylation of histone H4 at lysines 8 and 16 on activity of the Hat1 histone acetyltransferase. The Journal of biological chemistry 276, 43499-43502.
Miotto, B., and Struhl, K. (2010). HBO1 histone acetylase activity is essential for DNA replication licensing and inhibited by Geminin. Molecular cell *37*, 57-66.
Peterson, A.C., Russell, J.D., Bailey, D.J., Westphall, M.S., and Coon, J.J. (2012). Parallel reaction monitoring for high resolution and high mass accuracy quantitative, targeted proteomics. Molecular & cellular proteomics : MCP *11*, 1475-1488.
Phanstiel, D., Brumbaugh, J., Berggren, W.T., Conard, K., Feng, X., Levenstein, M.E., McAlister, G.C., Thomson, J.A., and Coon, J.J. (2008). Mass spectrometry identifies and quantifies 74 unique histone H4 isoforms in differentiating human embryonic stem cells. Proceedings of the National Academy of Sciences of the United States of America 105, 4093-4098.
Prestel, M., Feller, C., Straub, T., Mitlohner, H., and Becker, P.B. (2010). The activation potential of MOF is constrained for dosage compensation. Molecular cell *38*, 815-826.
Raja, S.J., Charapitsa, I., Conrad, T., Vaquerizas, J.M., Gebhardt, P., Holz, H., Kadlec, J., Fraterman, S., Luscombe, N.M., and Akhtar, A. (2010). The nonspecific lethal complex is a transcriptional regulator in Drosophila. Molecular cell 38, 827-841.
Rappsilber, J., Ishihama, Y., and Mann, M. (2003). Stop and go extraction tips for matrix-assisted laser desorption/ionization, nanoelectrospray, and LC/MS sample pretreatment in proteomics. Analytical chemistry *75*, 663-670.
Regnard, C., Straub, T., Mitterweger, A., Dahlsveen, I.K., Fabian, V., and Becker, P.B. (2011). Global analysis of the relationship between JIL-1 kinase and transcription. PLoS genetics 7, e1001327.
Schmidt, A., Gehlenborg, N., Bodenmiller, B., Mueller, L.N., Campbell, D., Mueller, M., Aebersold, R., and Domon, B. (2008). An integrated, directed mass spectrometric approach for in-depth characterization of complex peptide mixtures. Molecular & cellular proteomics : MCP *7*, 2138-2150.
Schotta, G., Sengupta, R., Kubicek, S., Malin, S., Kauer, M., Callen, E., Celeste, A., Pagani, M., Opravil, S., De La Rosa-Velazquez, I.A.*, et al.* (2008). A chromatin-wide transition to H4K20 monomethylation impairs genome integrity and programmed DNA rearrangements in the mouse. Genes & development *22*, 2048-2061.
Smith, E.R., Cayrou, C., Huang, R., Lane, W.S., Cote, J., and Lucchesi, J.C. (2005). A human protein complex homologous to the Drosophila MSL complex is responsible for the majority of histone H4 acetylation at lysine 16. Molecular and cellular biology *25*, 9175-9188.

Straub, T., Neumann, M.F., Prestel, M., Kremmer, E., Kaether, C., Haass, C., and Becker, P.B. (2005). Stable chromosomal association of MSL2 defines a dosage-compensated nuclear compartment. Chromosoma 114, 352-364.

Suganuma, T., Gutierrez, J.L., Li, B., Florens, L., Swanson, S.K., Washburn, M.P., Abmayr, S.M., and Workman, J.L. (2008). ATAC is a double histone acetyltransferase complex that stimulates nucleosome sliding. Nature structural & molecular biology 15, 364-372.

Taipale, M., Rea, S., Richter, K., Vilar, A., Lichter, P., Imhof, A., and Akhtar, A. (2005). hMOF histone acetyltransferase is required for histone H4 lysine 16 acetylation in mammalian cells. Molecular and cellular biology *25*, 6798-6810.

Tang, H., Fang, H., Yin, E., Brasier, A.R., Sowers, L.C., and Zhang, K. (2014). Multiplexed parallel reaction monitoring targeting histone modifications on the QExactive mass spectrometer. Analytical chemistry *86*, 5526-5534.

Thorne, A.W., Kmiciek, D., Mitchelson, K., Sautiere, P., and Crane-Robinson, C. (1990). Patterns of histone acetylation. European journal of biochemistry / FEBS *193*, 701-713.

Tropberger, P., Pott, S., Keller, C., Kamieniarz-Gdula, K., Caron, M., Richter, F., Li, G., Mittler, G., Liu, E.T., Buhler, M.*, et al.* (2013). Regulation of transcription through acetylation of H3K122 on the lateral surface of the histone octamer. Cell *152*, 859-872.

Verreault, A., Kaufman, P.D., Kobayashi, R., and Stillman, B. (1996). Nucleosome assembly by a complex of CAF-1 and acetylated histones H3/H4. Cell *87*, 95-104.

Yanez-Cuna, J.O., Arnold, C.D., Stampfel, G., Boryn, L.M., Gerlach, D., Rath, M., and Stark, A. (2014). Dissection of thousands of cell type-specific enhancers identifies dinucleotide repeat motifs as general enhancer features. Genome research *24*, 1147-1156.

Yang, X., Yu, W., Shi, L., Sun, L., Liang, J., Yi, X., Li, Q., Zhang, Y., Yang, F., Han, X.*, et al.* (2011). HAT4, a Golgi apparatus-anchored B-type histone acetyltransferase, acetylates free histone H4 and facilitates chromatin assembly. Molecular cell *44*, 39-50.

Ye, J., Ai, X., Eugeni, E.E., Zhang, L., Carpenter, L.R., Jelinek, M.A., Freitas, M.A., and Parthun, M.R. (2005). Histone H4 lysine 91 acetylation a core domain modification associated with chromatin assembly. Molecular cell *18*, 123-130.

Young, N.L., DiMaggio, P.A., Plazas-Mayorca, M.D., Baliban, R.C., Floudas, C.A., and Garcia, B.A. (2009). High throughput characterization of combinatorial histone codes. Molecular & cellular proteomics : MCP *8*, 2266-2284.

Zhang, K., Sridhar, V.V., Zhu, J., Kapoor, A., and Zhu, J.K. (2007). Distinctive core histone post-translational modification patterns in Arabidopsis thaliana. PloS one *2*, e1210.

Zheng, Y., Thomas, P.M., and Kelleher, N.L. (2013). Measurement of acetylation turnover at distinct lysines in human histones identifies long-lived acetylation sites. Nature communications *4*, 2203.

Table S1

Click here to download Supplemental Movies & Spreadsheets: Feller_Table_S1.xlsx

Table S2

Click here to download Supplemental Movies & Spreadsheets: Feller_Table_S2.xls

Table S3

Click here to download Supplemental Movies & Spreadsheets: Feller_Table_S3.xlsx

Table S4

Click here to download Supplemental Movies & Spreadsheets: Feller_Table_S4.xlsx

Table S5

Click here to download Supplemental Movies & Spreadsheets: Feller_Table_S5.xlsx

Table S6

Click here to download Supplemental Movies & Spreadsheets: Feller_Table_S6.xlsx